Master's degree in Biomedical Engineering

Master's Thesis

Experimental protocol to develop and validate a 3D patient-specific Finite Element Model of human knee joint after Total Knee Arthroplasty: Squat analysis

Supervisors:
Prof. Alberto Audenino
Prof.ssa Cristina Bignardi

Author:
Marco Giuseppe Branni

Tutor:
Prof. Bernardo Innocenti

Academic Year 2017/2018

ABSTRACT

In some cases of degenerative knee condition, total knee arthroplasty (TKA) can be a successful surgical treatment to restore the knee's functionality, if carried out correctly. Since each patient has different bone shapes and mechanical properties of soft tissues, the 3D complex roto-translation movement and the kinetics of the knee change as well. For these reasons, nowadays, several methodologies are carried out to analyse and predict the three-dimensional behaviour of a native or post-arthroplasty knee. To overcome the limitations of the in vivo analysis, such as low amount of analysed specimens for specific boundary conditions, and of the cadaver tests, in terms of high costs, lack of repeatability and ethical issues, the use of numerical modelling is becoming a fundamental tool to better understand the patient-specific knee joint anatomy and functionality.

The purpose of this research project was to produce a protocol in order to develop and validate a patient specific finite element model comparing numerical outcomes, in terms of kinematics and kinetics, with in vitro results obtained during cadaver test performed on the same specimen under the same boundary conditions.

Guide lines about experimental test were given, showing step by step the surgical specimen preparation and all the procedures to calibrate and utilise maps pressure sensors and motion capture systems. CT images, mechanical properties estimated through tensile test of ligaments, and boundary conditions applied during the experimental test, were used to develop the patient-specific Finite Element model. Therefore, the same active motor task simulated with the cadaver specimen was reproduced with a numerical approach.

A final comparison analysis between numerical and experimental outcomes showed that, the tibiofemoral kinematics were validated both in terms of translations and rotations. Instead, regarding to kinetics, while the patellofemoral contact areas and contact pressures predicted using FE model were validated for the main significant flexion angles, it could be validated only the tibiofemoral contact areas because the relative contact pressures measured during the cadaver test resulted uncorrected and in disagreement with the literature.

CONTENTS

LIST OF FIGURES

LIST OF TABLES

CHAPTER I – THE HUMAN KNEE JOINT

1.1 Anatomy of the knee

1.1.1 Bones

The knee joint represents one of the strongest and most important joints in the human body. It permits to link the movement between the lower leg and the thigh while supporting the body's weight and in our daily activities. The knee allows a wide range of motion for flexion–extension and internal–external rotation.

The knee is a synovial hinge joint that connects mainly the distal part of the femur and the proximal part of the tibia, but also includes the fibula and the patella, other two smaller bones. From the interactions between these bones derive the definition of three different joints: the medial and lateral tibiofemoral joints between the femur and the tibia, on the medial and lateral side respectively, and the patella-femoral joint, between the femur and the patella. The patella stands in front of the femur, on the anterior surface of the knee while its smooth joint-forming processes on its posterior surface face the femur.

Fig. 1-1. *Bones in the human knee.*

The femur is the longest, heavies and strongest bone in the skeleton, extending from the hip to the knee. It consists of a body and two extremities: the proximal end includes head, neck and greater and lesser trochanters. The head of the femur is covered by hyaline cartilage except over an avoid depression, known as fovea capitis femoris, and articulates with the acetabulum of the pelvis forming the hip joint. The neck represents a short portion that connects the head with the femoral body, and the greater and lesser trochanters, two prominences on antero-lateral and on postero-medial side, respectively. The distal end is characterised by the presence of two eminences, the medial and the lateral condyles, which articulate with the tibia and patella. Anteriorly, the condyles are slightly prominent and are separated by a smooth shallow articular depression called patellar surface, while on the posterior surface of the femur, a depression known as intercondylar fossa lies in between the

two condyles; it provides space for the anterior cruciate ligament (ACL) and posterior cruciate ligament (PCL), which stabilize the knee along its anterior/posterior axis. Each condyle presents a convex eminence, named medial and lateral epicondyles, to which the collateral ligaments are attached.

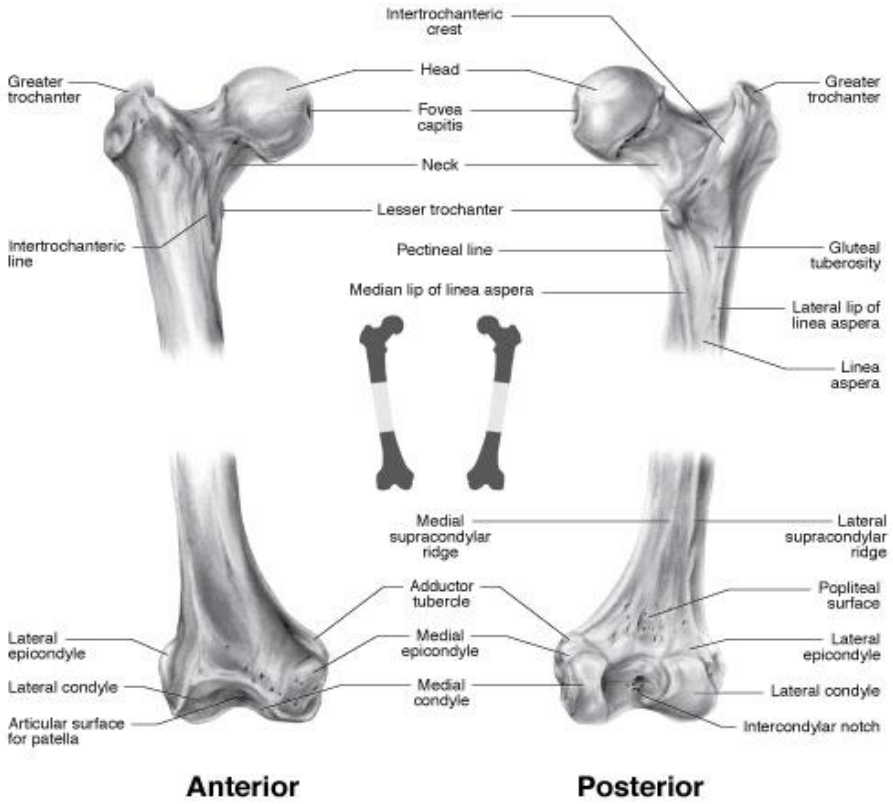

Fig. 1-2. *Proximal and distal ends of femur.*

The lower end of the femur presents a V-shaped articular surface occupying the anterior, inferior and posterior surfaces of both condyles. In the anterior surface is present the so called patellar surface, that presents a groove and articulates with the patella, while the lower and posterior parts of the articular surface represent the tibial surfaces, which articulate with the corresponding condyles of the tibia and menisci.

The tibia is situated on the medial side of the leg, and it is the second largest bone in the body, extending from the knee joint to the ankle. The tibia, such as the femur, is categorized as a long bone and is composed by a body and two extremities. At the proximal end of the tibia there are two bumps, the medial and lateral condyles. Located between the condyles is a region called the intercondylar area, which represents the main site of attachment for the ligaments and the menisci of the knee joint. Together with the medial and lateral condyle the intercondylar region forms a flat surface known as tibial plateau, which articulates with the femoral condyles to form the major articulation of the knee joint. Beneath the condyles is the tibial tuberosity, a large oblong elevation that serves for attachment of the patellar ligament.

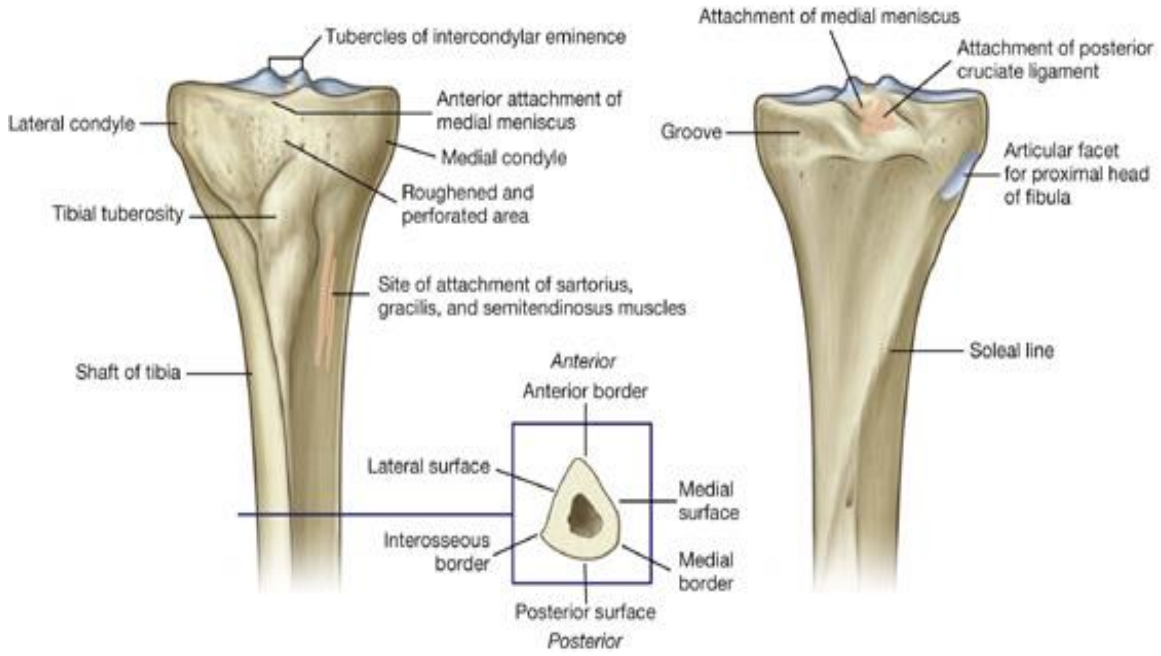

Fig. 1-3. *Anterior and posterior view of the proximal end of the tibia.*

On the lateral side of the tibia is located the fibula, which connects with the tibia in the proximal and distal extremity; it is not functional in the knee joint but represents an important site of attachment for muscles. The distal extremity of the tibia is smaller than the proximal one; the inferior face of the extremity presents a concave articular surface which, with the fibula and the talus, forms the ankle joint.

The patella is a flat, triangular-shaped sesamoid bone which lies in front of the femur on the anterior surface of the knee. It is formed by an anterior face, an articular (or posterior) face, divided into lateral and medial facets, articulating with the femoral patellar surface, and a distal apex, to whom the patellar tendon attaches.

1.1.2 Soft tissues

The knee joint includes a variety of ligaments, tendons, and soft tissue structures that maintain its flexibility, stability, and strength. Each bone has joint-forming surfaces covered in a thin layer of hyaline cartilage that gives them an extremely smooth surface and protects the underlying bone from damage. Between the femur and tibia there are two C-shaped fibrocartilaginous structures, called medial (inside) and lateral (outer) menisci; they are important for reducing contact stresses on the articular cartilage, shock absorption, circulation of synovial fluid and joint stability. The medial meniscus is tethered to the deep part of the medial collateral ligament and so is more prone to injury than the lateral meniscus which is more mobile. The lateral meniscus is smaller than the medial and is sometimes discoid in shape [1].

A joint capsule surrounds the bones of the knee and provide strength and lubrication. The outer layer of the capsule is made of fibrous connective tissue and, together with the ligaments of the knee, hold the joint in place. The joint capsule is lined the synovial membrane which produce an oily synovial fluid; it fills the hollow space between the bones and lubricates the knee to reduce friction.

Many strong ligaments surround the joint capsule of the knee to reinforce its structure and hold its bones in the proper alignment. The ligaments of the knee joint can be distinguished into extracapsular ligaments and intra-articular ligaments. The patellar ligament, medial collateral ligament (MCL),

lateral collateral ligament (LCL), oblique popliteal ligament, and arcuate popliteal ligament belong to the first category, while the intra-articular ligaments includes the anterior cruciate ligament (ACL), posterior cruciate ligament (PCL), and the posterior meniscofemoral ligament.

The patellar ligament is the anterior ligament of the knee joint, considered as the continuation of the tendon of quadriceps femoris, and extends from the inferior border of the patella to the tibial tuberosity of the tibia. Two fibrous bands, known as the medial and lateral retinacula, originate from the vastus medialis and lateralis and, passing on either side of the patella, insert medially and laterally of the tibial tuberosity, merging with the knee capsule. These two structures contribute medially and laterally to the patellar ligament, granting the alignment of the patella with the patellar surface of the femur.

The MCL includes a superficial portion and a deep portion. The superficial one originates on the medial epicondyle and can be further subdivided into anterior and posterior portions. The anterior margin lies free except at its attachment sites to the tibia and femur, and it is separated from the medial meniscus and deep capsular ligament by a bursa, whereas the posterior margin passes obliquely backwards to an insertion in the medial meniscus [2].

The lateral collateral ligament (LCL) originates from the lateral femoral epicondyle, joins the bicep femoris tendon and attaches to the head of the fibula. LCL is separated from the lateral meniscus by the popliteus tendon. The main function of MCL is to restrain valgus movement of the knee joint but it is important also for the control of external rotation. The lateral collateral ligament restrains against varus rotation as well as resisting internal rotation [1].

The oblique popliteal ligament and arcuate popliteal ligament reinforce the joint capsule on the posterior aspect. The oblique popliteal ligament is a broad and flat ligament representing the expansion of the tendon of the semimembranosus, and it arises from the medial tibial condyle and passes toward the lateral femoral condyle, where it blends in with the rest of the joint capsule. The arcuate popliteal ligament is a thick and fibrous ligament that arises from the posterior fibular head and passes over the tendon of the popliteus, spreading over the posterior surface of the knee.

The ACL has a complex structure that reflects its important contribution to knee-joint function. The ACL is attached to a fossa on the posterior aspect of the medial surface of the lateral femoral condyle. The femoral attachment forms of a circular segment, with a straight anterior border and a convex posterior border. From its femoral attachment, the ACL runs anteriorly, medially, and distally to the tibia [3]. The ACL helps to resist anterior displacement of the tibia on the femur during the flexion of the knee and control the screw home mechanism of the tibia in terminal extension of the knee. A secondary function of the ACL is to resist varus or valgus rotation of the tibia, especially in the absence of the collateral ligaments. The ACL also resists internal rotation of the tibia [1].

Directly behind the ACL is located the posterior cruciate ligament (PCL). It PCL arises from the posterior intercondylar area and passes on the medial side of the ACL to attach to the anterior part of the lateral surface of the medial condyle of the femur. The PCL is the strongest ligament of the knee and acts as the primary restraint to posterior tibial translation and a secondary restraint to external tibial rotation [4].

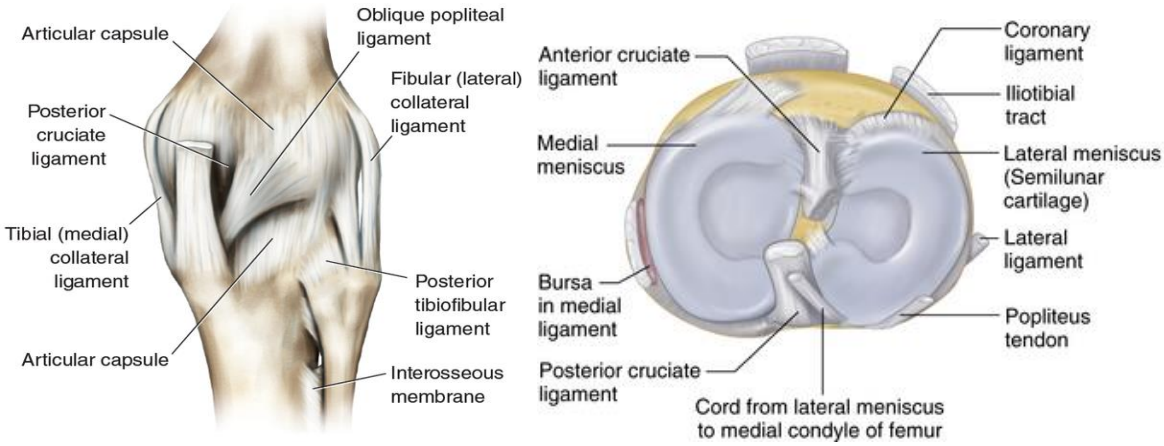

Fig. 1-4. *A view of knee joint ligaments.*

The knee is characterized by a complex kinematic in which the main motion are the flexion-extension and a slight medial and lateral rotation. These movements of the joint take place thanks to the muscles, divided in extensors and flexors. Along the anterior surface of the thigh extends the quadriceps femoris, the most important muscle that stabilize the knee joint. The quadriceps femoris include four muscles: vastus lateralis, vastus medialis, vastus intermedius, and rectus femoris. These large muscles originate from the ilium and femur and insert on the tibia. Contraction of the quadriceps group allows the extension of the leg at the knee and the flexion of the thigh at the hip. The four quadriceps muscles are linked just above the patella forming the quadriceps tendon, which attaches the quadriceps muscles to the patella. The patella is attached to the tibia by its tendon, known as patellar tendon. Together, the quadriceps muscles, quadriceps tendon and patellar tendon provide the straightening of the knee.

The hamstring muscle group extends across the posterior surface of the thigh and is responsible for the flexion movement; it is composed by the semimembranosus, the semitendinosus, the long and the short head of the biceps femoris. The gracilis, sartorius, gastrocnemius, and popliteus contribute weakly to the flexion movement. The sartorius, the semimembranosus, the semitendinosus, the popliteus and the gracilis determine the medial rotation, while the lateral rotation is due to the biceps femoris.

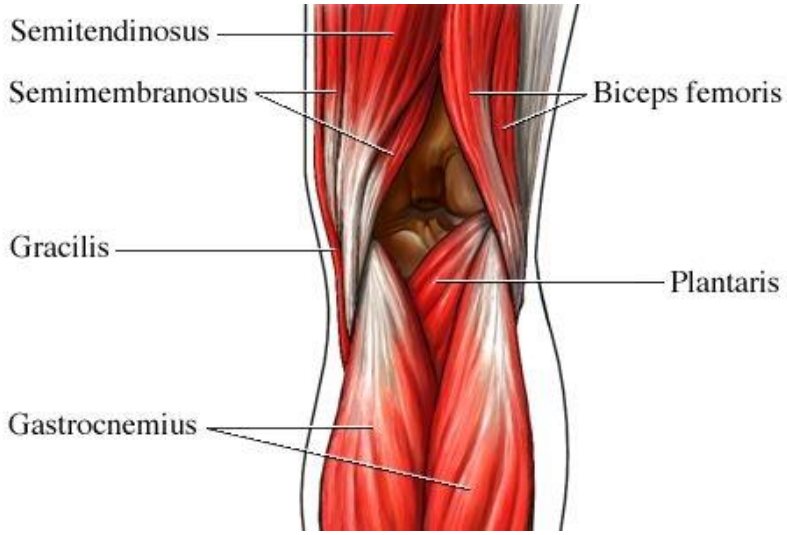

Fig. 1-5. *A view of knee joint muscles*.

1.2 Kinematics of the Healthy Knee

The knee joint plays two main roles: it allows locomotion with stability and minimum energy requirements from the muscles and it transmits, absorbs and redistributes forces during the activities of daily life [5]. These functions can occur thanks to the presence of two distinct joints/articulations, the tibio-femoral joint and the patello-femoral joint.
The knee joint is not a pure hinge joint but moves with a complex set of translations and rotations. It is a bicondylar, modified-hinge joint that exhibits 6 degrees of motion: these may be characterized as 3 rotations (flexion and extension, external and internal rotation, varus and valgus angulation) and 3 translations (anterior and posterior glide, medial and lateral shift, compression and distraction [6].

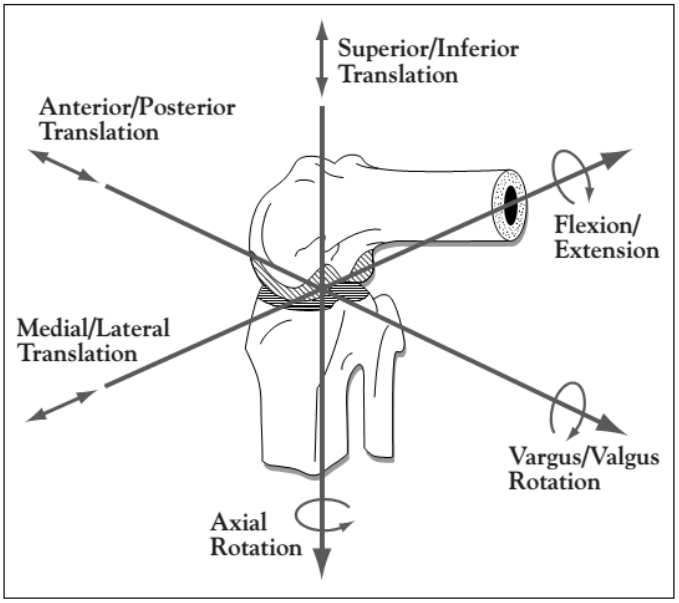

Fig. 1-6. Six degrees of freedom of the knee joint, which include 3 rotational and 3 translational motions [6].

Medio-lateral translation (M-L) and flexion-extension (F-E) occur along and about an epicondylar femoral axis. Joint distraction and internal-external rotation (I-E) occur along and about a tibial long axis. Anterior-posterior translation (A-P) and varus-valgus (V-V) rotation occur along and about a floating axis, which is perpendicular to both femoral epicondylar and tibial long axes.
The rotation of the TF joint in the sagittal plane (flexion-extension) represents the primary motion. The full extension, that corresponds to zero degrees of flexion, is usually defined when the long axes of the tibia and femur are aligned in the sagittal plane. An active knee flexion can be obtained primarily by the hamstring contraction and usually reaches 130°, whereas passive flexion can reach 160° [5]. A small hyperextension, in the order of 3-5 degrees, is also possible.
The wide range of flexion angles is due to a mechanism known as femoral rollback, in which the rotation of the femoral condyles is coupled with a posterior sliding of the articular surface. Thanks to this mechanism, the posterior dislocation of the femoral condyles that could happen at high flexion angles in case of a pure rolling of the femur on the tibia, is avoided [7], [8]. Some differences can be highlighted in the antero-posterior motion of the lateral and medial side of the femur: in fact, smaller displacements and an almost complete sliding characterize the medial side, while the lateral compartment presents bigger displacements and a rolling and sliding combined movement.
The anatomical difference that exists between the medial and lateral tibial condyle (the lateral that is shorter than the medial one) leads to a “screw-home mechanism”, in which the tibia rotates internally

during flexion - from full extension to 20° flexion - and externally during extension - from 20° to full extension. This rotation is responsible for the tightening of the ligamentous structures that lock the knee, assuring maximal stability. The varus-valgus rotation, known also as adduction-abduction, reaches higher angles during flexion of the knee and lesser ones (from 6 to 8 degrees) during full extension. This movement is restricted by the collateral ligaments, by co-contraction of the quadriceps, by hamstrings muscle groups or by some combination of them. The tibio-femoral joint kinematics presents also other complex aspects (Fig. 1-7).

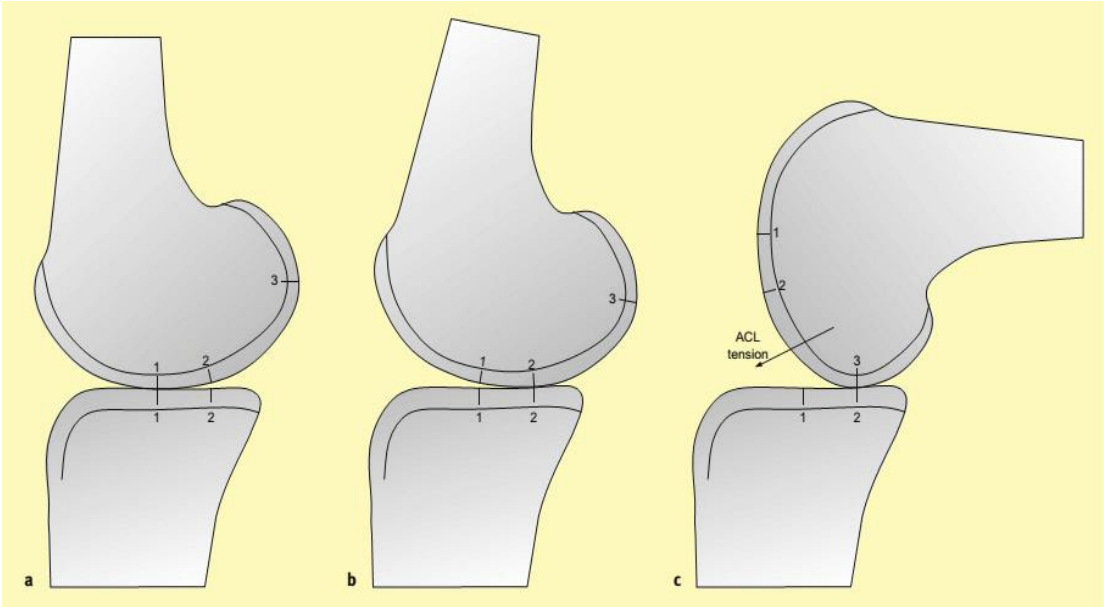

Fig. 1-7. *Knee joint kinematics during gait. a) Extension; b) Early flexion; c) Deep flexion*

When full extended, the contact area between the femur and the tibial plateaus is large and presses anteriorly on the meniscal horns. During the flexion of the knee, the contact area with the tibial plateaus reduces, leading to a decrease of the radii of curvature of the femoral condyles. Moreover, the tibia rotates during flexion; the medial tibial plateau is slightly concave whereas the lateral tibial plateau is flat or slightly convex in the sagittal plane. The femoral condyles present circular sagittal sections and the anterior cruciate ligament (ACL) is in tension; this means that the femur slides anteriorly and rolls posteriorly at the same time. During high flexion, the contact between the femoral condyles and the posterior meniscal horns occurs with very little cartilage-to-cartilage contact, especially where the meniscus is constrained from displacing further posteriorly off the tibial posterior rim (medial side). Moreover, tibial internal rotation occurs leading to the displacement of the posterior horn of the lateral meniscus with the posterior rim of the tibial plateau. Regarding the patella-femoral joint (Fig. 1-8), when the tibio-femoral joint is full extended, the patella and the femur meet each other at the distal end of the patella. As flexion increases, the patella engages into the femoral trochlear groove and the contact area spreads across the width of the patella and moves proximally.

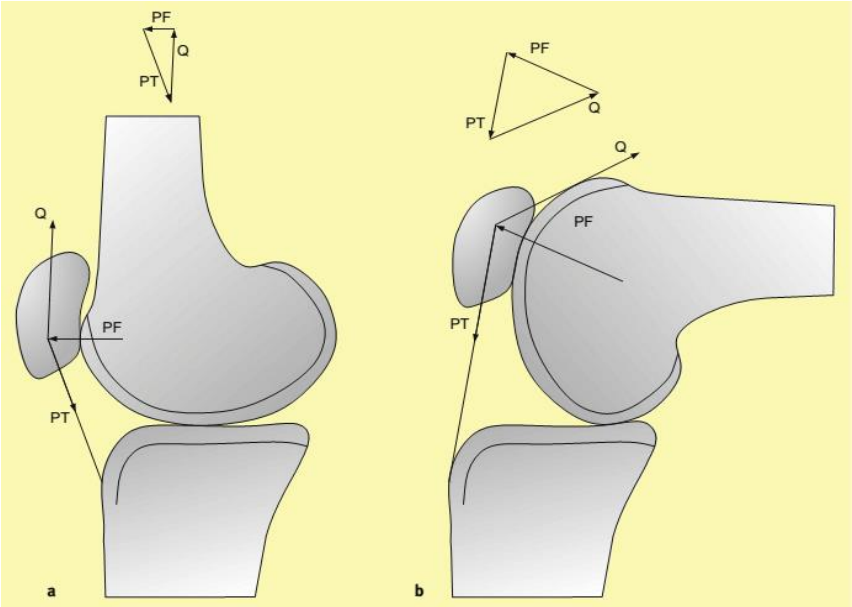

Fig. 1-8. *Patello-femoral joint kinematics and loads during extension (a) and 90°flexion (b)*

In the patella-femoral joint, when the knee is about to extension, the lines of action of the patellar tendon and quadriceps muscle are almost co-linear in the sagittal plane (Fig. 1-8a) leading to a small joint force. However, if the knee flexes, the angle between the lines of action of the patellar tendon and the quadriceps muscle reduces: this result in increasing patello-femoral joint force up to approximately 70° knee flexion (Fig. 1-8b). Observing the frontal plane of the extended patella-femoral joint, can be seen a resultant lateral force acting on the patella; this is often called the Q-angle effect. The Q-angle is approximately 12-15°in males and 15-18°in females in the extended knee and reduces with flexion because of the reversal of the screw-home mechanism [5].

1.3 Alignment of the lower limbs

The reciprocal alignment of femur and tibial bones is crucial in terms of stability and functionality of the knee joint. For this reason, a correct evaluation of the alignment of lower limbs appears to underlie the diagnosis of arthritic conditions of the knee joint; one of the most important seems to be the frontal plane alignment, which could be related to degenerative pathologies such as osteoarthritis.
The alignment of the lower limbs is determined by the orientation of an anatomical and a mechanical axis of the tibia and the femur. The anatomical axis is represented by a line drawn in the centre of the medullary cavity of the bone, while the mechanical axis describes the axis along which the load is applied. Usually the mechanical axes orientation is preferred to measure the alignment compared to anatomical axes, since those are easier to identify.
A neutral alignment of the knee, is characterized by the lining up of the mechanical axis of the tibia and femur and by an angle of 180° between them, called hip-knee-ankle angle (HKA), which coincides with the load bearing axis (LBA), crossing the centres of ankle, knee and hip [9]. The femoral mechanical axis is inclined in respect to the vertical axis of 3°. It links the femoral head centre with the mid-condylar point located between the cruciate ligaments, while the tibial mechanical axis joints the centre of the tibial plateau with the centre of the tibial plafond. In the tibia, the anatomical axis and the mechanical axis coincide, while the anatomical axis of the femur is 6° inclined in respect to the mechanical axis [10], [11].

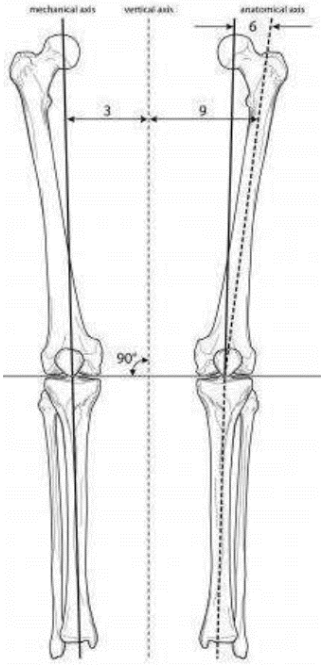

Fig. 1-9. *View of anatomical and mechanical axis of the lower limbs [11].*

When the alignment is incorrect, the center of the knee is medially or laterally displaced in respect to the load bearing axis, leading to an alteration in the loading conditions of the joint. A pathologic alignment in the frontal plane can be described by two configurations: valgus malalignment and varus malalignment, in relation to the mechanical and anatomical axis directions.
In case of varus malalignment the center of knee is lateral to the load bearing axis, while in valgus it is medially translated. In a varus condition, the distal part of the femur is twisted outward the center of the body, while the distal part of the tibia is twisted inward (bow-legs); in the valgus condition, the proximal part of the joint is twisted inward, while the distal part is twisted outward the center of the body (knock-knee).

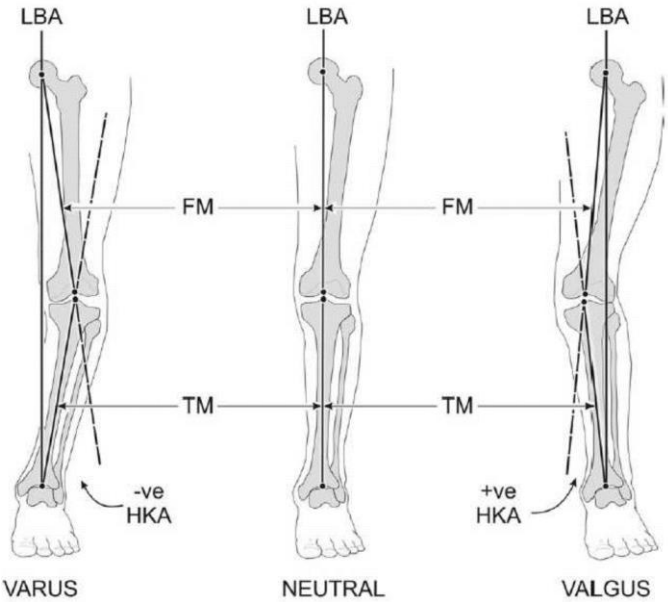

Fig. 1-10. *A Fig. Varus, Neutral and Valgus alignment of the lower limbs. LBA=Load Bearing Axis, TM=Tibial Mechanical Axis, FM=Femoral Mechanical Axis, HKA= Hip-KneeAnkle angle [9]*

1.4 Total Knee Arthroplasty

1.4.1 Introduction

The knee joint has to bear very high forces in all the human daily activities and works for countless cycles during the life. For these reasons the knee joint can undergo to an unexpected reduction of its functionality, particularly in patients with a not physiologic native knee. When the damage is irreparable, a total or partial knee replacement could be necessary.
One of the main causes of knee damage is the worsening of the articular cartilages, which could be due to degenerative pathologies, such as arthritis, or caused by an alteration of the physiological loads acting on the cartilages. However, beyond the pathological situations, also catastrophic events might need a knee replacement surgery.

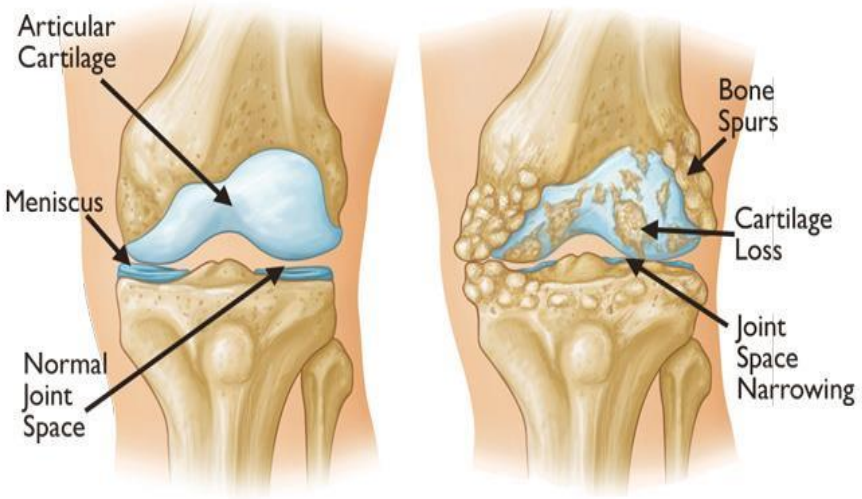

Fig. 1-11. *A comparison between a healthy human knee and a knee affected by osteoarthritis*

Arthritis is inflammation of one or more joints and its main symptoms are joint pain and stiffness, which usually worsen with age. The most common types of arthritis are the osteoarthritis, the rheumatoid arthritis and the post-traumatic arthritis.
Osteoarthritis affects both elder and middle-aged persons and is characterized by the progressive degradation of the articular cartilage. This can be due to several causes, such as hereditary, metabolic and mechanical. Rheumatoid arthritis is an autoimmune disorder that affects the knee but also the other joints and internal organs. It leads to chronic inflammation and thickening of the synovial membranes that surround the joint. Post-traumatic arthritis can affect people who have experienced fractures, ligament injuries or meniscal tears.
As stated above, these pathologies lead to the degradation of the articular surfaces. The main functions of femoral condyles and meniscus are to reduce stress on subchondral bone and to minimize friction, this means that when they are degraded they interpose between the distal section and the proximal section of the joint in a non-physiologic way, causing a bone-to-bone contact. This contact is painful and reduces significantly the mobility of the patient. Inflammation and pain are treated with anti-inflammatory drugs and physical therapy if they are mild; however, when the pain is chronic and the motility of the patient is compromised, the knee replacement total or partial surgery is necessary to restore the correct movement and to relieve the patient from pain.

1.4.2 TKA components

The surgical procedure in which a knee prosthesis is implanted is known as Total Knee Arthroplasty (TKA). TKA is usually made by three or four components (Fig. 1-12).

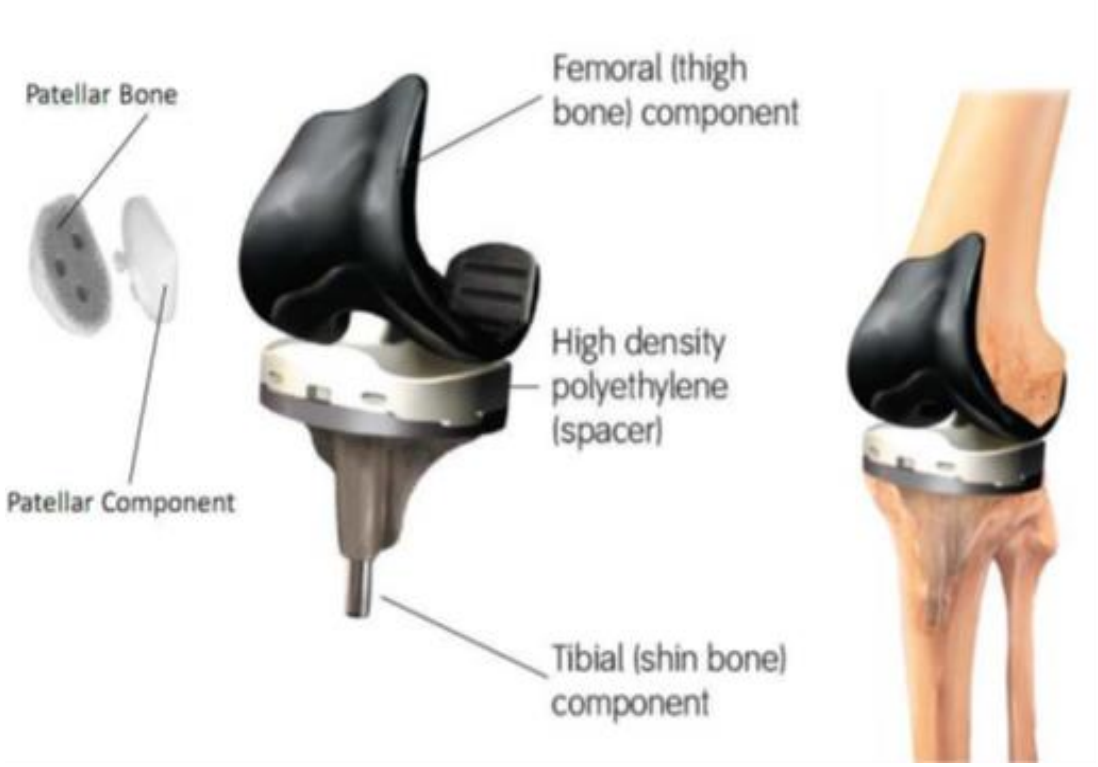

Fig. 1-12. *TKA prosthesis components.*

The femoral component is usually made of Cobalt-Chromium alloy. It restores the femoral condyle curvature and replaces the damaged articular cartilage, rebuilding the distal part of the femur. The tibial component consists of the tibial insert and the tibial tray: the first one is generally made of Ultra-High-Molecular-Weight-Polyethylene (UHMWPE) and mimes and substitute the cushion function of the menisci, while the tibial tray is made of a specific biocompatible Titanium alloy. Moreover, it is also possible to use the all-polyethylene solution which provides good results with no significant differences compared to the traditional configuration [12]. The patellar component substitutes the cartilage covering the posterior face of the bone and articulates with the patellar face of the femur. However, the patellar replacing is not always performed and the decision rest with the surgeon, which judges the condition of the patients.

1.4.3 TKA designs

Nowadays there is a wide variety of TKA designs available, distinguished according to the degrees of constraint, bone loss and soft tissue resection. For uncomplicated primary knee replacement, the most commonly used types are the posterior-stabilised (PS) and cruciate-retaining (CR) designs. When a PS is implanted, the Posterior Cruciate Ligament (PCL) and the Anterior Cruciate Ligament (ACL) are lost during surgery. Since PCL and the ACL are responsible for the antero-posterior stability, an intercondylar spine on the tibial component, known as post, is necessary to replace their function. The post articulates with a cam on the femoral component, in order to prevent non-physiological anterior movement of the femur with respect to the tibia during flexion [13]. The

implantation of CR prosthesis requires resection of the anterior cruciate ligament (ACL) but it need not the cutting of PCL during surgery, since it provides the antero-posterior stability. It is chosen in case of arthritis with minimal bone loss, minimal soft tissue laxity or with a varus/valgus deformity. Current total knee prosthesis (TKP) devices can be subdivided into two groups according to their different fundamental design: fixed-bearing knees, characterized by a polyethylene tibial insert locked with tibial tray, and mobile-bearing designs which facilitate movement of the insert relative to the tray [14]. Fixed-bearing prosthesis provides low contact stress thanks to its high conformity bearing surface, but, on the other hand, produces high torque at the bone-implant interface predisposing to component loosening. Then mobile-bearing knee prosthesis was introduced with the aim of reduce polyethylene wear and component loosening. The mobile-bearing design ensures both congruity and mobility in the tibiofemoral bearing surface, allowing low contact stress and low constraint force. This enables to improve wear resistance and, theoretically, to minimize loosening. Moreover, this design also solves the kinematic conflict of fixed-bearing knee because a high conforming articular surface can now coexist with free rotation [15].

1.4.5 Surgical technique for TKA

The surgical intervention varies according to the type of the prosthesis has to be implanted. However, the general steps are the removal of the Anterior Cruciate Ligament, the guided cut of the femoral condyles and the tibial plate through specific surgical instrumentations. The Posterior Cruciate Ligament is removed if a PS prosthesis is implanted. The bones are resected along planes that are identified by specific anatomical landmarks in accordance with the specific TKA model [16]. Most commonly, the surgeon begins with making an incision on the front of the knee to allow access to the knee joint. Regardless of approach, it is essential maintain careful attention to ligament balancing and protecting neurovascular structures.

The capsule is opened generally on the inside edge of the kneecap and muscles and tendons are then pulled away to expose the arthritic bone ends. The distal femur resection starts with the placement of a special, customized knee instrumentation device on the end of the femur. This device ensures that the bone is cut in the proper alignment to the leg's original angles and it is used to cut several pieces of bone from the distal femur so that the artificial knee can replace the worn surfaces with a metal surface.

The metal prosthesis is cut so it matches the taper almost exactly and then the component is attached to the end of the femur using an epoxy cement [17]. To perform the tibial resection, 10 mm of tibial proximal bone are removed [18] along a plane that is orthogonal to the mechanical axis; also in this case, the procedure requires the use of a specific device. After that, an intramedullary hollow enables to fit the stem of the tibial tray, by giving stability between the implant and the bone [19]. The plastic spacer is then attached to the metal tray of the tibial component. Trial implants are placed over the resected bone surfaces to assess joint stability, ligament balance, and range of motion. If satisfactory, final components are inserted. At this point, the patella is flattened before returning to its normal position, and it is adjusted with an additional plastic component to ensure a proper fit with the rest of the implant. Final hemostasis is then obtained, and the joint is irrigated and closed [20].

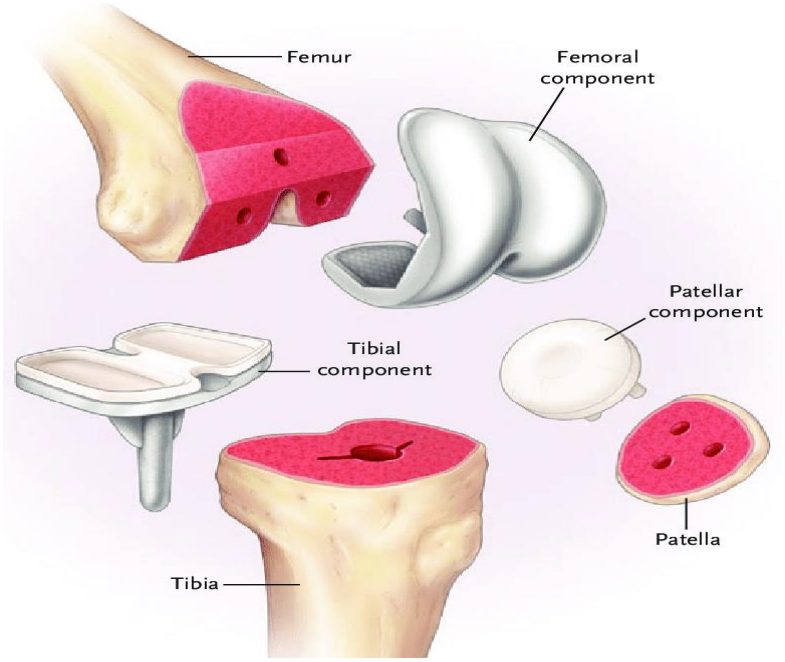

Fig. 1-13. *Components of Total Knee Arthroplasty.*

Precise resections are made in the distal end of the femur, the proximal end of the tibia, and the posterior surface of the patella to fit the corresponding surfaces of the three arthroplasty components.

1.4.6 Complication of the TKA

In order to supervise the outcomes of surgical procedures and to assure an accurately measuring of healthcare quality, a reporting of complications is essential. Several reasons can lead to complications after surgical operations, such as an evolving disease process, a surgical error, a medical error, a nursing error, patient noncompliance, and events without error beyond physician or patient control such as falls or trauma.

Total knee arthroplasty (TKA) is a safe, cost-effective treatment that alleviates pain and restores the knee function of those patients with arthritis who do not respond to conservative treatment. It is a commonly performed procedure worldwide with a high rate of patient satisfaction [21]. Nevertheless, complications may occur, causing significant morbidity. Several studies have attempted to predict factors which may increase complication rates in TKA. The most common adverse effects, reported by several studies, are listed below:

- Infection in a prosthetic total knee joint, a serious complication which can be difficult to treat;
- Thromboembolic disease. It is a severe complication of TKA. Potential disadvantages of routine DVT prophylaxis following TKA include bleeding and wound problems as well as cost, drug side-effects and inconvenience for the patient.
- Vascular injury following TKA. It is a rare complication, but it may have disastrous outcome. In particular, the popliteal artery is the commonest major vessel at risk.
- Tourniquet-related nerve injury. The utilisation of a tourniquet is common in total knee arthroplasty, but it may be associated with nerve injury because of the compression and/or ischemia. However, this complication appears to be rare if the tourniquet pressures is low and it is used for shorter time periods.
- Superficial wound complications following TKA. They are common and include erythema, superficial surgical site infection, postoperative drainage and skin necrosis.

- Periprosthetic patellar fractures. It is usually the commonest fractures complicating total knee arthroplasty. The risk of a patellar fracture in association with a total knee arthroplasty is lower intra-operatively than it is in the postoperative period [21]. Predisposing intra-operative factors include aggressive clamping of the patella during the resurfacing, over-reaming of the patella, slippage of the reamer, aggressive bone resection. During postoperative period, periprosthetic patellar fractures can be due to direct trauma or indirectly caused by eccentric quadriceps muscle contraction.
- Pain during the initial postoperative period.
- Stiffness. It may arise from an improper implant position or size, inadequate bone resection, improper soft-tissue balancing, anterior tibial slope, instability, infection, reflex sympathetic dystrophy, heterotopic ossification, poor patient compliance, poor pain management or subacute infection.
- Metallosis, metal allergy and metal ions. Metallosis is a rare complication and can be caused by implant loosening, demineralization of bone and subsequent fracture following TKA [21].

CHAPTER II – AIM OF THE STUDY

In contrast to the past, when a numerical analysis in orthopaedic research was mainly limited to a simplistic approach, such as single structures or tissue types investigation and bidimensional model, nowadays fully three-dimensional, non-linear, multi-structures and tissues, multi-joints systems, can be developed applying different boundary conditions to simulate specific motor task. In this context, when clinical research and questions cannot be answered, the coupling of numerical analysis to experimental clinical procedures represents the best method to investigate the knee behaviour.
Since knee kinematics and kinetics differ among patients, a subject-specific analysis become fundamental to determinate the knee functionality. In fact, this approach permits to improve and predict clinical outputs and, at the same time, to help industry in generating new devices.
Therefore, the aim of this study is to realize a protocol to develop and validate a patient-specific finite element model of human knee after total knee arthroplasty, in order to simulate an active squat.
The research project is subdivided in three main parts. First, experimental cadaver tests were performed in UZ Gent Hospital University to collect kinetics and kinematics experimental data recorded using a pressure maps sensors and infrared cameras respectively. The second part of this work is focused on the development of patient-specific finite element model. Starting from clinical images obtained from the human specimen used during the cadaver test, it was reconstructed bones geometry. In addition, a tensile test of the ligaments, extracted at the end of the in vitro analysis, was conducted in order to estimate specific mechanical properties of MCL and LCL. It was simulated the TKA surgery and the identical initial spatial configuration was replicated using specific landmarks coordinates. Moreover, the experimental squat was exactly replicated, applying as boundary conditions and constrains the test-rig input data.
The last part is based on the validation of the FE model. Concerning to kinematics validation, internal-external and varus-valgus rotations, medial-lateral, antero-posterior and compress-distract translations were compared to the experimental ones. Moreover, contact pressures and contact areas on the patellofemoral and tibiofemoral joints were contrasted to validate the kinetics.

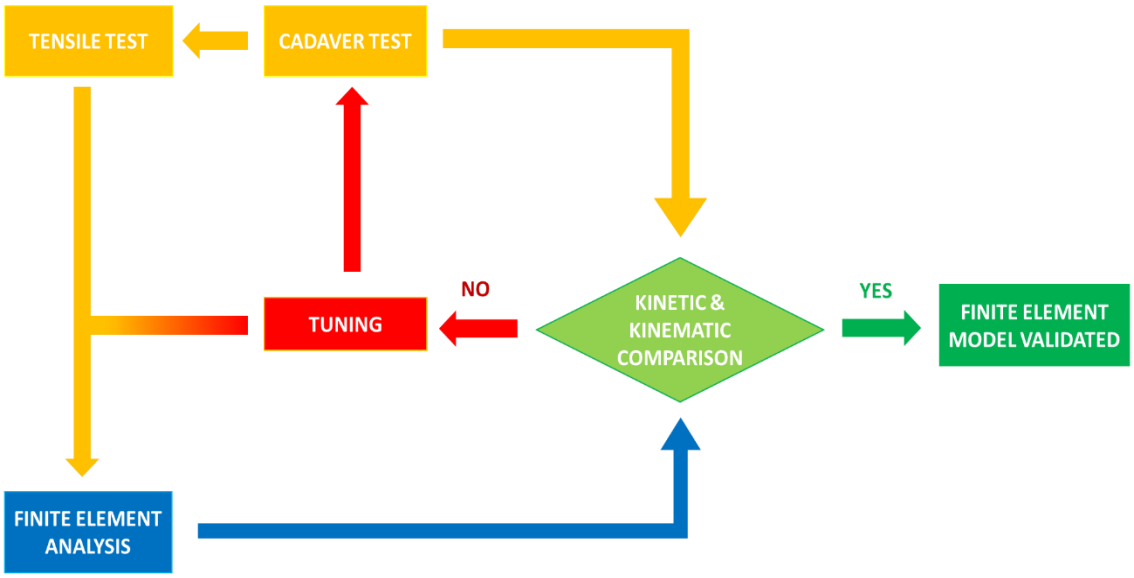

Fig. 2-1. The flowchart describes the project plan followed in this thesis

CHAPTER III – CADAVER TEST

3.1 Background

Several types of knee simulators are developed to study knee kinetics and kinematics. In general, two types can be distinguished: Oxford simulators and robotic simulators. The Oxford simulator type adjusts the quadriceps load to create knee flexion/extension while leaving kinematic freedom (six DOF) to the knee. This characteristic introduces a direct relationship between the magnitude of the quadriceps force applied and the knee kinematics, which is the major limitation. Instead, robotic simulators permit to control the position of the femur relative to the tibia, which is controlled based on the reaction forces measured at the clamping. By additionally adding active controlled muscle activation of quadriceps, medial and lateral hamstring, these robotic simulators allow studying the knee biomechanics simulating daily life activities [22].

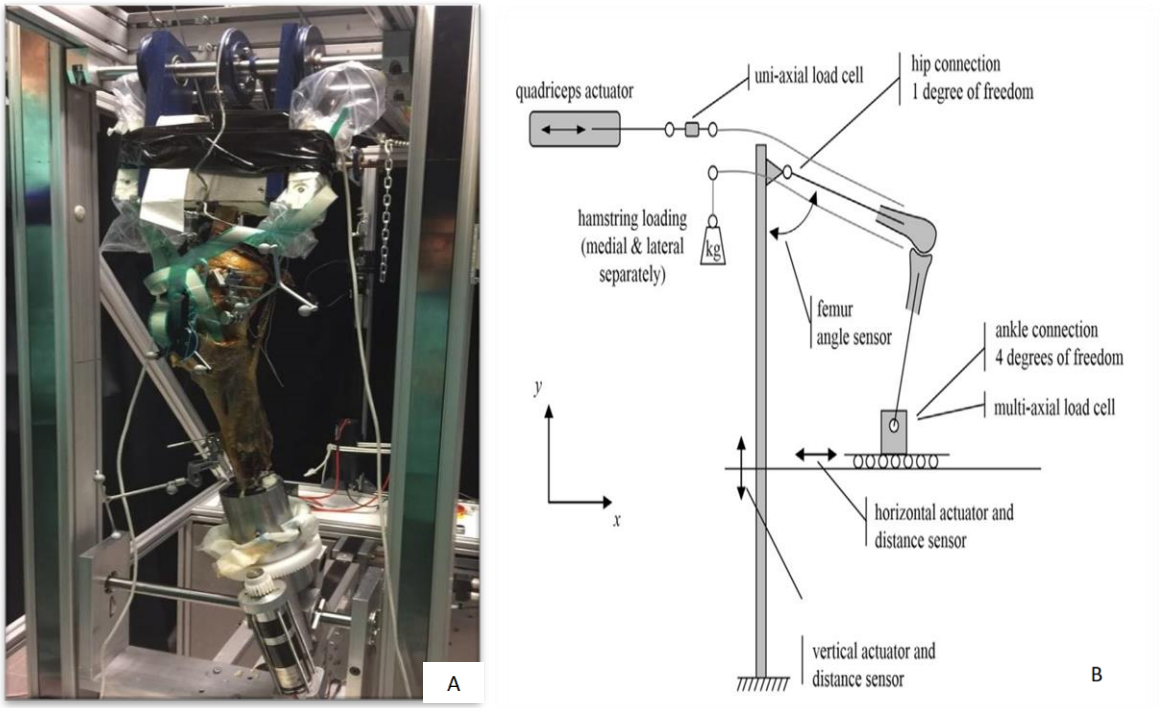

Fig. 3-1. Squat simulated by Test Rig (A). Schematic representation of knee simulator (B).

Therefore, the focus of this chapter lies in evaluating kinetics and kinematics of the knee joint during in vitro testing. A dynamic knee test-rig simulator system was customized for this study. Relative design and control allows to independently control the applied kinematic and kinetic boundary conditions to simulate a specific active motor task (figure 3.1 B). Thereby, controlling only the flexion, the knee is left with five degrees of freedom. In details, kinematic boundary conditions are controlled from the ankle while kinetic conditions are controlled from the hip. This peculiarity allows a fixed positioning of the muscle actuator and a more constant alignment of the simulated muscle forces through pulley systems. A sinusoidal quadriceps forces and two constant hamstring forces are generated using a servomotor (Parker Hannifin Corp, Cleveland, OH, USA). The controller of these motors is synchronized with the actuators, controlling the ankle position using a dedicated Ni LabVIEW programming frame.

3.2 Methodology

3.2.1 General strategy

Five fresh frozen cadaver specimens were used for the ex vivo testing, four for the pilot tests, and one for the final test. The specimens consist of a complete limb, disarticulated at the level of the hip, which has been frozen. Using a test-rig knee simulator, an active squat movement is simulated. During that motor task, the position of the femur, the tibia and the patella are quantified by tracking three different markers set using an OptiTrack Motion Capture System. Moreover, the stress distribution in both main joints, tibiofemoral and patellofemoral, are estimated using an ultra-thin pressure and force sensors (Pressure Mapping Sensor 4000, Tekscan). The ex vivo experimental set-up was guided by the following sequence. A general description of all steps is given.

3.2.2 Materials and tools list

- Specimens
- Test-rig
- OptiTrack Motion Capture System
- Pressure Mapping Sensors

With regard to the Specimens:
- CT scanner
- Oscillating saw or hand saw
- Auxiliary materials (i.e., pins, screws, scalpels, sutures)
- Potting jig
- Alignment guides
- Cutting guides
- Cement for bone potting and for implant
- TKA and relative tools for implant insertion (e.g., hammer, inserter, etc.)

With regard to the OptiTrack Motion Capture System:
- Wonder
- Ground plane
- Markers sets of Femur and Tibia

With regard to the Pressure Mapping Sensors:
- Electronic scanner (The Evolution™ Handle)
- Loading frame
- Teflon
- Metal blocks

3.2.3 Methodological sequence

Experimental tests can be planned in three major parts: sensors and tools preparation, specimen preparation and cadaver test. During the first part, which can go on for days or weeks, clinical imaging are accomplished in order to reconstruct STL files of all bones. In addition, design of guides for mounting the specimens in the test setup, cutting and alignment guides are developed and printed. Moreover, pre-conditioning and calibration of the sensors are done, possibly few days before the test. The second main part is pertinent to specimen's preparation. First of all, de-skinning of the leg and installation of markers sets are made; afterward, the opening of knee joint and the matching between STL bones and cadaver bones are carried out in order to utilise capture IR system. Then, both bones are embedded in containers and the surgeon performs a TKA. Finally, specimen is fixed in the knee robot simulator and Tekscan sensors are placed. Finally, during the last part, performance of the ex vivo squat is evaluated by means of data acquisition of kinetic and kinematic data set.

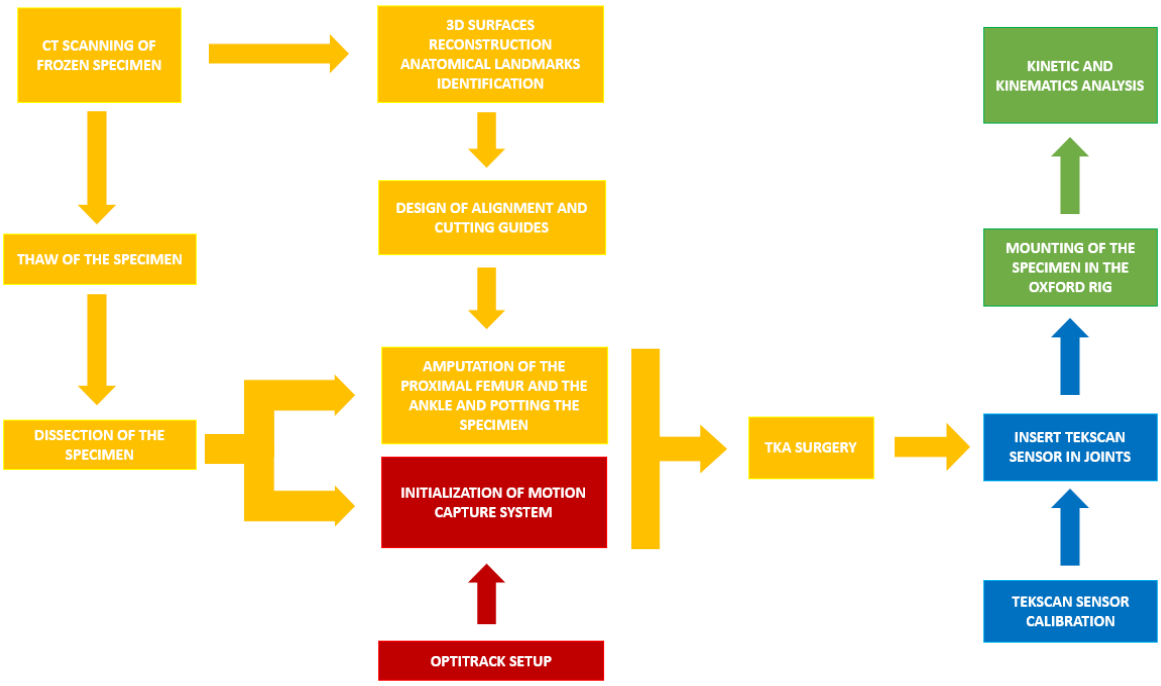

Fig. 3-2. *The flowchart describes the methodological sequence followed to conduct a cadaver test.*

3.2.3.1 Sensors and tools preparation

1. CT scanning of frozen specimen

A few days or weeks before the testing, the specimens were transported in frozen state in an isolating box to the CT scan. Fresh frozen amputated legs were analysed using a helical CT scan (General Electric Lightspeed VCT, Milwaukee, WI, USA). After that, the specimens were replaced in frozen state to preserve tissues. The images were obtained at 120 kV and 450 mA, with a slice thickness of 1.25 mm and a pitch of 0.5 mm/rev (Figure 3-3). Raw data were processed using a bone filter and the images were stored in DICOM format.

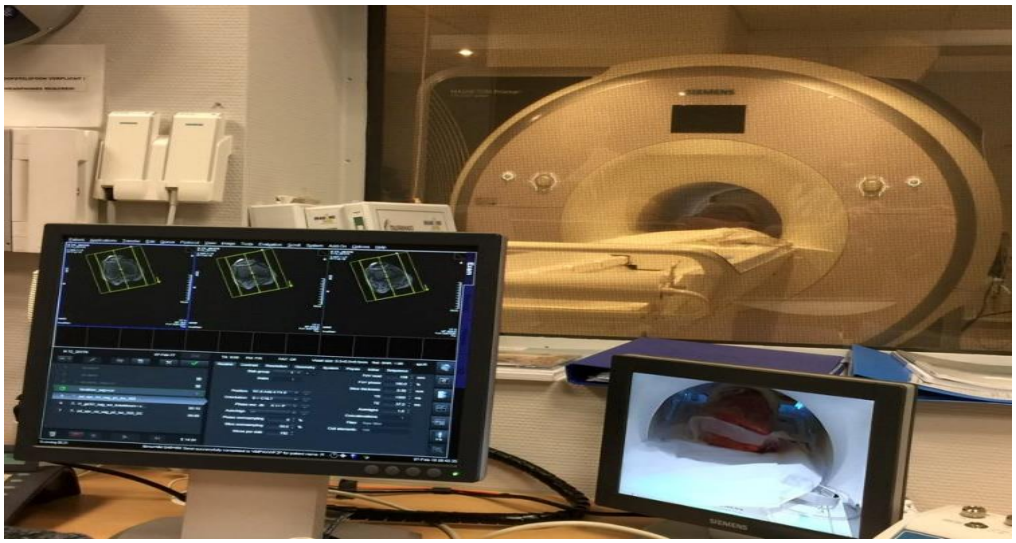

Fig. 3-3. *Specimen's TC scan.*

2. 3D surfaces reconstruction and anatomical landmarks identification.

The CT scans were processed using ScanIP® (Simpleware, Synopsys, Exeter, UK) to reconstruct 3D surfaces of the region of interest. 2D and 3D techniques were used to segment the DICOM files to define three masks: femur, tibia and patella. Manual segmentation was selected as best option to allow good accuracy in the reconstruction necessary to precisely identify anatomical landmarks. A threshold was applied defining manually lower and higher greyscale values (Figure 3-4). Moreover, a sensitive smoothing algorithm was applied to generate more accurate and faithful surfaces (Figure 3-5).

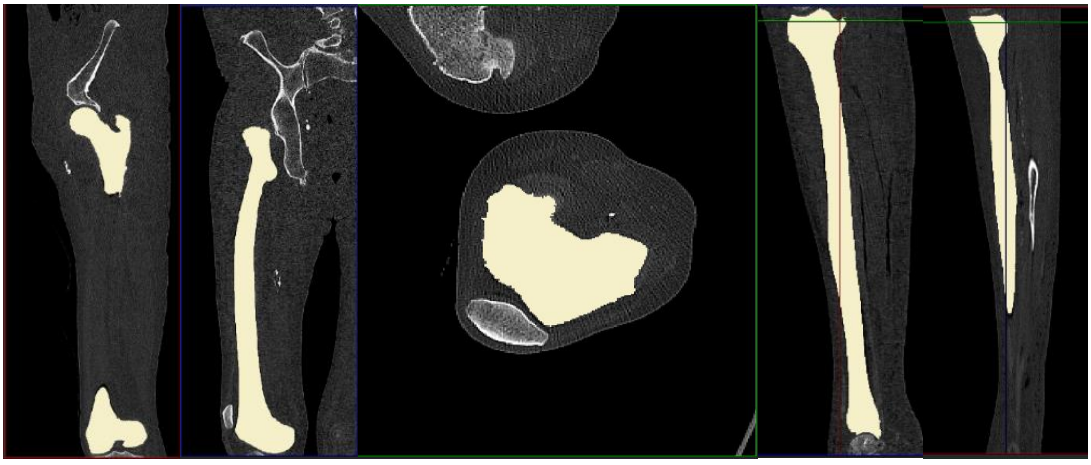

Fig. 3-4. *Femur and tibia segmentation.*

Fig. 3-5. *Application of Recursive Gaussian Filter to bones segmentations.*

Afterwards, all needed anatomical landmarks were evaluated and exported in a list of coordinates. In accordance to work published by Victor [23] were identified the followed anatomical landmarks of the femur, tibia and patella:

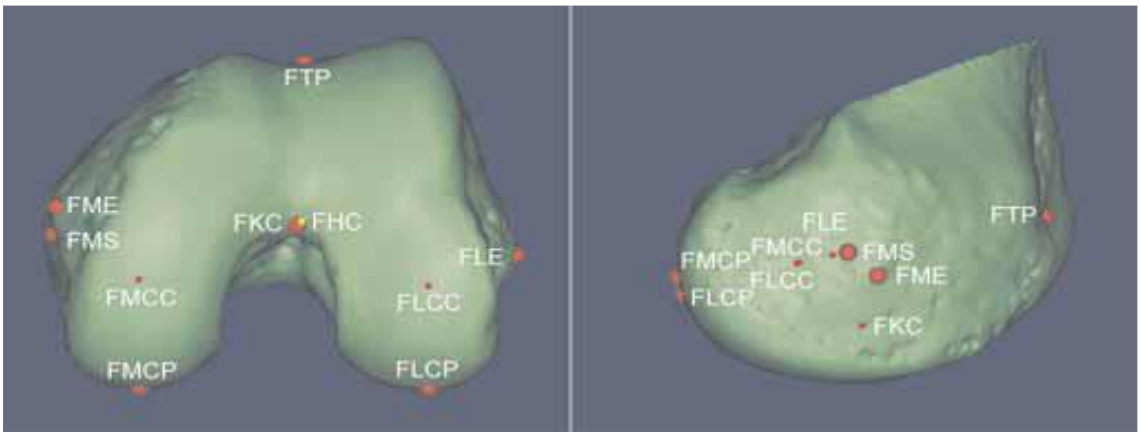

Fig. 3-6. *3D view of the relevant points of distal femur.*

Table. 3-1. *Abbreviations of the relevant points of distal femur.*

Abbreviations	Description
FHK	Femoral Hip Centre
FKC	Femoral Knee Centre
FMCC	Femoral Medial Condyle Centre
FLCC	Femoral Lateral Condyle Centre
FME	Femoral Medial Epicondyle
FMS	Femoral Medial Sulcus
FLE	Femoral Lateral Epicondyle
FTP	Femoral Trochlea Proximal
FMCP	Femoral Medial Condyle Posterior
FLCP	Femoral Lateral Condyle Posterior

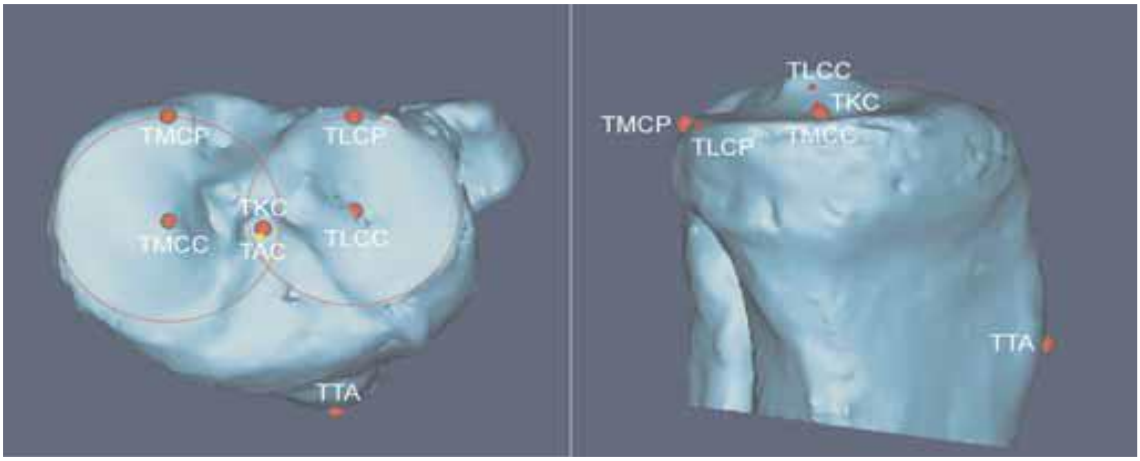

Fig. 3-7. *View of the relevant points of proximal femur.*

Table. 3-2. *Abbreviations of the relevant points of proximal femur*

Abbreviations	Description
TAC	Tibial Ankle Centre
TKC	Tibial Knee Centre
TMCC	Tibial Medial Condyle Centre
TLCC	Tibial Lateral Condyle Centre
TMCP	Tibial Medial Epicondyle Posterior
TLCP	Tibial Lateral Condyle Posterior
TTA	Tibial Tubercle Anterior

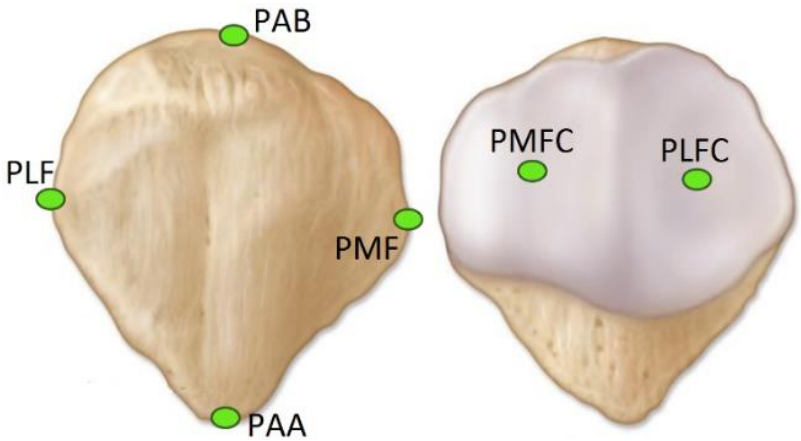

Fig. 3-8. *3D view of the relevant points in 3D model of patella.*

Table. 3-3. *Abbreviations of the relevant points of patella.*

Abbreviations	Description
PAA	Patellar Anterior Apex
PAB	Patellar Anterior Base
PMF	Patellar Medial Facet
PMFC	Patellar Medial Facet Center
PLF	Patellar Lateral Facet
PLFC	Patellar Lateral Facet Center

3. Design of alignment and cutting guides.

To hold appropriate posture of the specimen during cadaver test, both bone ends are encased in a container that can be mounted on the knee simulator. The optimization of the bone-machine interface and the use of a custom-made 3D printed-guides in the potting of a distal femur and proximal tibia permit to create a safe and reproducible experimental environment. Moreover, even the location of the cutting plane along the mechanical axis is a source of deviation from the correct alignment. [24]. To overcome this issue, two potting containers (fig. 3-9) and two specimen-specific 3D-printed cutting guides were designed to restore the anatomical alignment in the knee simulator with a reasonable accuracy.

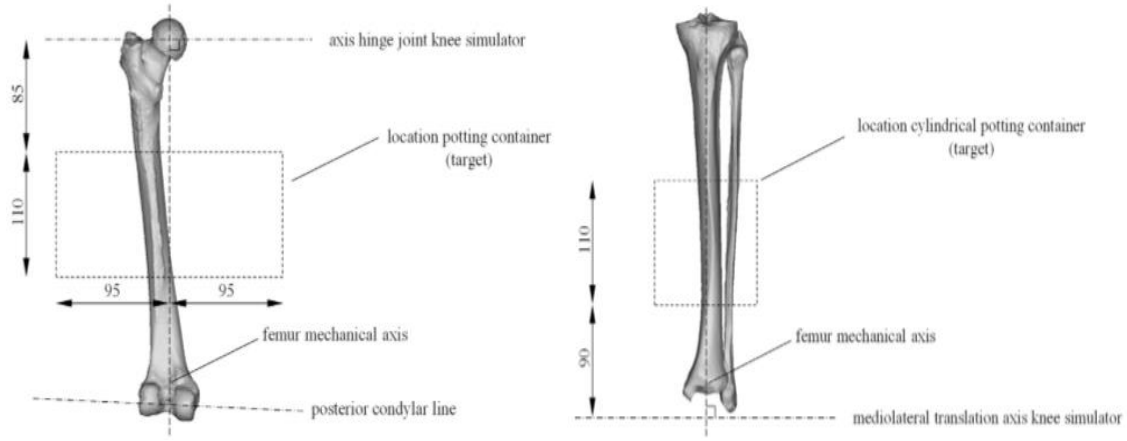

Fig. 3-9. *Femur and Tibia containers design to restore anatomical alignment.*

CAD files relative to two container and cutting guides, 3D patient-specific reconstruction bones and anatomical landmarks of tibia, femur and patella were used to achieve this anatomical alignment using Matlab® R2017b (Mathworks).

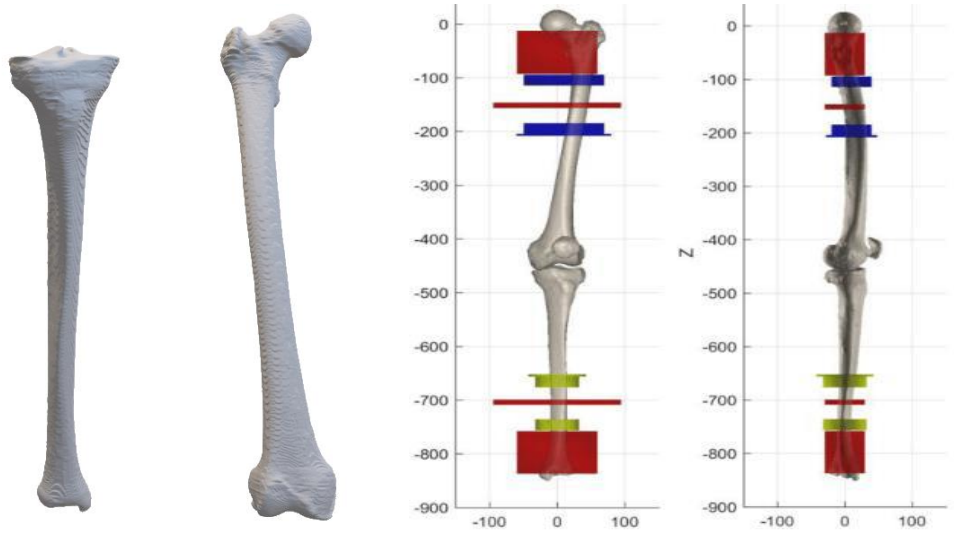

Fig. 3-10. *3D patient-specific reconstruction of femur and tibia (A). Anatomical Alignment (B).*

Once the mechanical alignment has completed, a subtraction of bones from the alignment guides and cutting guides was done using Mimics Research Edition 17.0 (Materialise). Finally, using SolidWorks the final design of the alignment and cutting guides was made removing the excess

material. In details, the alignment guides were split in two-parts, relative design was bettered using a locking mechanism (figure 3-11) and extra cavities were removed optimizing the 3D printing (figure 3-12 and figure 3-13).

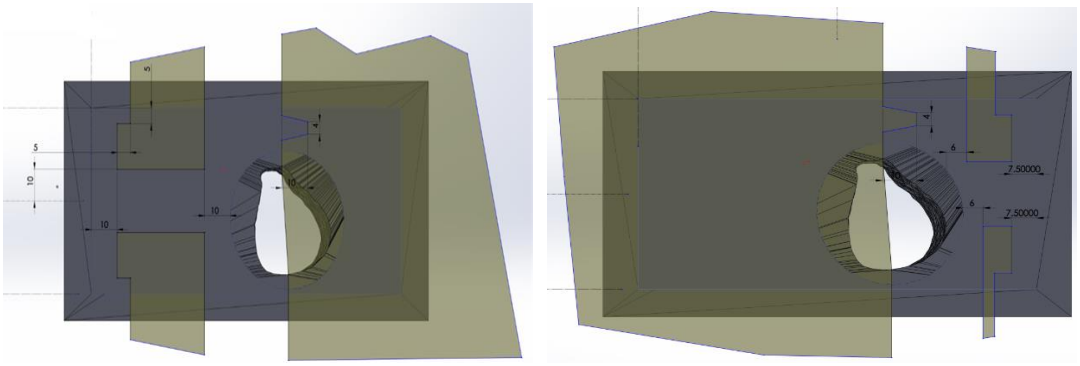

Fig. 3-11. *Sketch of a locking mechanism.*

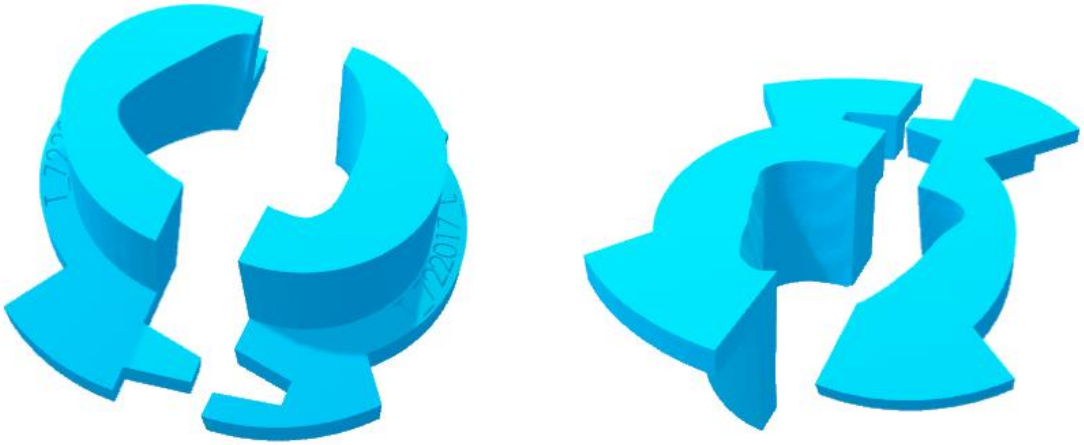

Fig. 3-12. *Final lower and upper Alignment Tibia Guide.*

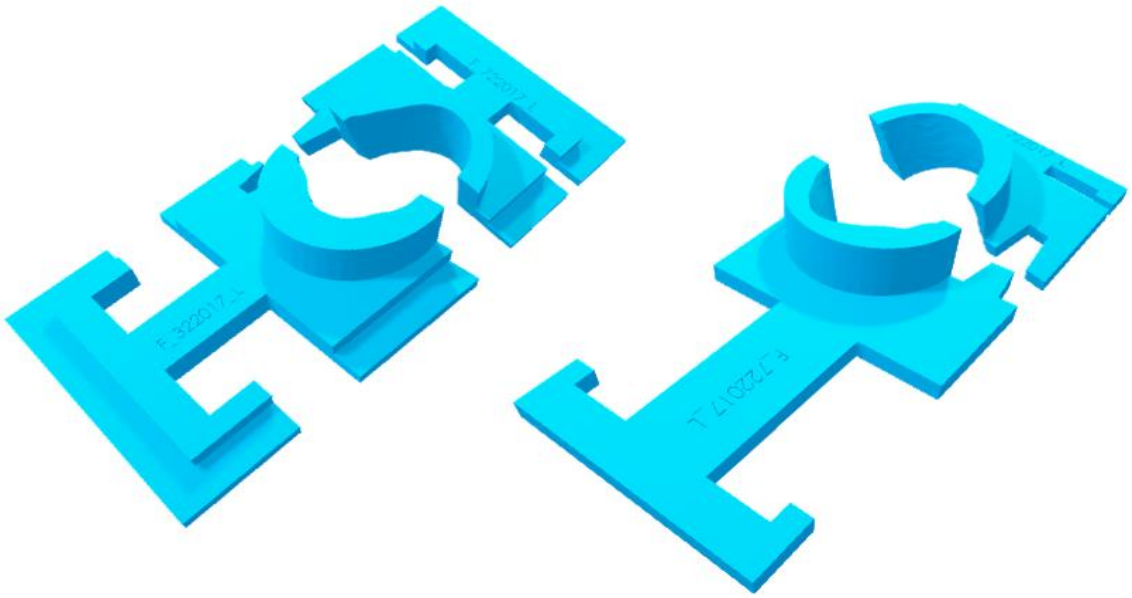

Fig. 3-13. *Final lower and upper Alignment Femur Guide.*

The cutting guides were processed to allow a suitable fitting with bones and excess material was removed (figure 3.14).

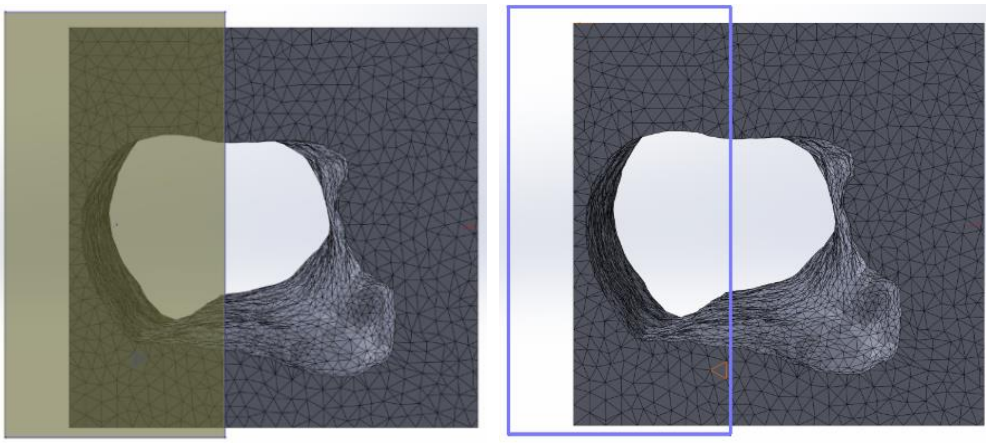

Fig. 3-14. *Sketch of a excess material on femur cutting guide.*

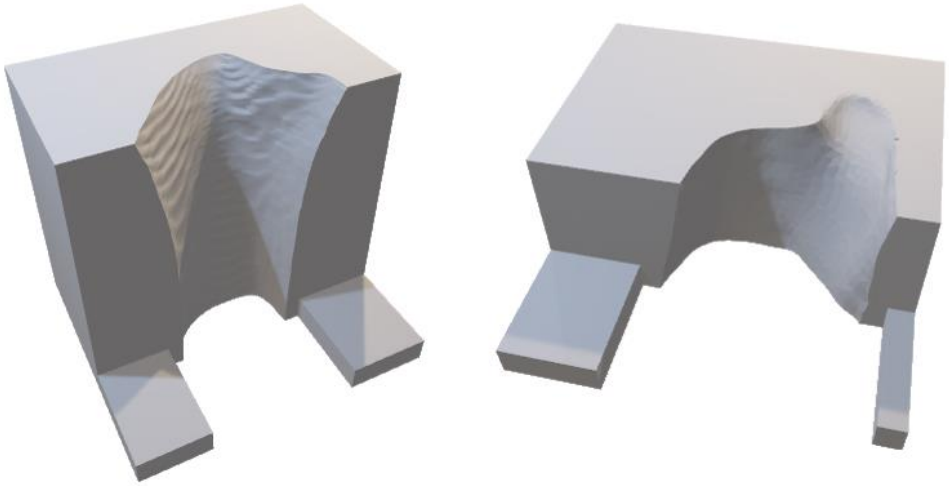

Fig. 3-15. *Final Femur and Tibia cutting guide.*

Fig. 3-16. *Final guides 3D printed*.

4. Tekscan sensor calibration

To obtain an appropriate quantification of knee kinetic two pressure mapping systems were inserted in patellofemoral joint and in tibiofemoral joint. Tekscan sensors consist of a matrix of row and column electrodes created by printing conductive silver ink onto a thin polyester film substrate. The electrodes are coated with a piezo-resistive ink such that a sensing cell is created at each intersection point in the matrix. An electronic scanner connected to the tail of the sensor permits to measure changes in the resistance of the cells. [25]

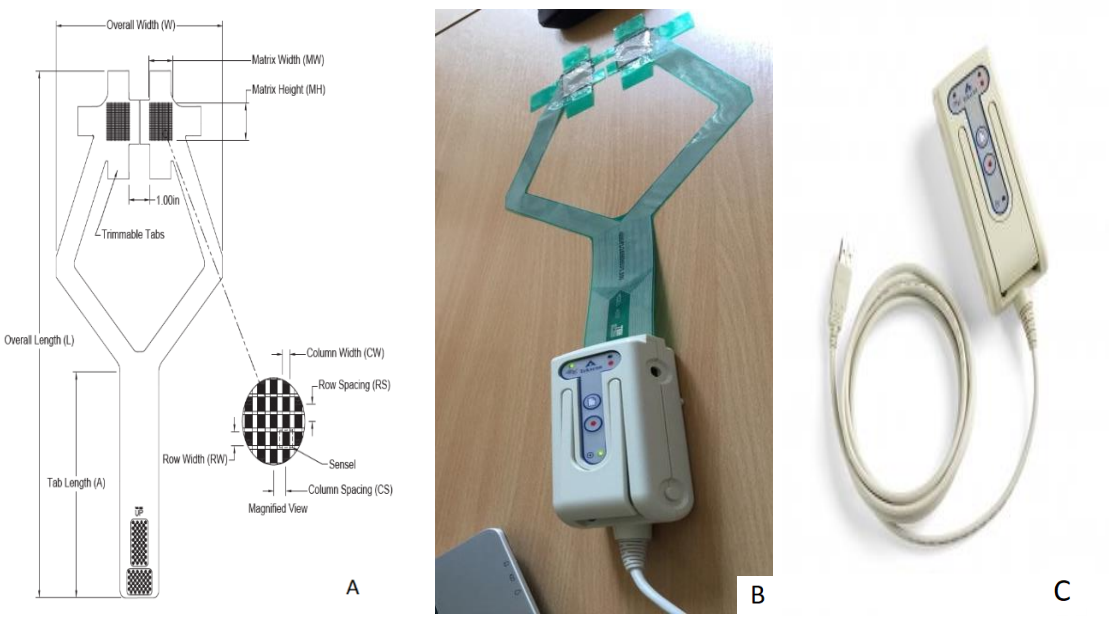

Fig. 3-17. *Pressure Mapping Sensor 4000 design (A). Tekscan sensor connected to laptop during test (B). Handle Tekscan scanner (C).*

In order to calibrate these sensors, a specific protocol was developed. Sensor calibration was performed using two metal blocks covered by a rubber layer and a loading frame (Lloyd LS1 1kN Advanced Material Testing System) that provides a uniform load distribution in the whole surface.

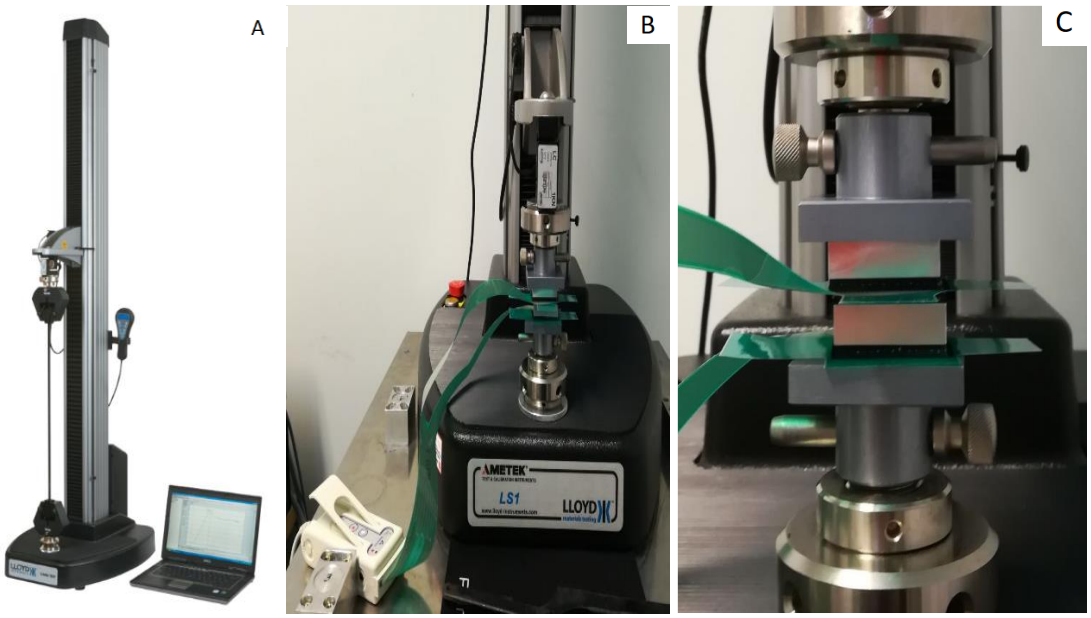

Fig. 3-18. *Lloyd LS1 (A). Tekscan sensors under load during calibration (B-C).*

Sensors were placed under six different loads from 100N to 750N, as show in figure 3-23, for intervals of 30 seconds to control the high level of precision during the calibration. The I-Scan software allows for up to a 10-point sensor calibration with a minimum suggested being a 3-point calibration. Then the computer software, distributed with the Tekscan system, will fit the points following a power calibration curve provided (figure 3-19).

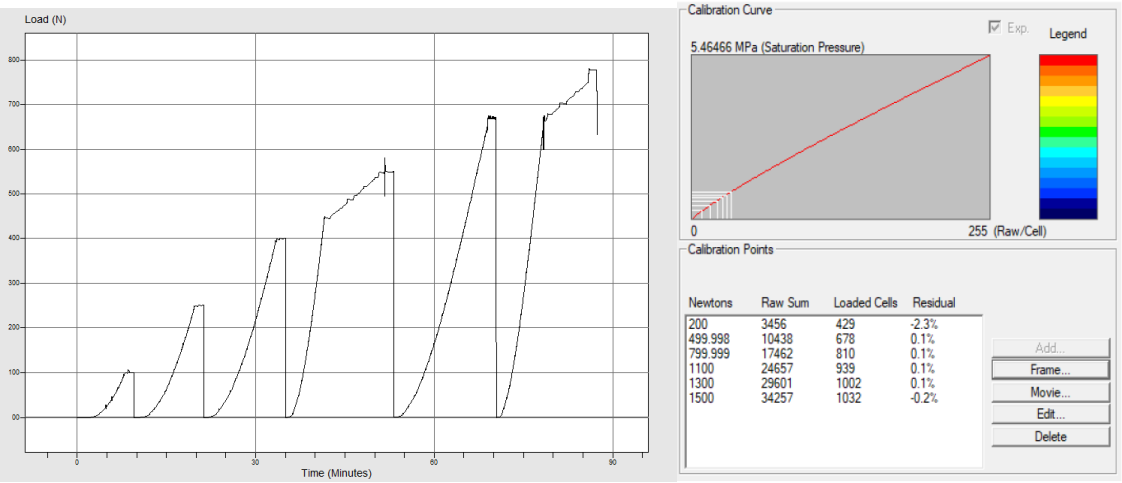

Fig. 3-19. *Loading curve applied and calibration curve calculated with I-Scan Software.*

5. Opti-Track setup

Motion capture system (OptiTrack ®) were used to describe kinematic behaviour of human knee. Four infrared cameras (figure 3-20) were placed and configured to fully cover the capture volume around the test rig to track the movement of markers sets fixed on specimen.

Fig. 3-20. *Set-up of OptiTrack*

Each camera was mounted securely so that they remain stationary during capture. All extraneous reflections or unnecessary markers were removed or ignored, through the Mask Tool, from the capture volume before calibration. Camera calibration was performed using a CW-500 calibration wand kit (Figure 3-21 B).

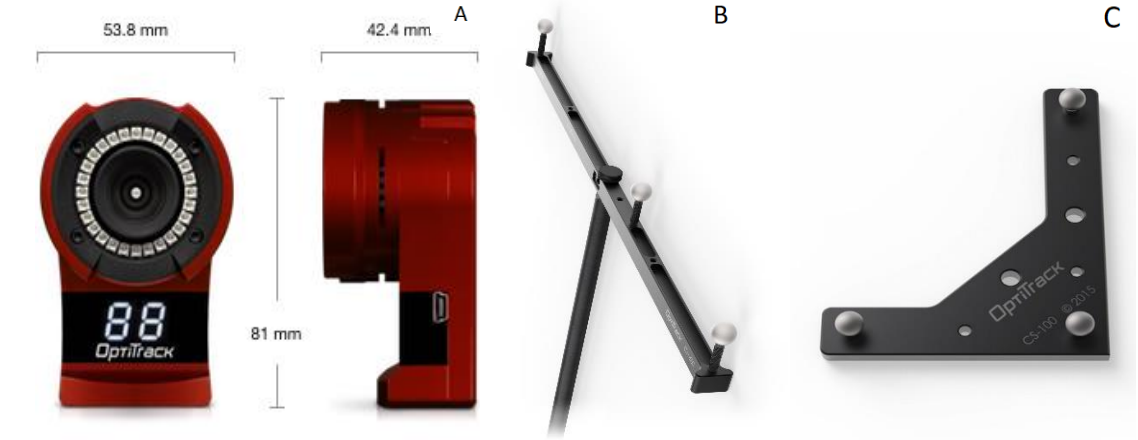

Fig. 3-21. *InfraRed camera (A). CW-500 calibration wand kit (B). Calibration square (C).*

In details, the wand was waved in front of the cameras repeatedly, allowing all cameras to see the markers. Through this process, each camera captures sample frames in order to compute their respective position and orientation in the 3D space. When sufficient amounts of calibration samples are collected by each camera, calibration for the capture volume was calculated.

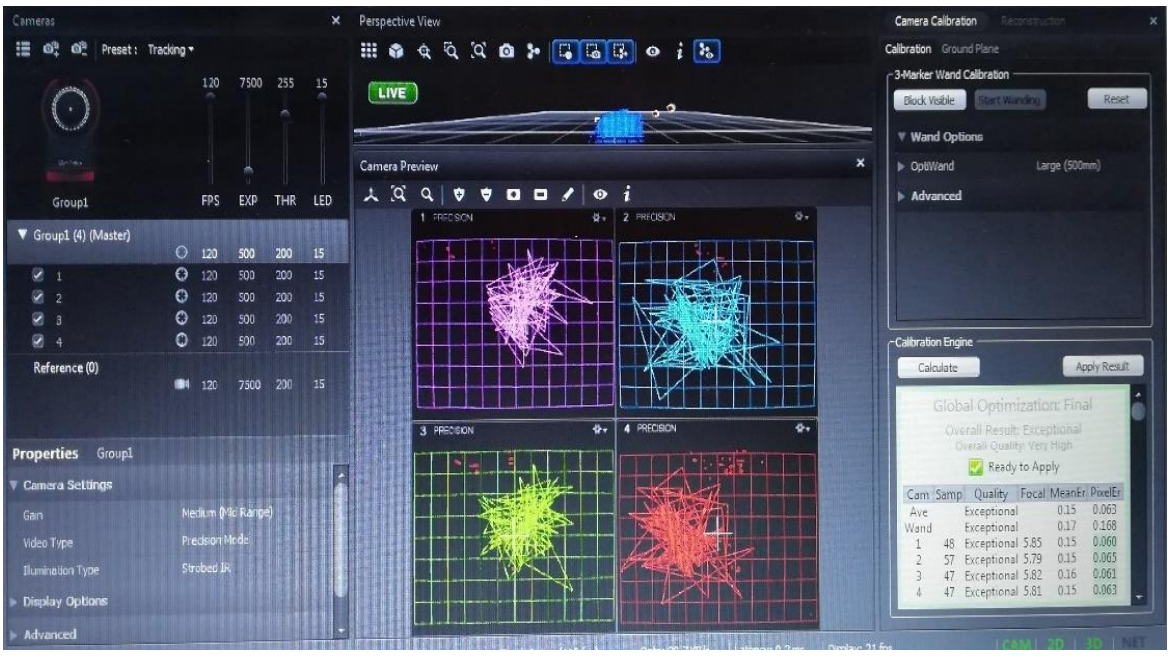

Fig. 3-22. *Cameras calibration.*

Lastly, placing the calibration square (figure 3-21 C) in the capture volume the ground plane and the origin were set. The position and orientation of the calibration square will be referenced for setting the coordinate system during recording.

3.2.3.2 Specimen preparation

1. Thaw of the specimen

Two days before the cadaver test the specimens were removed from the freezer and left in their plastic wrappings and placed on a suitable surface at room temperature. After that, a saline water solution to prevent them dehydration was sprayed and a number tag was applied on each bone for identification.

2. Dissect the specimen

Skin and fat tissues were stripped by the surgeon in order to isolate the knee joint volume (figure 3-23). Using blunt dissection techniques quadriceps, lateral and medial hamstring tendons were preserved.

Fig. 3-23. *Cadaver specimen before dissection (A), during dissection (B) and after dissection (C).*

3. Initialization of motion capture system

The concept used to analyse knee kinematics is to track the patient's anatomy in three-dimensional space. To achieve this goal three retroreflective marker sets were fixed on the bones (figure 3-29) and a lab tool, developed in Matlab, connected with Motive, motion capture dedicated software, was used. Femur and tibia positions were estimated in real-time detecting infrared light that is reflected by the retroreflective surface of the markers.

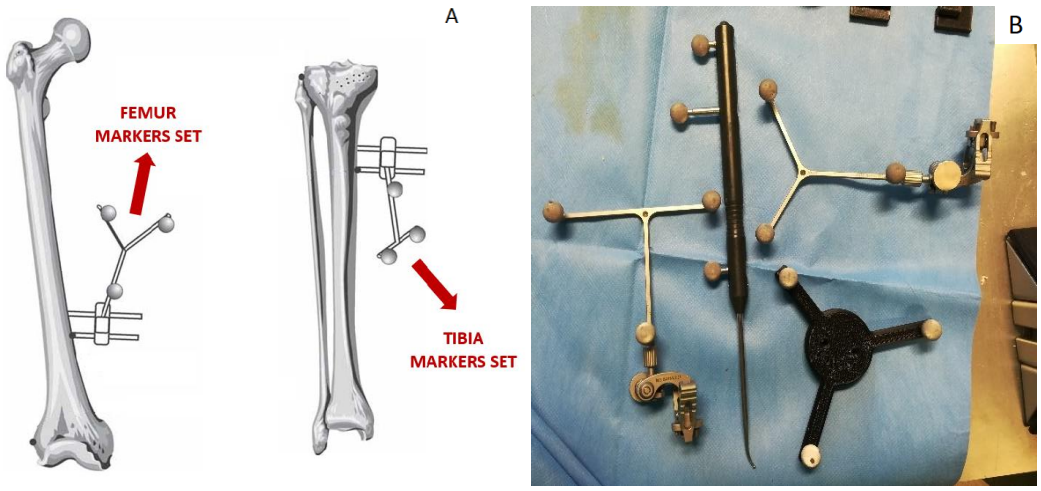

Fig. 3-24. *T-shape and Y-shape markerset of femur and tibia (A). Pointer and markersets during cadaver test (B).*

Once fixed the marker sets, in Motive one rigid body for each marker set was created in order to identify the three bones.

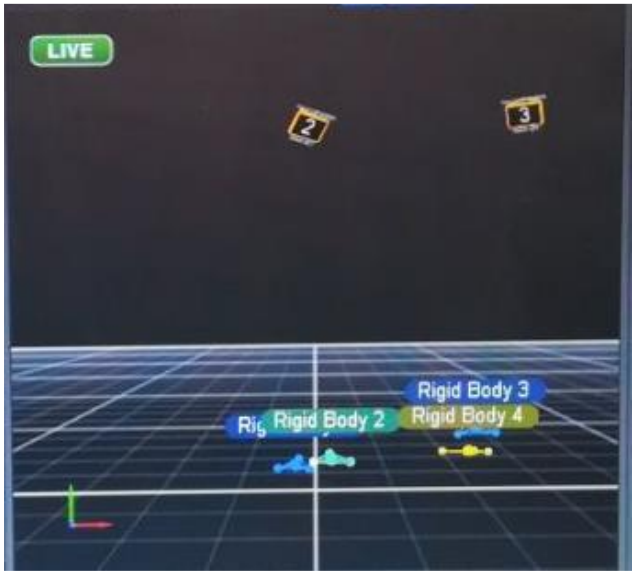

Fig. 3-25. *Rigid bodies setting.*

In additional, 3D bones reconstructions (STL files) and relative landmarks coordinate were given as input on lab tool. A pointing device was used to scan bones for the purpose to collecting points clouds directly on the specimen (figure 3-26 A). Applying a sophisticated algorithm, the collected points were matched with the anatomical landmarks evaluated on the 3D bones (figure 3-26 B) in order to determine knee kinematics.

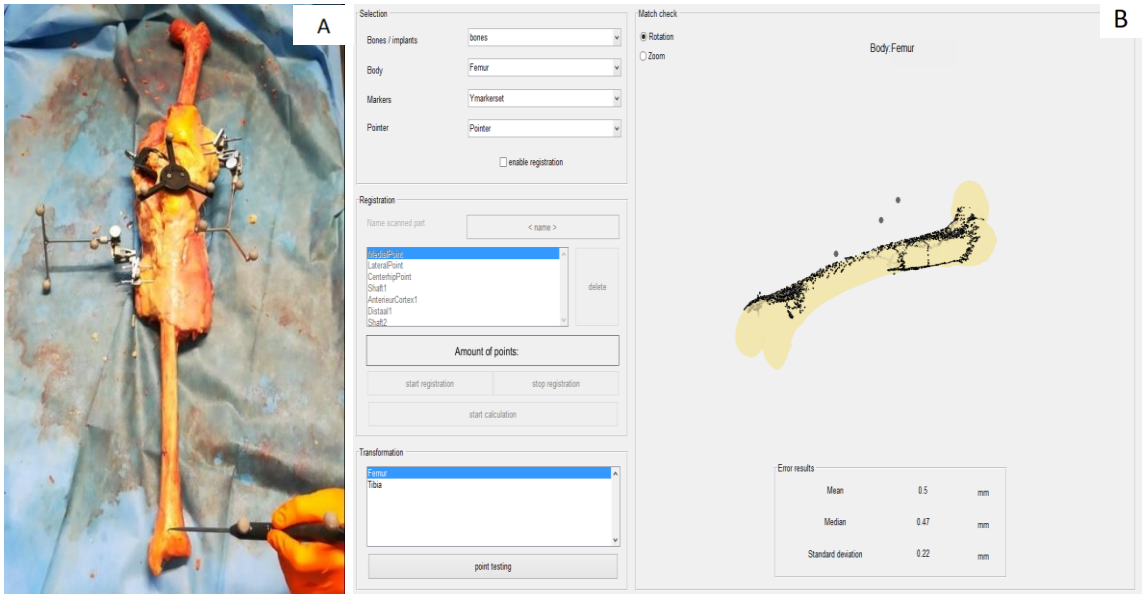

Fig. 3-26. *Points cloud recorded by means Wand (A). Graphical user interfaced used for Motive initialization (B).*

4. Amputation of the proximal femur and the ankle and potting the specimen

At this stage, using electric saw and the two cutting guides proximal femur and distal tibia were amputated. Afterwards, tibia and femur were aligned by means respectively alignment guides and then they were fixed in two containers with polymethylmethacrylate (PMMA). Moreover, a screw was used to fix the PMMA and to prevent a possible cement relative rotation around the container.

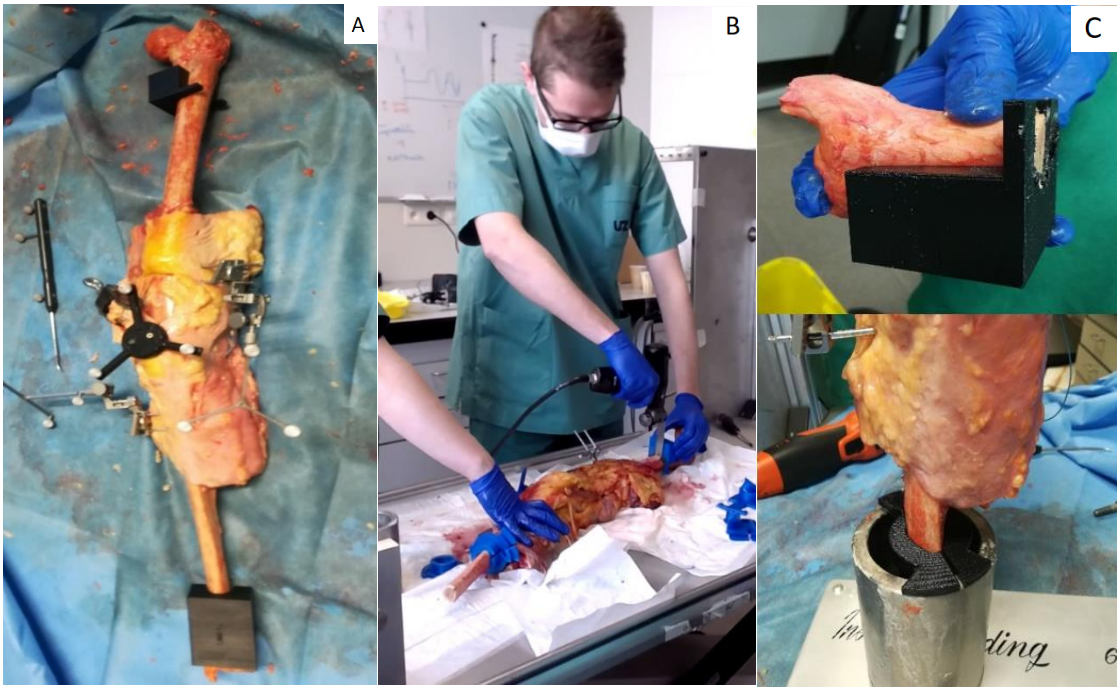

Fig. 3-27. *Marker sets fixed on specimen (A). Potting preparation (B). Head femur cutted and distal tibia potted (C).*

5. Insertion of the knee prosthesis

A standard parapatellar lateral incision was used to expose the knee joint. The patella was everted and the integrity of collateral ligament was checked. The size of components and the thickness of insert were selected by surgeon as in surgical practice. By surgery techniques PS TKA implant was embedded and patella was resurfaced. The components were fixed with PMMA.

Fig. 3-28. *TKA surgery.*

6. Insert Tekscan sensor in joints

Two calibrated sensors were placed between knee joints surfaces in which the contact stress is to be measured. Placed correctly in the knee joint space, sensors were sutured around soft tissue to maintain sensor placement.

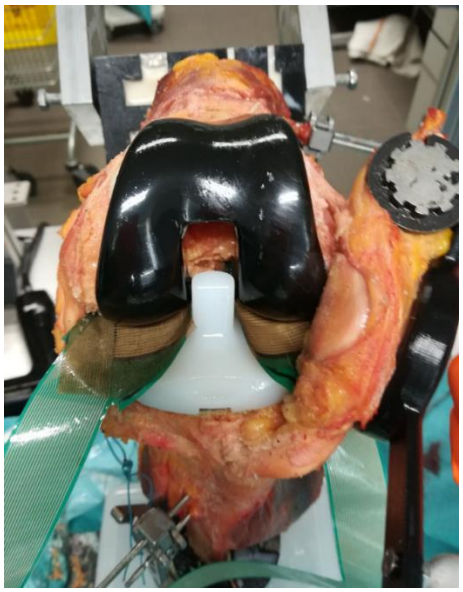

Fig. 3-29. *Implant of the prosthesis and placement of Tekscan sensor.*

7. Mounting of the specimen in the oxford rig

Lastly, the specimen was mounted onto the mechanical test-rig with the containers rigidly fixed to the hip actuator and the ankle load cell (figure 3-35)

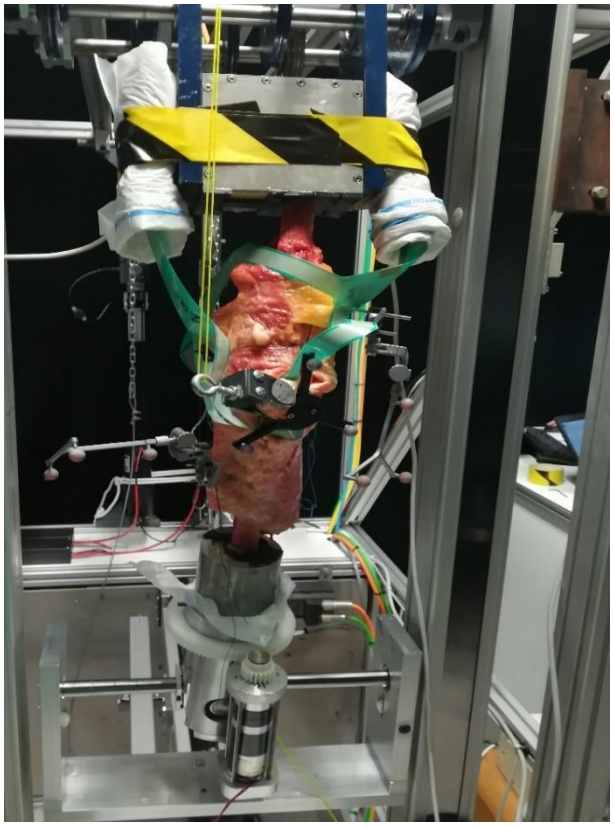

Fig. 3-30. *Positioning of the specimen on the Test Rig.*

3.2.4 Test Rig: simulation of an active squat

The test rig simulates a specific active motion pattern. As previously described, a squat was simulated controlling independently the applied kinematic and kinetic boundary conditions. The ankle position in the sagittal plane is controlled with two linear electric servo actuators that drive a linear positioner (figure 3-30). At the same time, a sinusoidal quadriceps force and two hamstring forces are applied by a servomotor and by linear ball actuator respectively. The controller of these motors is synchronized with the actuators controlling the ankle position using a dedicated NI LabVIEW programming frame (figure 3-32).

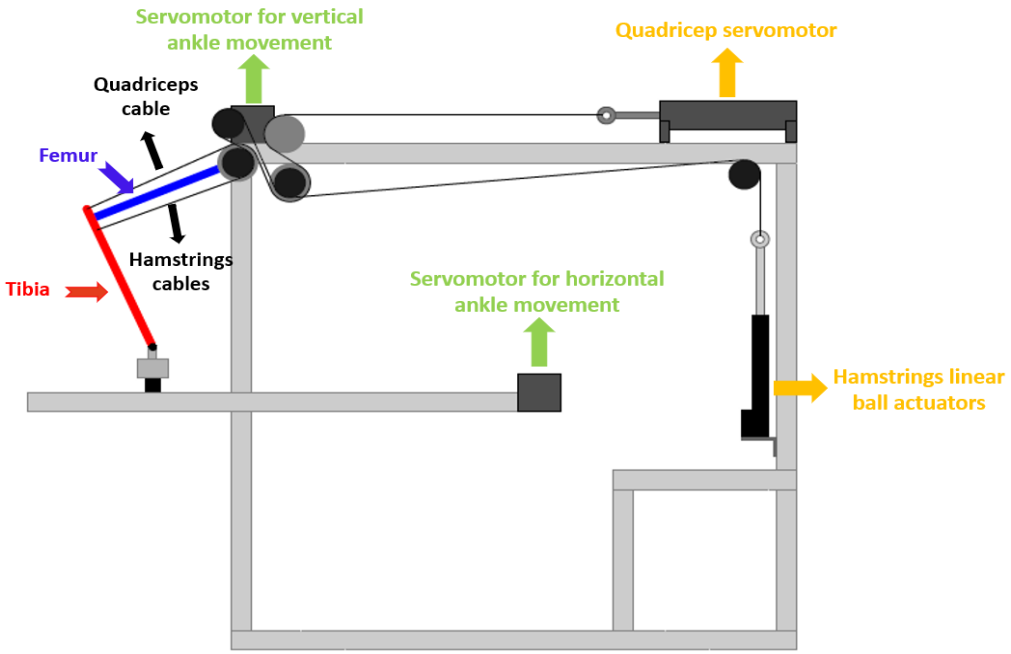

Fig. 3-31. *Schematic representation of Test Rig.*

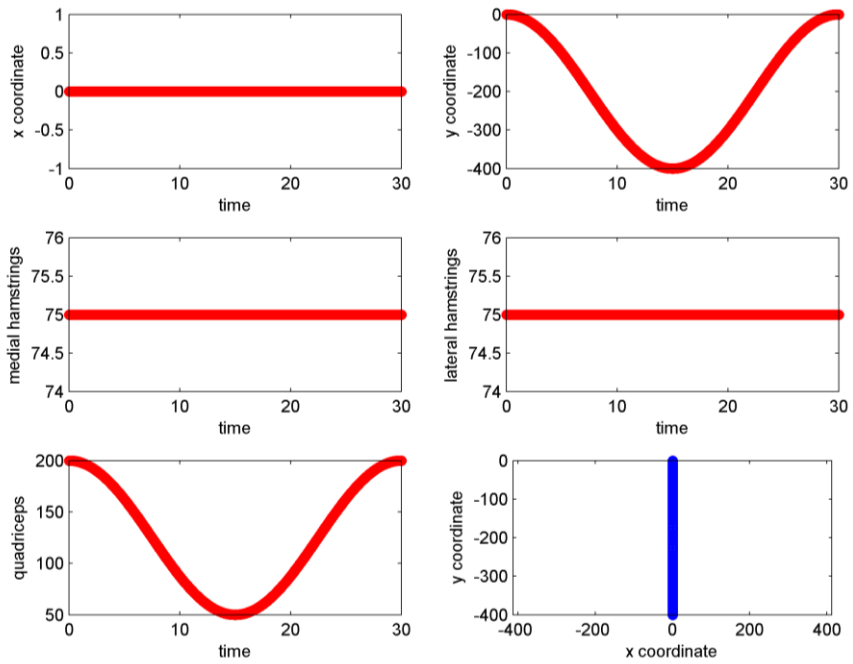

Fig. 3-32. *LabVIEW Input data.*

Initially, the knee was placed in mid-flexion. By exerting loads to simulate quadriceps and hamstrings the knee was pulled into full extension. Therefore, the knee was initialized at a position of 20° of flexion to replicate squat motion. A dynamic analysis was performed, and motion and pressures were recorder during full cycle. In details, the position of the rigid bodies consisting of the femur and tibia, with their respective reference frame was followed by the 3D motion analysis system measuring kinematics of the knee joint during squat test. At the same time, measurements of interfacial contact area and stress in articulating joints were performed using Tekscan sensors.

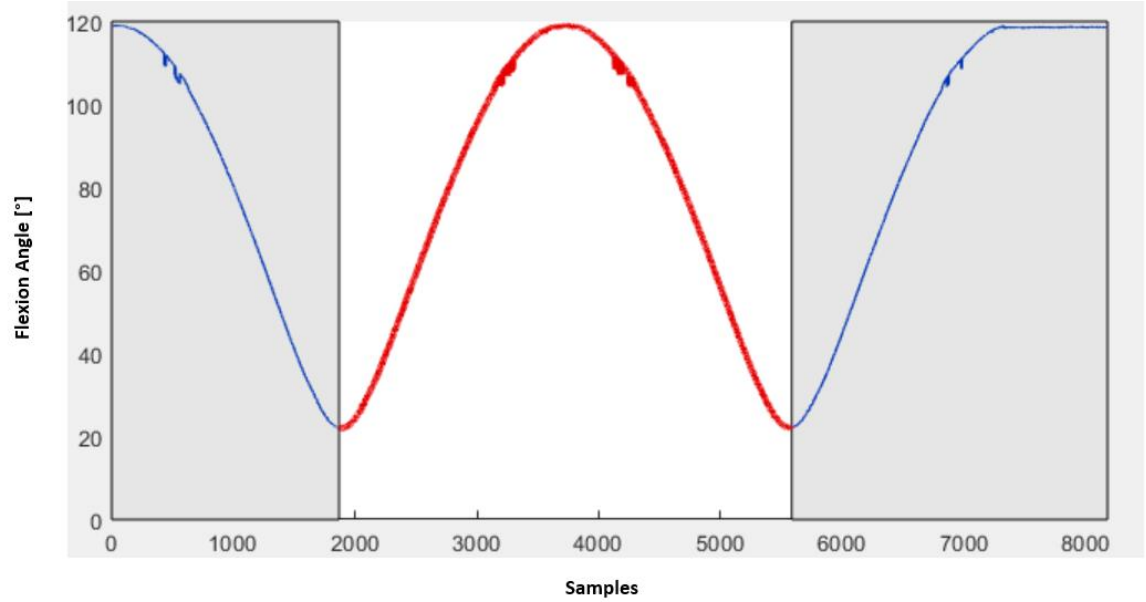

Fig. 3-33. *Squat pattern simulated.*

With regard to the description of the kinematic behaviour of knee, Grood and Suntay methodology [26] was used to describe six degrees of freedom, consisting of three rotations and three translations as illustrated in figures 3-34 and 3-35.

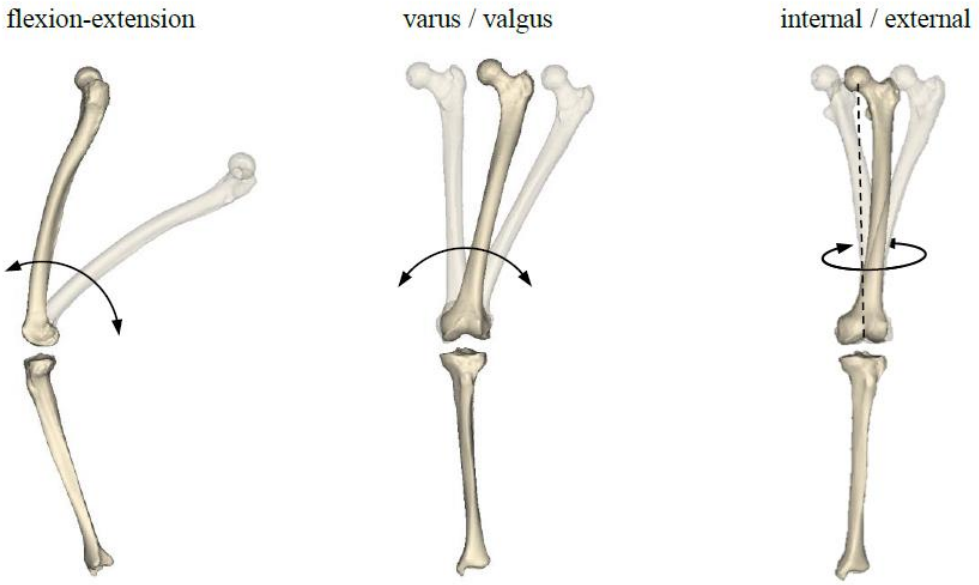

Fig. 3-34. *The three translations of the tibial-femoral knee joint with the femur moving relative to the fixed tibia*

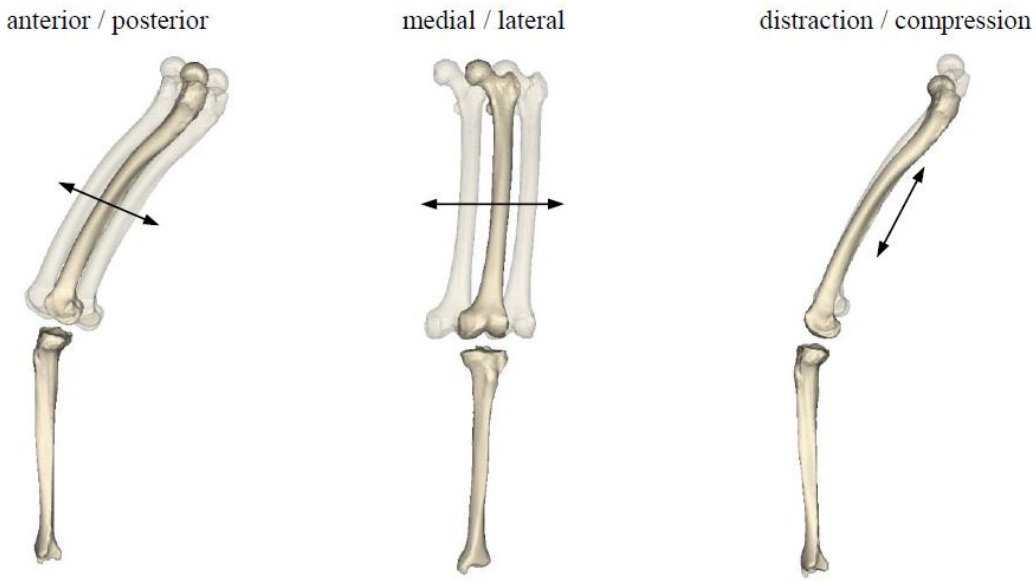

Fig. 3-35. *The three rotations of the tibial-femoral knee joint with the femur moving relative to the fixed tibia*

A Cartesian coordinate system for each bone was defined to set up a joint coordinate system. To achieve this goal, four anatomical reference points for femur and tibia were used.

Table 3-4. *The anatomical reference points for femur and tibia used to create a Cartesian system for each body.*

Points	Femur	Tibia
p_1	Femoral Hip Center FHC	Tibial Knee Center TKC
p_2	Femoral Knee Center FKC	Tibial Ankle Center TAC
p_3	Femoral Medial Condyle Center FMCC	Tibial Medial Condyle Center TMCC
p_4	Femoral Lateral Condyle Center FLCC	Tibial Lateral Condyle Center TLCC

Medio-lateral axis, anterior-posterior-axis and mechanical axis were calculated in according to following equations:

$$\text{Mechanical Axis} = \frac{p_1 - p_2}{||p_1 - p_2||} \quad (3.1)$$

$$\text{Anterior-Posterior Axis} = (\text{Mechanical Axis}) \times \frac{p_3 - p_4}{||p_3 - p_4||} \quad (3.2)$$

$$\text{Medio-Lateral Axis} = (\text{Anterior-Posterior Axis}) \times (\text{Mechanical Axis}) \quad (3.3)$$

The substitution of the coordinates of the anatomical reference points in the previous equations defines both the Cartesian coordinate systems. For clarity, capitalized letters X, Y, Z are used to denote the femoral cartesian coordinate system axes with I, J and K as the respective base vectors, and small latter x, y, z are used with i, j, k as their respective base vectors for the tibial Cartesian coordinate system.

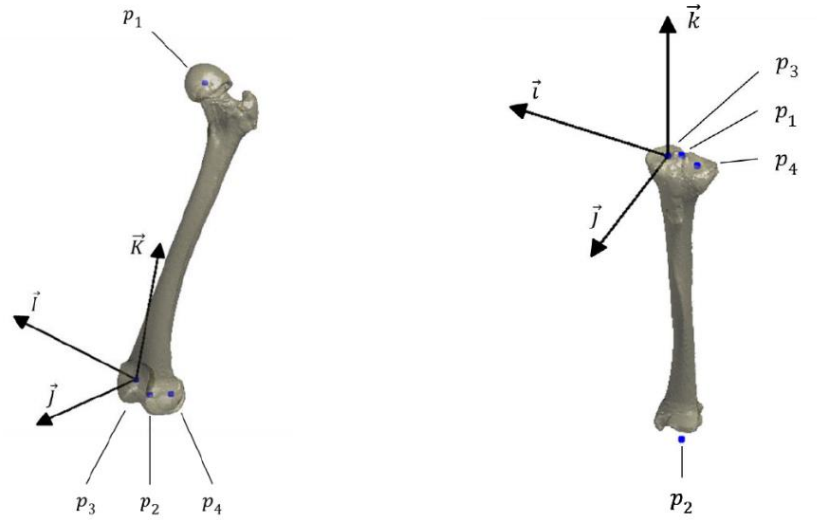

Fig. 3-36. *Visualisation of the anatomical reference points together with the resulting Cartesian coordinate system of (a) femur and (b) tibia, with origin p3.*

In order to obtain a coordinate system that describes the motion of femur relative to the fixed tibia, the joint coordinate system is derived according to following equations:

Mechanical Axis:	$\overrightarrow{e_1} = \vec{I}$	(3.4)
Anterior-Posterior Axis:	$\overrightarrow{e_2} = \overrightarrow{e_3}$ x $\overrightarrow{e_1}$	(3.5)
Medio-Lateral Axis:	$\overrightarrow{e_3} = \vec{k}$	(3.6)

Namely, the joint coordinate system is composed by two fixed axes, Medio-Lateral Axis $\overrightarrow{e_1}$ and $\overrightarrow{e_2}$ Mechanical Axis, and one floating axis, the cross product of both $\overrightarrow{e_2}$. In according to these choses, the flexion-extension occurs about the femoral fixed axis $\vec{I}$, the internal-external rotation about the tibial fixed axis $\vec{k}$ and valgus-varus about the floating axis $\overrightarrow{e_2}$.

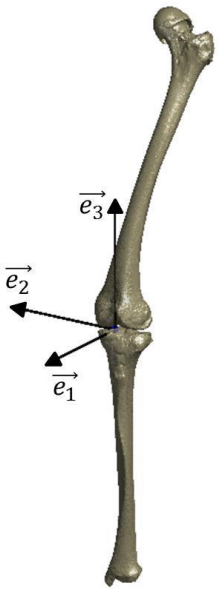

Fig. 3-37. *Visualisation of the femoral-tibial joint coordinate system, with origin p3.*

Flexion-extension angle, called α, is obtained from the angle formed between the floating axis, $\overrightarrow{e_2}$, and the femoral anterior axis, $\vec{J}$. The following equation permit to estimate the relative magnitude:

$$\cos(\alpha) = \vec{J} \,.\, \overrightarrow{e_2} \tag{3.7}$$

Since cos(α) = cos (−α), a sign correction has to be applied for α when the following inequality is satisfied:

$$\sin(\alpha) = \overrightarrow{e_2} \,.\, \overrightarrow{K} > 0 \quad \rightarrow \quad \cos(-\alpha) = \vec{J} \,.\, \overrightarrow{e_2} \tag{3.8}$$

Intern-external rotation, ϒ, is defined as the angle formed between the floating axis, $\overrightarrow{e_2}$, and the tibial anterior axis $\vec{j}$:

$$\sin(\gamma) = \overrightarrow{e_2} \,.\, \vec{\imath} \tag{3.9}$$

The valgus-varus angle, β, is identified as the angle between the tibial and femoral body fixed axes:

$$\cos(\mu) = \vec{I} \,.\, \vec{k} \quad \rightarrow \quad \beta = \mu - \frac{\pi}{2} \tag{3.10}$$

The three translations are computed by subtraction of the position of origin of the tibia from the position of origin of the femur and projecting the resulting vector on each axis of the joint coordinate system. Both for the medial side of the bone and for the lateral side, medio-lateral (q_1), anterior-posterior (q_2) and distraction-compression (q_3) were calculated using the following equations:

$$\overrightarrow{H_{medial}} = (p_3)_{tibia} - (p_3)_{femur} \tag{3.12}$$
$$q_{1,medial} = \overrightarrow{H_{medial}} \,.\, \overrightarrow{e_1} \tag{3.13}$$
$$q_{2,medial} = \overrightarrow{H_{medial}} \,.\, \overrightarrow{e_2} \tag{3.14}$$
$$q_{3,medial} = -\overrightarrow{H_{medial}} \,.\, \overrightarrow{e_3} \tag{3.15}$$
$$\overrightarrow{H_{lateral}} = (p_4)_{tibia} - (p_4)_{femur} \tag{3.16}$$
$$q_{1,lateral} = \overrightarrow{H_{lateral}} \,.\, \overrightarrow{e_1} \tag{3.17}$$
$$q_{2,lateral} = \overrightarrow{H_{lateral}} \,.\, \overrightarrow{e_2} \tag{3.18}$$
$$q_{3,lateral} = -\overrightarrow{H_{lateral}} \,.\, \overrightarrow{e_3} \tag{3.19}$$

Furthermore, in Tab 3-5 the applied sign convention about translations and rotations is explained.

Table. 3-5. *The sign convention used in practise for (a) translations and (b) rotations.*

Translation	Sign
Medio – Later (q_1)	+ / -
Anterior – Posterior (q_2)	+ / -
Distraction – Compression (q_3)	+ / -
Flexion – Extension (α)	+ / -
Valgus – Varus (β)	+ / -
Internal – External (γ)	+ / -

3.3 Experimental results

3.3.1 Kinetics

To evaluate the kinetics involved during the squat, contact pressures and contact areas were estimated using two Tekscan sensors systems placed respectively on the tibial insert and on the patellar component. Figure 3-38 reports a resume of the contact pressure outputs for tibiofemoral and patellofemoral joints, observed during the flexion. Concerning to tibial insert, the contact zone moves from anterior to posterior, both in the lateral and medial side, especially in the last part of flexion being before located in the central part. Similar behaviour is showed for the patellar component, where the contact zone moves from inferior to superior side increasing the flexion angle.

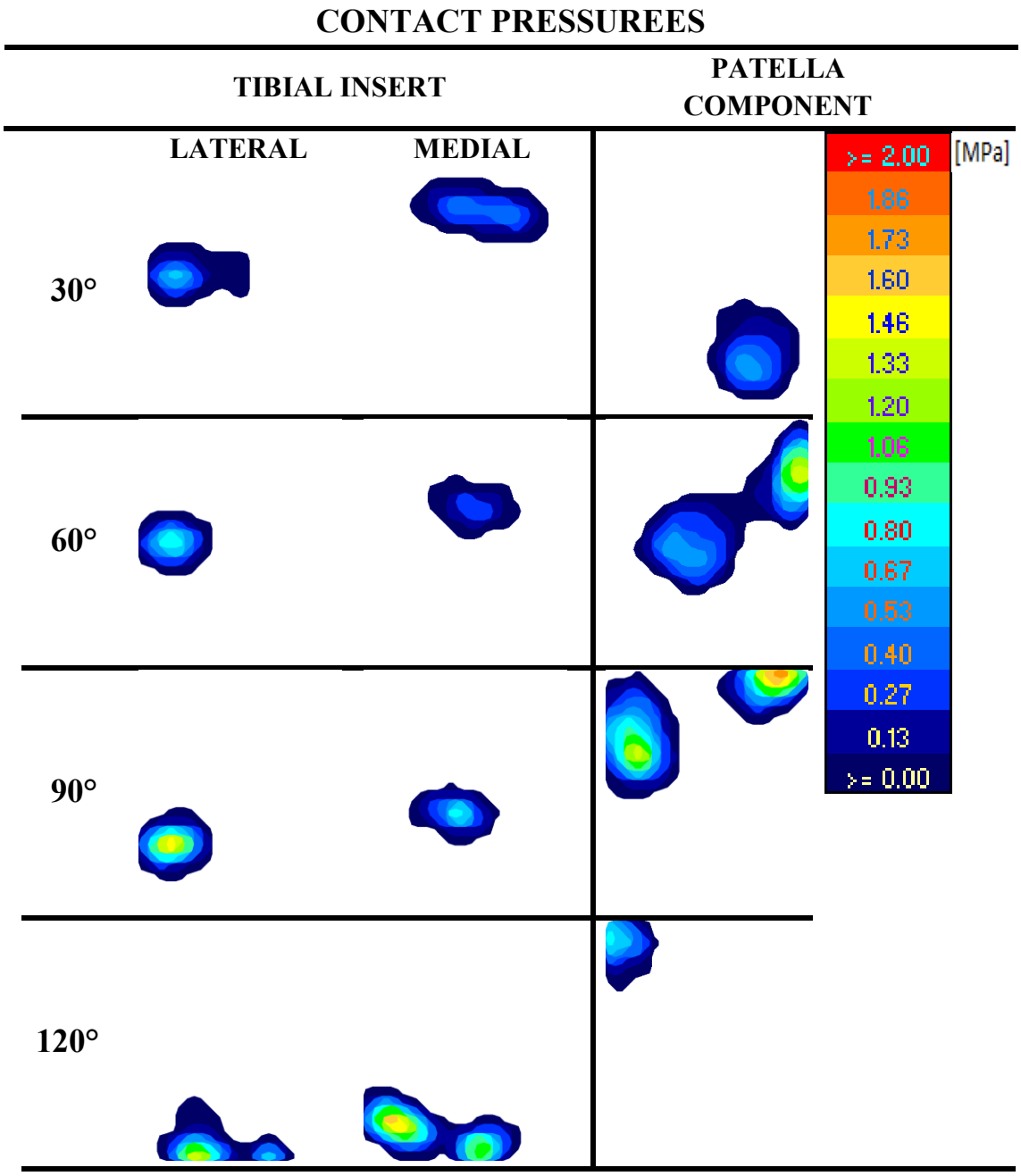

Fig. 3-38. *Contact pressure on medial and lateral tibial insert and on the patellar component at each 30 of flexion.*

Regarding to tibial insert, quantitative results of contact pressures on tibial insert observed during the flexion are showed in figure 3-39. During the flexion, contact pressure increases achieving values in a range between 0 and 2 MPa. Maximum values of pressure are mainly located on the medial side around 120 degrees of flexion.

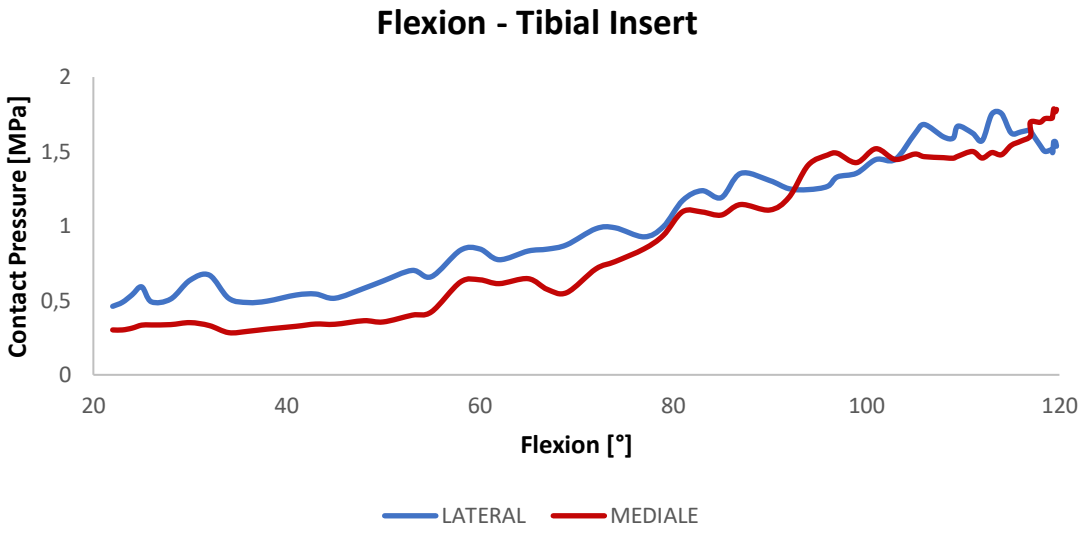

Fig. 3-39. *Contact pressure on the medial and lateral tibial insert during flexion.*

A comparable trend is recorded in the tibial insert during the extension, with similar average values (figure 3-40). The pressure is in a range of 0 - 2 MPa, with maximum values exhibited at beginning of extension.

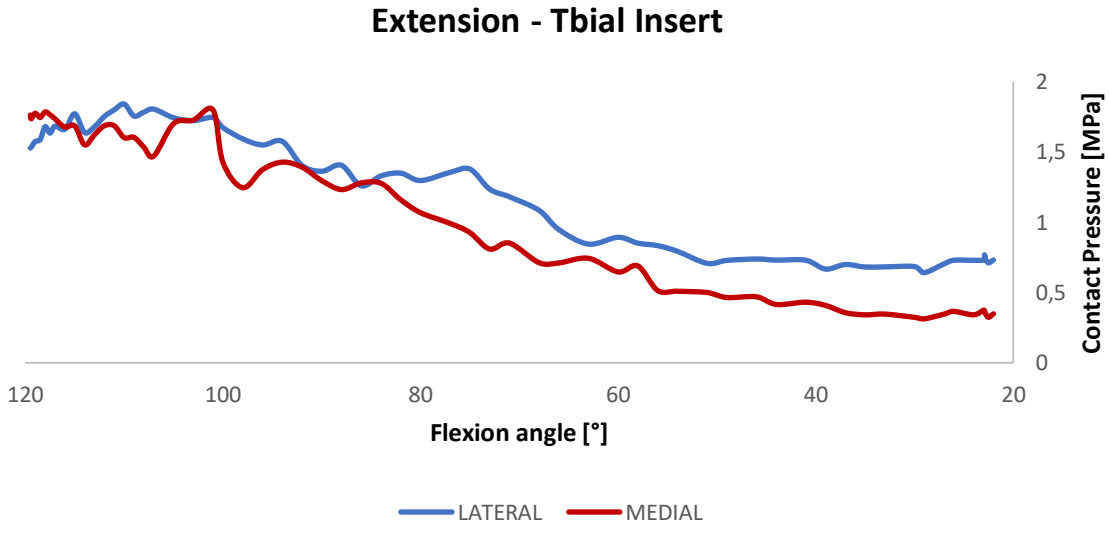

Fig. 3-40. *Contact pressure on the medial and lateral tibial insert during extension.*

Observed contact pressures trends are similar to the data found in literature for similar boundary conditions, with the exception of the lower values recorded. In fact, literature data of tibial insert show higher values of contact pressures with a range of 0-20 MPa. This can be consequent to the use

of Tekscan sensors and their experimental complications. Probably disagree results can be provoked by calibration protocol adopted. As explained in paragraph above, the Tekscan sensors were calibrated using a loading frame interfaced with the pressure maps through two planar surfaces, whereas during cadaver test, the measurements were conducted inside the specimen in a complex environment. Even the mere fact of placed sensor with a certain amount of inaccuracy in terms of bowed setting in the joint space could have affected the measurement.
Figure 3-41 and figure 3-42 show the contact area for flexion and extension movement recorded on tibial insert. Lateral side remains steady during all flexion movement with an average value of 110 mm^2. Instead, medial side shows higher values at the beginning and at the end of movement, with maximum values of 140 mm^2 and minimum values between 70 and 100 degrees.

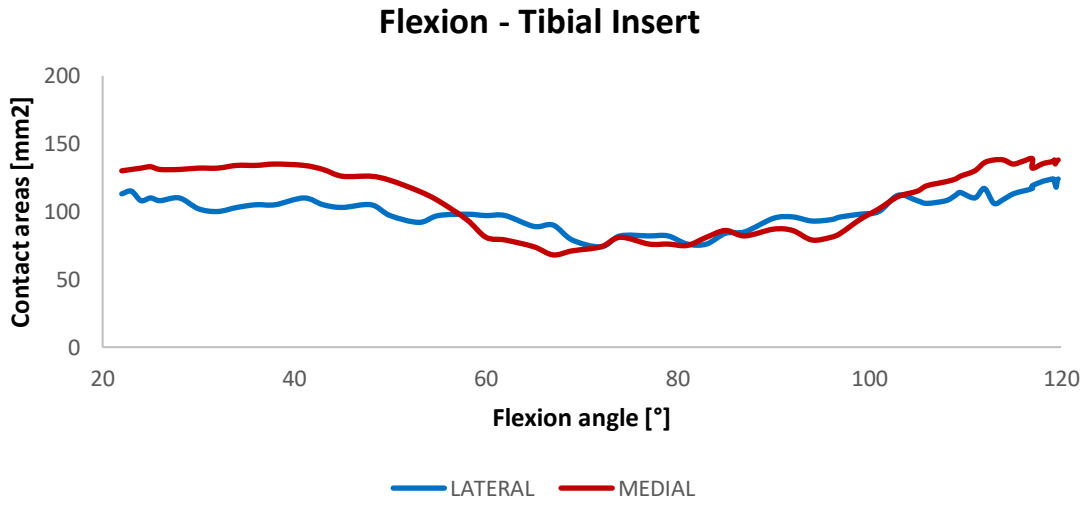

Fig. 3-41. *Contact area on the medial and lateral tibial insert during flexion.*

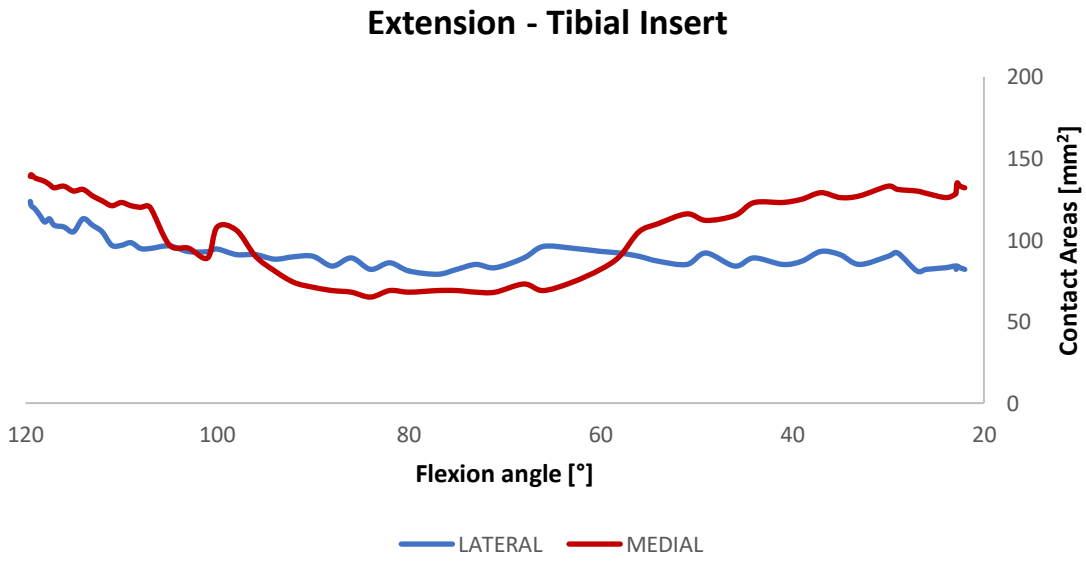

Fig. 3-42. *Contact area on the medial and lateral tibial insert during extension.*

Regarding patellar component, figure 3-43 shows a growing trend of contact areas with the knee flexion that reaches its maximum value of 200 mm^2 around 90 degrees. After that, in contrast with the literature, experimental data shows a decreasing until 120 degrees. This decrease could be associated with a shift of sensor in full extension that forges results.

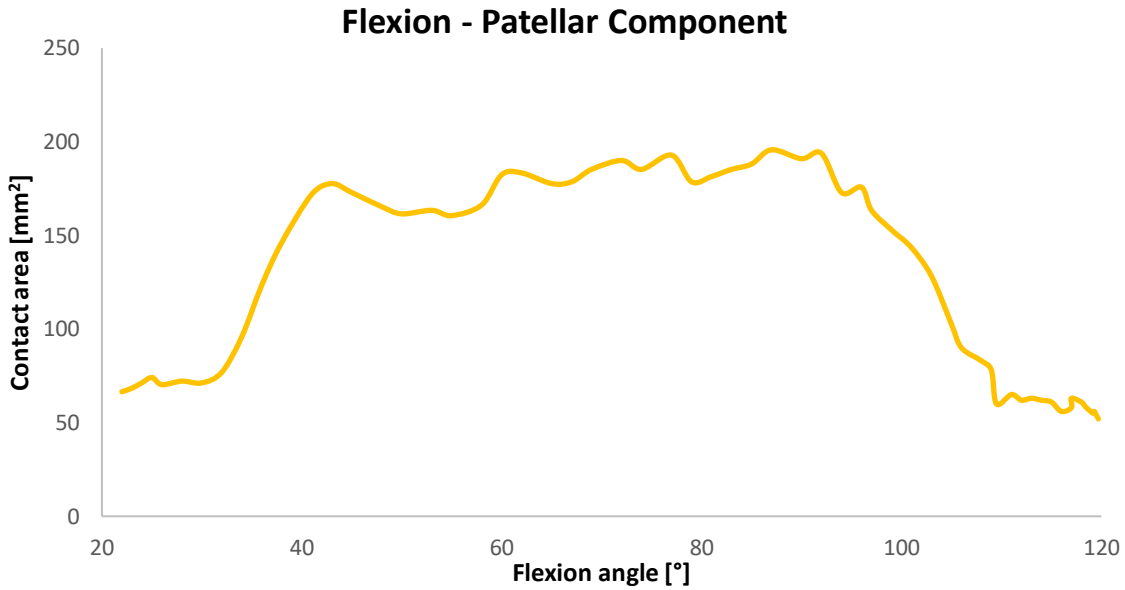

Fig. 3-43. *Contact area on the patella component during flexion.*

With regard to contact pressures for patellar component, figure 3-44 shows a growing trend with the flexion, achieving maximum values of 1.7 MPa at 80 degrees. As explained above, in full flexion experimental trend is disagreed with literature data due to sensor shift.

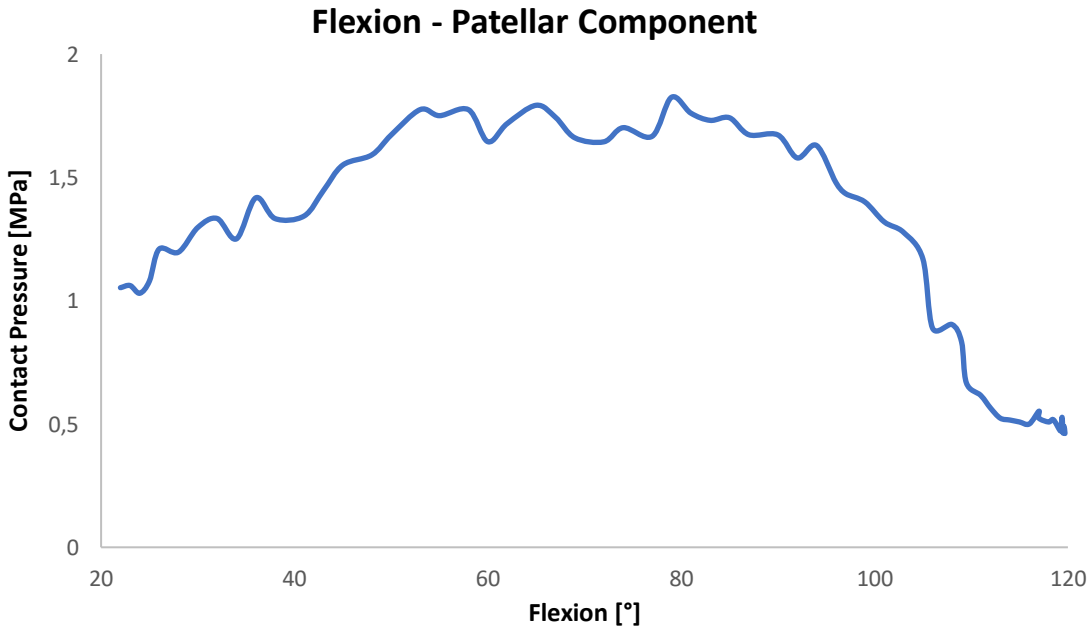

Fig. 3-44. *Contact pressure on the patella component during flexion.*

3.3.2 Kinematics

As mentioned before, regarding to kinematics, a motion capture system was used to estimate internal-external and valgus/varus rotations and antero-posterior, medial-lateral and compress-distract translations.

The analysis of internal-external rotation of the femur on the tibia illustrated in figure 3-45, shows an average of 6° of external rotation in the first 70 degrees of knee flexion, while then a decrease trend up to 1° of external rotation is reported at the end of the observed movement. Concerning to varus-valgus rotation, figure 3-46 is characterized by initial growth of 3 mm from 20 to 90 degrees and a subsequent decrease of 1 mm until full-flexion. Both experimental rotations results are in agreement with the literature data.

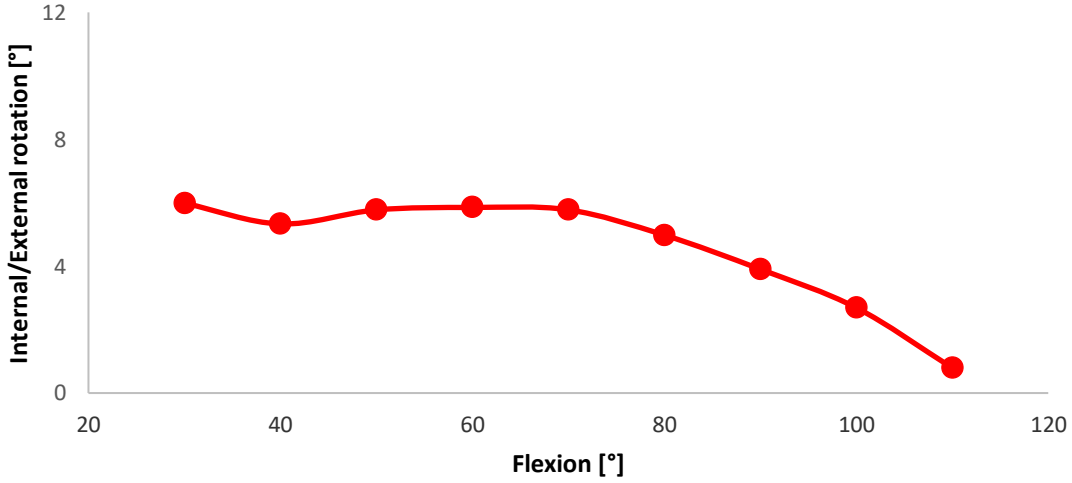

Fig. 3-45. Internal-external rotation at each 10 degrees of flexion.

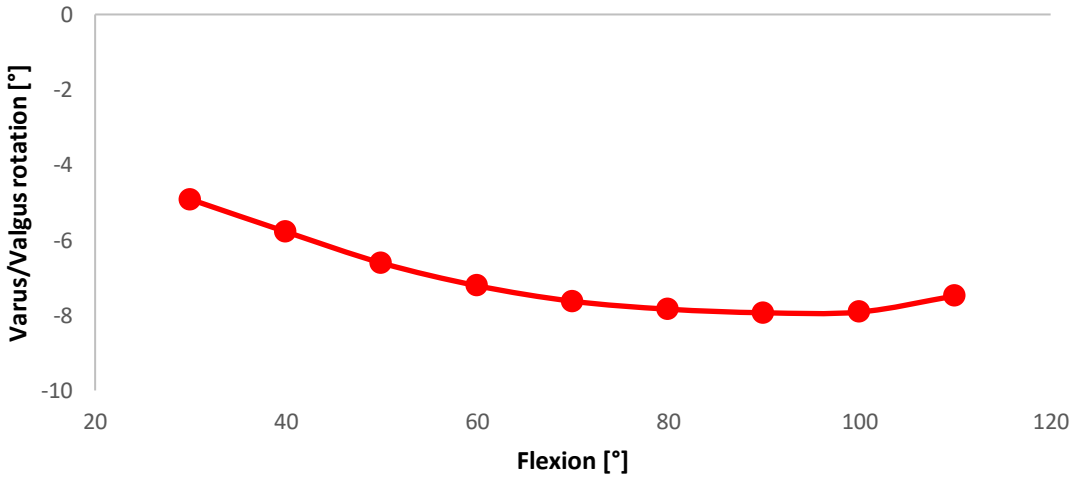

Fig. 3-46. Varus-Valgus rotation at each 10 degrees of flexion.

Figure 3-47 shows that the anterior-posterior translation is posteriorly oriented with increasing knee flexion in average range of 15 mm, in agreement with values reported in literature [177]. The range

of movement in this direction is reduced to 5 mm considering the range of flexion between 30-60 degrees. Medial-lateral translation has a range of 2 mm (figure 3-48) with a symmetric behaviour for medial and lateral femur condyle. Lastly, the compression-distraction translation showed in figure 3-49 reports a range of 2 mm with maximum values at 100 degree of flexion both for medial and lateral side. Kinetics translations are in accordance with the literature data [216].

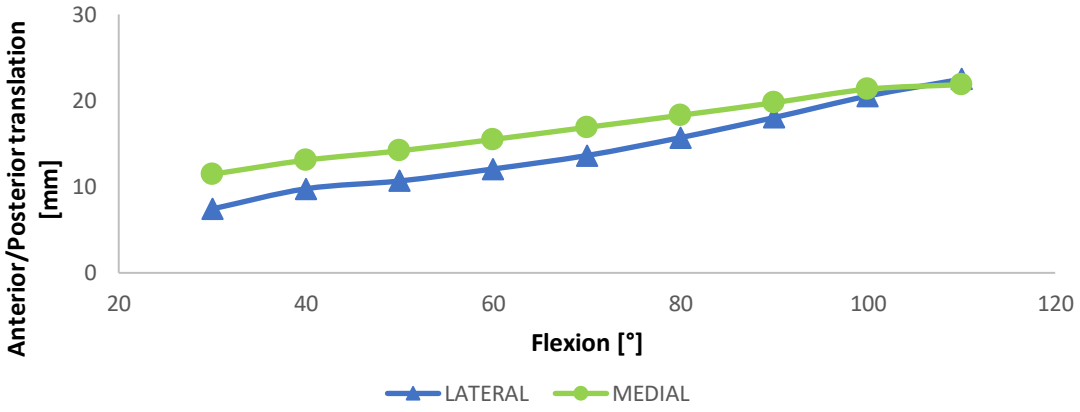

Fig. 3-47. Anterior-posterior translation of medial and lateral condyles at each 10 degrees of flexion.

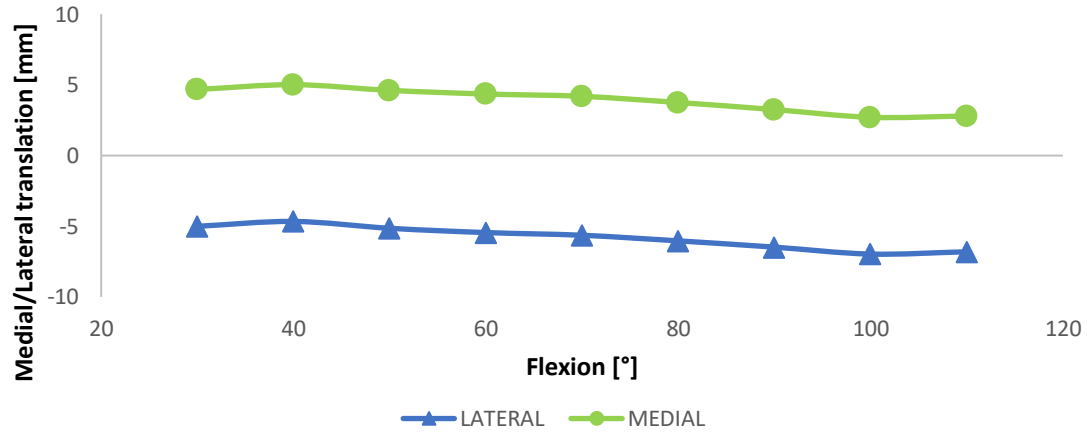

Fig. 3-48. Medial-lateral translation of medial and lateral condyles at each 10 degrees of flexion.

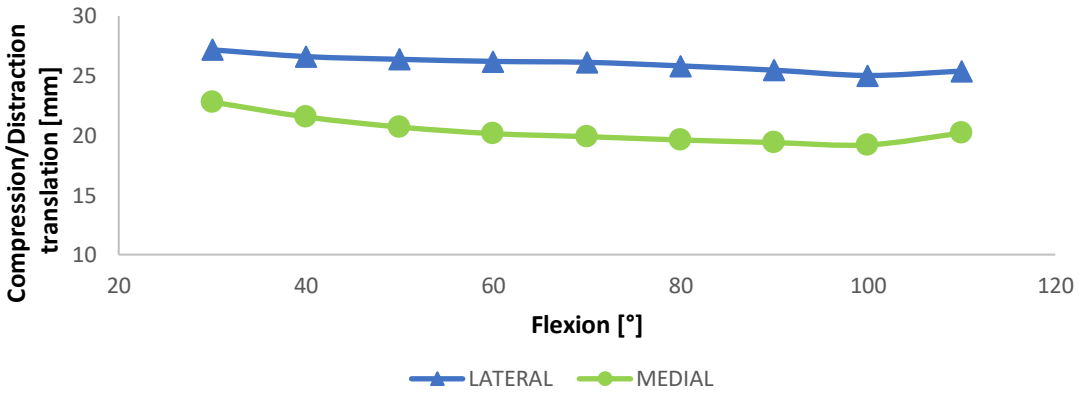

Fig. 3-49. Compression-distraction translation of medial and lateral condyles at each 10 degrees of flexion.

CHAPTER IV – FINITE ELEMENT ANALYSIS

4.1 Background

4.1.1 Introduction

The finite element method (FEM) is a numerical procedure technique used to find and solve problems in engineering and mathematical physics. Typical problem areas of interest in engineering and mathematical physics that are solvable by use a Finite Element Analysis include structural analysis, heat transfer, fluid flow, mass transport, and electromagnetism. [27]

All these engineering problems are analysed with a mathematical approach. Generally, when the description of the laws of physics are space- and time-dependent, mathematical models are grounded on partial differential equations (PDEs) with a set of corresponding boundary and/or initial conditions. The PDEs derived by applying the fundamental laws of physic, representing balance of mass, force or energy, to a system or a control volume. [28]

For the vast majority of problems involving complicated geometries, loadings and material properties, these analytical mathematical solutions cannot be obtained. Basing upon discretization methods it is possible, thankfully, approximate the PDES with numerical model equations, which can be solved using numerical methods. Therefore, the finite element formulation of the problem results in a system of simultaneous algebraic equations, rather than requiring the solution of differential equation.

In more detail, FEM consists in a discretization of space of the system to be analysed in sub-regions in which integral formulations are used to create a system of algebraic equations. Reason why in the finite element method, instead of solving the problem for the entire body in one step, the idea is to formulate the equations for each finite element and combine them in order to obtain the solution of the whole body. [27].

In general, a finite element analysis consists of three principal steps:

- The pre-processing, also called model preparation, is the first and the most work intensive step of the FEA. The goals of this phase are to develop an appropriate finite element mesh, assign suitable material properties, and apply boundary conditions. First of all, the parts of the system to be analysed are re-constructed from a CAD draw or from a clinical images segmentation. Materials models and properties about each parts of the model are defined in order to replicate the true capability to endure external forces. After that, the geometry is divided into a number of discrete and small "element" connected at discrete points called "nodes". In certain of these nodes will have applied boundary conditions in terms of constraints or loads.
- During the processing or solver phase the dataset prepared by the pre-processor is used as input to the finite element code itself, which constructs and solve a system of linear or nonlinear algebraic equations:

  $$K_{ij}u_j = f_i$$

  where u and f are respectively the displacements and the externally forces applied at the nodal points. The formation of the K matrix is dependent on the type of problem being considered [29]. Seeing as the solving of that system requires significant amount of time, often the solving can be accelerated applying parallel processing techniques on several CPUs.
- The postprocessing phase permits to investigate the results of the numerical analysis. Displaying the calculation results, such as displacements, stresses and nodal forces, a result interpretation can be done.

4.1.2 Finite Element Analysis in Biomechanics

In the last decades, thanks to the progresses in computing power and development of more sophisticated data handling algorithms, biomechanical numerical models are gaining always more frequently relevance in orthopaedic research. Until few years ago, simplistic approaches based on linear analyses and single structure or tissue types only have limited the use of finite element analysis in the biomechanical research. Instead, nowadays the use of a numerical approach is essential to analyse and predict the 3D behaviour of a knee, native or with implant.
To perform research on knee behaviour, several methodologies are carried out: in vivo analyses such as fluoroscopy and gait analyses, or ex-vivo experimental using human knee specimens. Unfortunately, in both cases several limitations affect these procedures. In fact, in the majority of the cases, clinical observations during surgery or during follow-up are related to patients in which pathology is already present. On the other hand, the lower amount of analysed specimens and the limited number of simulated boundary conditions affect the extracted outputs and the accuracy achieved. In this context, the use of a validated numerical approach is able to solve several of experimental limitations, giving to surgeons a powerful tool. Simulating fully three-dimensional, nonlinear, and multi-joint systems under different load conditions and specific patient's geometries, FEA helps surgeons to answer unresolved questions related to clinical complications [30]. The analysed structures in Orthopaedic Biomechanics are patient-specific morphology, which highly inhomogeneous and which changes over lifetime, depending on physiological loads, health and nutrition. Bone morphology is mainly determined by genetic factors, but also by mechanics. In detail, bone has the ability to adapt to mechanical loads, i.e. the external and internal structure of bone is transformed depending on the load occurring in the bone. Especially about the implant technology and arthroplasty, bone transformation plays an important role. If the biomechanical distribution of forces in and around the treated joint is reconstructed inappropriately during surgery, or if the design of the implant is improper, the so-called 'stress shielding' can occur. If the forces are mainly transferred by the implant, adjacent bony regions get minimally loaded and are subsequently degraded. Clearly even an overloaded bone region responds remodelling itself increasing bone volume and density [31]

4.2 Methodological sequence

A Finite Element Analysis developed in Abaqus/CAE (Simulia, Dassault Systèmes, Rhode Island, United States) was performed to supply surgeons a patient-specific numerical knee model in replying to clinical or research questions.
As shown in the Workflow (4.1), the development of a numerical model of native or after implant knee requires subject-specific and/or literature data sources like general input. First, high quality clinical images, performed on an intact lower limb specimen used for experimental tests, have been used to reconstruct biological geometries of interest. As regard implant components geometry are usually utilised CAD-data design supplied from the manufacturer. Moreover, material models and properties for bone, soft-tissues and implants are necessary. Since model is generated using specific boundaries, in order to replicate a real motor task, interactions among parts, forces and constrains as inputs should be applied, using as template previous cadaver test data or more generally standards reported from literature.
Once the input data are defined, the next fundamental step is the Finite Element model configuration. To generate the best mesh, leading to the least possible approximations, several options can be set in meshing a component. The accuracy of the outputs depends on selected element type and on chosen

element size. To reach a prefixed accuracy in the outputs, convergence tests are accomplished to select the minimum number of elements necessary for each parts of the model with a requested reasonable computational time.
According to the clinical/research question several outputs should be requested from the numerical simulations. As example, to understand knee behaviour during a specific motor task, implant contact forces and contact pressure, bone stresses, ligament strains and bone kinematics can be determined from a Finite Element Analysis. Undoubtedly, a first check and a validation of the Finite Element Model should be done in order that outputs have a real meaning and scientific relevance.

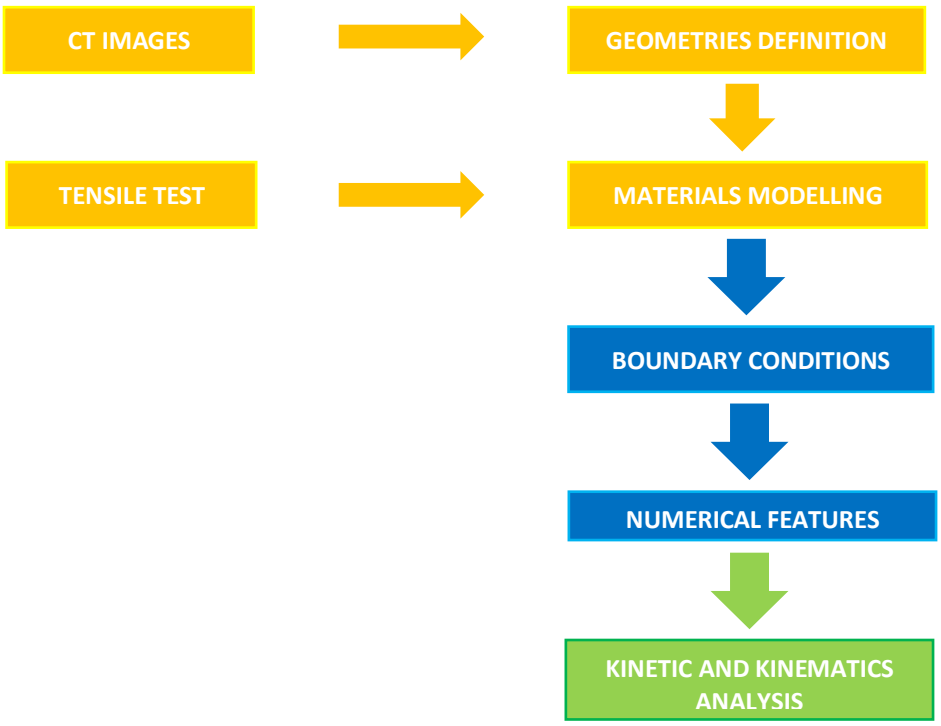

Fig. 4-1. *The flowchart describes the methodological sequence followed to develop a patient-specific FE model.*

4.3 Geometries definition

4.3.1 Bones

The reconstruction of bones geometries for all cadaveric knee specimens, as reported in Chapter 3.2.3 "Sensors and Tools Preparation", were performed using DICOM-files obtained with a 64-row helical multidetector computer tomography scanner.
In detail, femur, tibia and patella bones geometry was reconstructed, one more time, using ScanIP® (Simpleware, Synopsys, Exeter, UK) to segment CT scans. Compared to 3D reconstruction, in order to design Alignment and Cutting guides, in this case a more accurate manual segmentation was realised. The most proximal femur part and most distal tibia part have been removed to reduce the numerical complexity, maintaining the zone of interest. After that, for each bone morphology a cortical mask and a cancellous mask were done utilising a Boolean subtraction function.

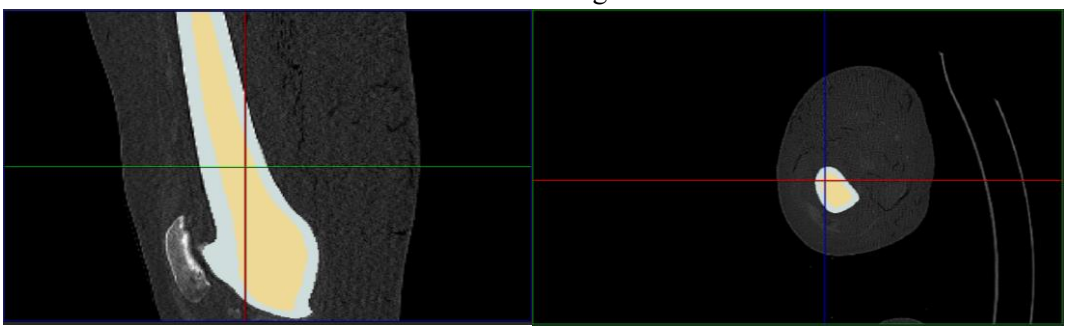

Fig. 4-2. *Bones segmentation.*

Furthermore, a filter algorithm was applied, on in this one, to realise a smoother and more regular surface. (figure 4.1 – A-B-C).

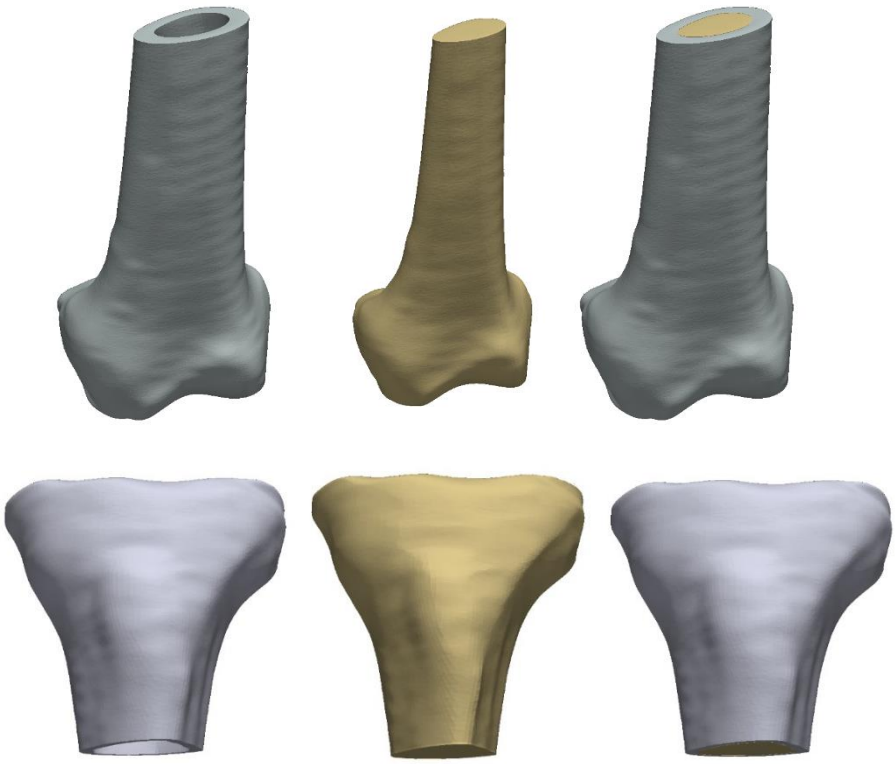

Fig. 4-3. *3D cortical and cancellous bones reconstruction.*

4.3.2 Ligaments

Concerning ligaments geometries, MRI images had a very low quality (figure 4.3) and they could not be used for the reconstruction of medial collateral ligament (MCL), anterior and posterior bundles, and of lateral collateral ligament (LCL).

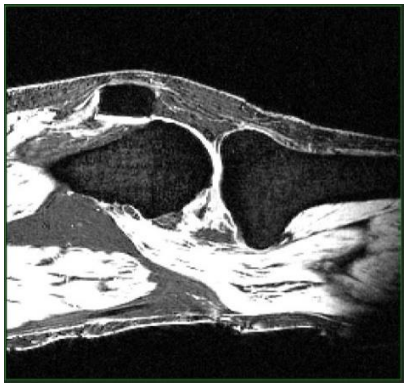

Fig. 4-4. *MRI images.*

Table. 4-1. *The radius of the profile of the considered ligaments.*

Ligaments	Radius [mm]
MCL	2.1
pMCL	2.1
LCL	2.4

In this study, even though a 2D or 3D reconstruction is more accurate since also the shear and transversal forces are considered 1D model approach was taken, Therefore, ligaments have been sketched as beams structures, directly in FEA software. Moreover, lengths and relative circular cross area sections were assigned to ligaments after a meticulous and accurate experimental measurement done during the cadaver test.

4.3.3 TKA

For the purpose of replicate a virtual Total Knee Arthroplasty, whole CAD-design files granted from the manufacturer was utilised. The same surgical technique done during cadaver test, with the same prosthesis in terms of femoral component dimensions, tibial tray dimensions, articular insert thickness, universal stem size and patellar component were adopted.

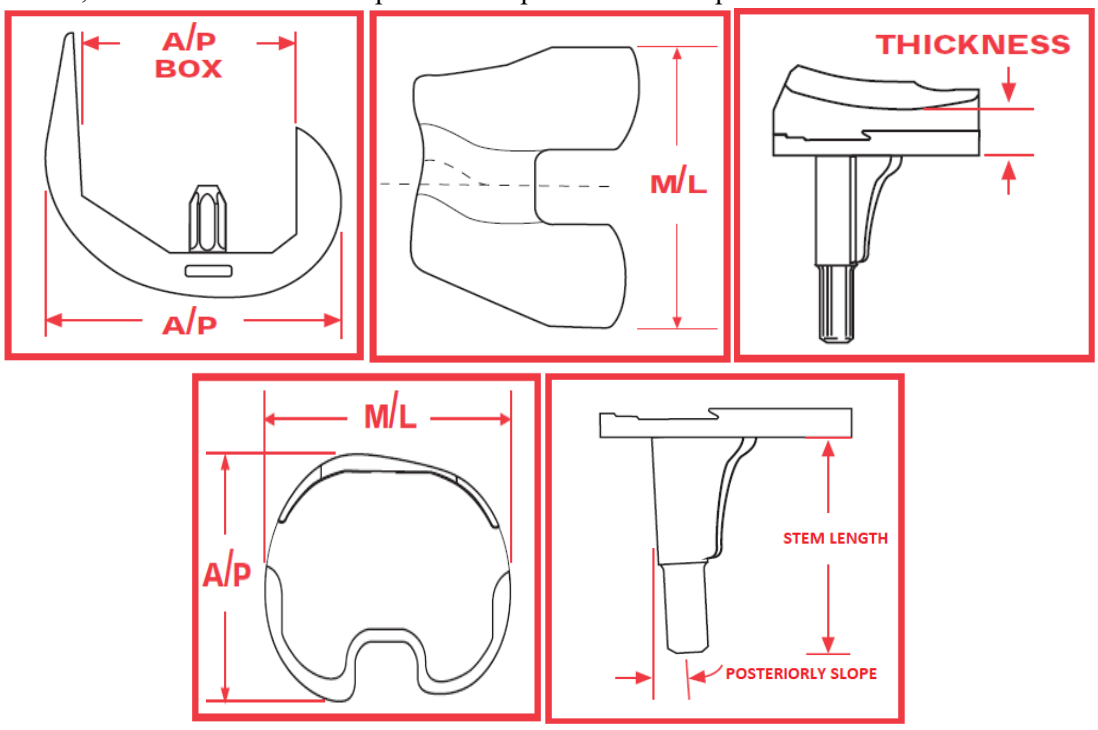

Fig. 4-5. *Designs of femoral component, tibial tray and articular insert.*

4.4 Materials Modelling

Once defined all the needed geometries, a literature-proved data and ex-vivo measurements obtained by tensile test, were used to characterize the material behaviour of bones and ligaments. Regarding to prosthesis, mechanical properties data released from manufacturer has been used. Usually, to simplify the model in terms of computational time requests, and due to the lack of information, all these materials are modelled as linear elastic materials.

4.4.1 Bone

For femoral, tibial and patellar bones, a healthy material property was simulated. Collecting data from the literature, the cortical bone was considered transversely isotropic, in which the third axis was taken parallel with anatomical axis of the femur and the cancellous bone was considered linear isotropic. Both bones material properties and them bone densities adopted in this research project are reported in the table 4.3.

Table. 4-2. *Material properties characterizing the bones.*

Materials	Young's Modulus [MPa]			Poisson's Ratio			Density [Kg/m^3]
	E_1	E_2	E_3	υ_1	υ_2	υ_3	
Cortical Bone	11500	11500	1700	0.51	0.31	0.31	1.8
Cancellous Bone	2130			0.3			1.3

4.4.2 Ligaments

Regarding ligaments, a mechanical uniaxial tensile test was performed to determinate the MCL and LCL specific-patient mechanical properties. In fact, at the end of cadaver test, both collateral ligaments, belonging to the human specimen tested in ex-vivo, were extracted, cleaned from fat and dried, in order to estimate Young's modulus and Poisson ratio.
Generally, during a tensile test, the displacement among points in the bundle of ligament is different from the clamps displacement. This undesired effect can be explained by a different spatial elongation behaviour of ligament and by a possible relative sliding during test between specimen and clamps. Due to the reasons explained above, four antireflecting markers were consequently drawn, directly on the ligament surface (figure 4-6), and an additional camera registration synchronised with loading machine was employed to measure the real ligaments displacement.

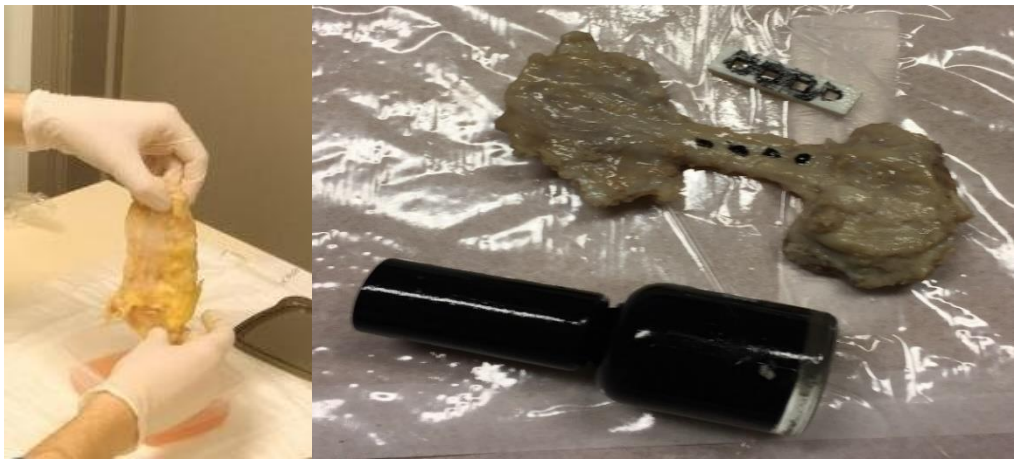

Fig. 4-6. *Ligaments preparation to tensile test.*

The tensile test was performed utilising an advanced material testing machine (LS1, LLOYD Materials Testing). A load cell of 250 N, driven by Nexygen plus dedicated software, was utilized to achieve an appropriate accuracy. A camera (HD Logitech webcam) (figure 4-7), fixed on an adjustable shelf, was perfectly aligned to the vertical plane where ligaments will be stretched. Moreover, camera was placed in an adequate distance to captured contour of the markers of all specimen surface during the whole test, with a sampling rate of 1000 Hz.

Fig. 4-7 *Camera and black-white chessboard utilised.*

Before starting the tensile test, once the camera was placed in the final position, a camera calibration was performed using a standard black and white chessboard (figure 4-7). An algorithm recognizes the position of all four corners and assigns them known values. Thereby, using ICY open source software, in the post-processing analysing the record it will be possible to find the initial length and width of the specimen and their variations during all the test.

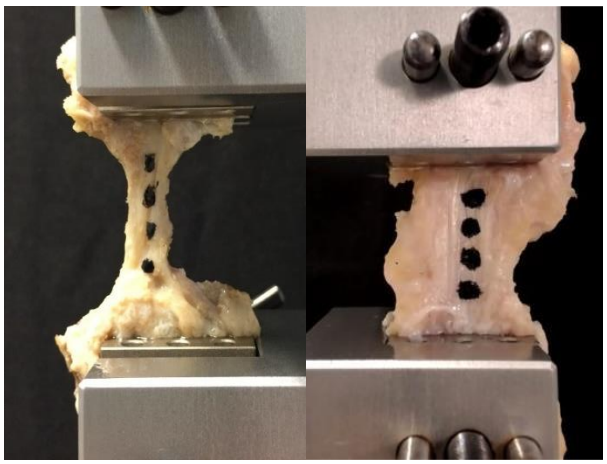

Fig. 4-8. *Ligaments clamped in the tensile machine ready for the characterization.*

After the markers treatment, specimen was clamped in the tensile machine and a quasi-static test was performed setting 1 mm/min of velocity for both ligaments. In the post-processing, first the images recorded were cut to contemplate only the region of interest. Secondly, all markers were automatically recognised by size parameters and threshold upper and lower limits. In order to estimate the width a central portion of the ligaments was considered and compared to the black background.

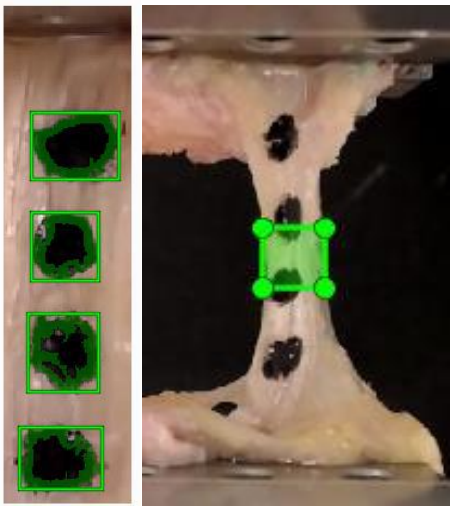

Fig. 4-9. *Ligament markers detection and width estimation.*

Through the true displacement variation, it was possible to obtain the true strain ε_l of both ligaments:

$$\varepsilon_l = \ln\frac{L(t)}{L_0}$$

Where, $L(t)$ is the instantaneous longitudinal distance between two markers and L_0 is the initial distance between two markers. Most of the time, the material displacement identified by markers in the post-processing is smaller than the clamps displacement calculated in real-time.

During tensile test the cross-sectional area of specimen varies. As simplifying assumption, the thickness was assumed constant, but using a black and white threshold imaging technique it was possible to estimate the specimen mean width variation (Figure sopra).

Through the estimate of cross sectional area variation, it is possible to obtain the true stress of the material:

$$\sigma = \frac{F(t)}{A(t)}$$

Where, $F(t)$ is the load acquired by the tensile machine and $A(t)$ is the specimen cross section area instantaneous variation.

Therefore, the Young's modulus was defined by dividing true stress by true strain:

$$E = \frac{\sigma}{\varepsilon_l}$$

and Poisson ratio was defined as transversal strain ε_t divided by true longitudinal strain ε_l

$$\nu = \frac{\varepsilon_t}{\varepsilon_l}$$

Where, ε_t is estimated using the instantaneous and the initial specimen width:

$$\varepsilon_t = \ln\frac{width(t)}{width_0}$$

Finally, for MCL and LCL stress-strain curve, relative Young' modulus and Poisson ratio were obtained:

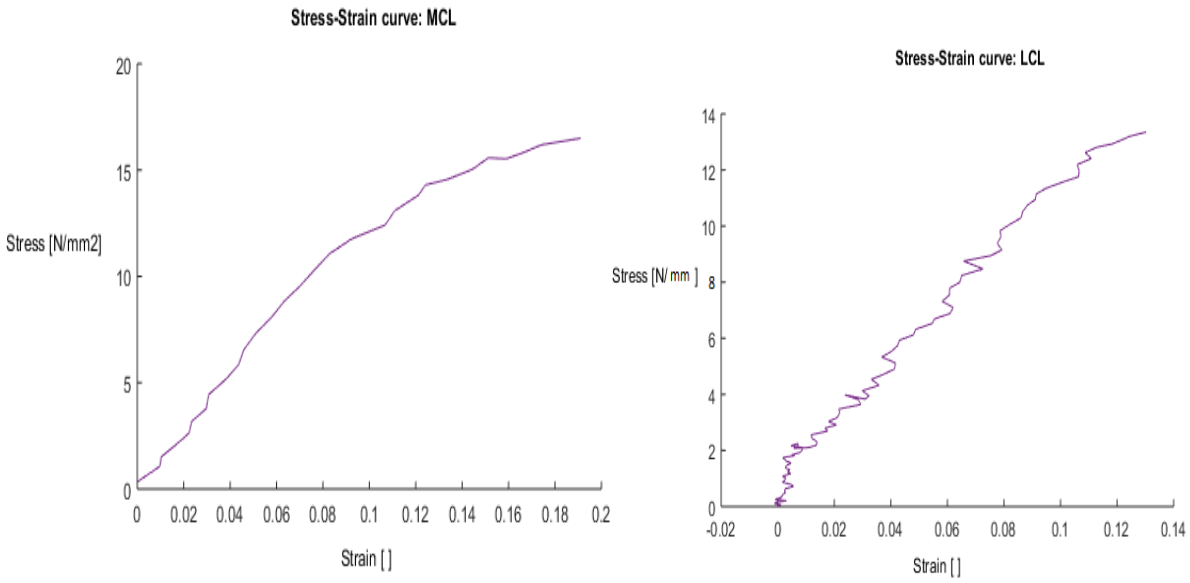

Fig. 4-10. *MCL and LCL stress-strain curve.*

Table. 4-3. *Material properties characterizing the soft tissues.*

Materials	Young's Modulus [MPa]		Poisson's Ratio	Density [Kg/m^3]
	Literature	Tensile Test		
LCL	280	120	0.4	0.31
MCL	224	150	0.4	0.31

The mechanical properties were compared with the literature data and an average mechanical properties model was implemented. In addition, MCL and LCL were modelled adding a pre-strain characteristic. The importance of considering the pre-strain is reported in literature to affect the outputs proving reliable stability during the simulated tasks [31]. The pre-strain effect was modelled inducing a heat contraction with a temperature field that cause a ligaments tension at the beginning of the simulation.

4.4.3 TKA

All TKA components are estimated with a linear and isotropic model. In particular, the femoral component and patellar component are made from Cobalt Chrome, instead the insert of TKA is made in Polyethylene (table 4.4). As regard tibial tray, it is made of Titanium.

Table. 4-4. *Material properties characterizing the TKA components.*

Materials	Young's Modulus [MPa]	Poisson's Ratio	Density [Kg/m^3]
CoCr	240000	0.3	8.272
Titanium	110000	0.3	4.510
Polyethylene	720	0.4	9.297

4.5 Relative position of the structures of the knee model

Once defined and assigned all the needed geometries and their materials behaviour, the same initial position of specimen during cadaver test was replicated being very careful to the correct relative positions among bones.

Fig. 4-11. *Subject-specific knee bones model.*

Precise positions of femur and tibial was attained using anatomical landmarks based on Victor et al. [23]. In detail, these points were identified both in the 3D CAD and in the human specimen before starting with the cadaver test using motion capture system. Calculating the roto-translation matrix of these point in two different coordinate systems, the correct knee configuration was replicated.
Moreover, to replicate the TKA surgery, made in the human specimen, the instructions provided by the manufacturer to the surgeon were followed. The resection of bones was performed through Boolean functions, implemented in Abaqus, to remove unnecessary material (figure 4-12). Finally, ligaments and patellar tendon were added to ultimate the reconstruction of final knee structure.

Fig. 4-12. *Cut Surgical Technique.*

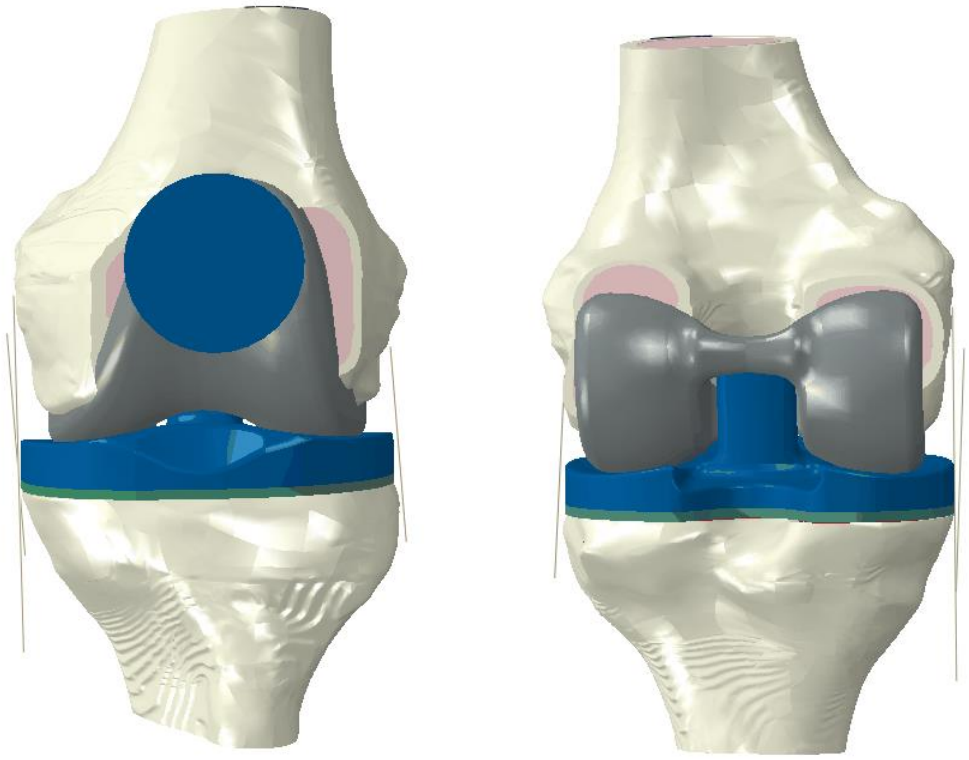

Fig. 4-13. Model assembly in frontal and posterior view.

4.6 Interactions

Specific interactions were considered among structures to simulate real boundary conditions. First, the effect of the cement in the femoral component and in the tibia tray is simulated with a Tie Constrain between femur and tibia bones respectively (Fig. 4-14)

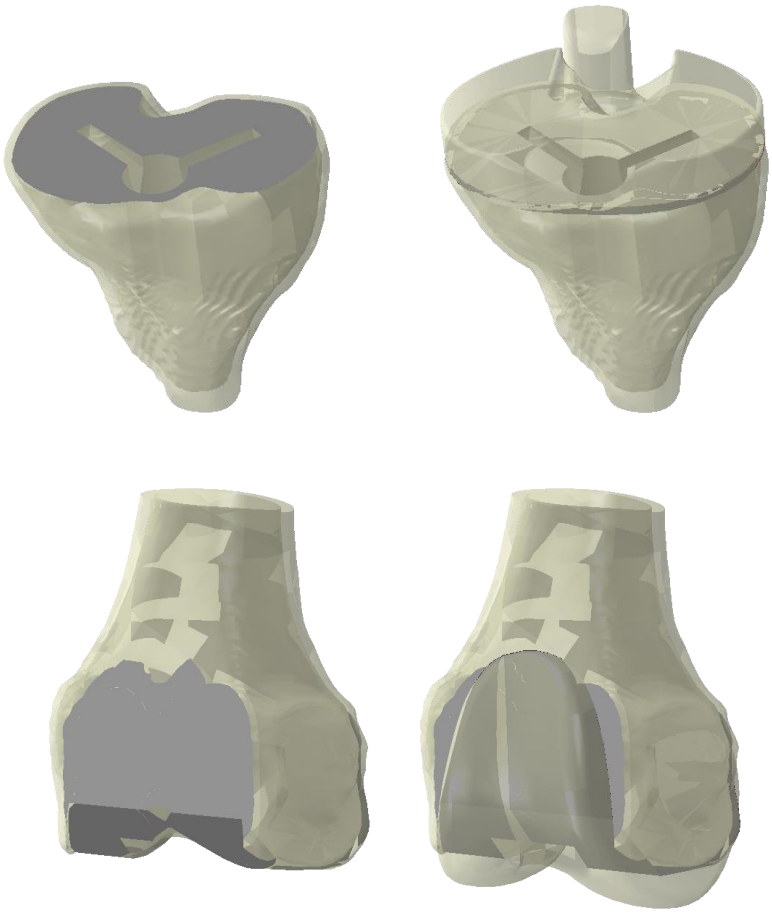

Fig.4-14. *Cement effect modelled as tie constrain.*

Secondly, between the femoral component and the tibial insert, and between patellar component and femoral component, a surface-to-surface contact has been defined to replicate the contact that occur during the simulated squat. For these interactions, a coefficient of friction of 0.01 was set in the tangential direction.

Fig.4-15. *Femoral-tibia contact modelled as surface-to-surface contact.*

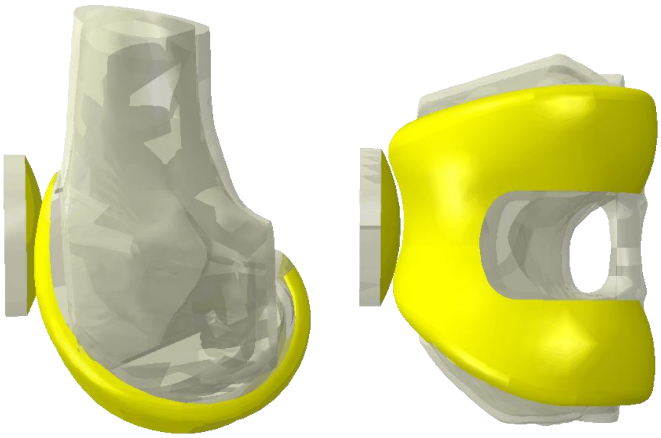

Fig.4-16. *Femoral-patella contact modelled as surface-to-surface contact.*

Afterwards, femur bones and femoral TKA component were simulated like a rigid body while tibial insert, tibial bones and patellar component are considered deformable. Moreover, ligaments and patellar tendon were coupled with their relative region of bones by coupling, and some reference points were defined in order to apply and to transmit specific forces and boundary conditions.

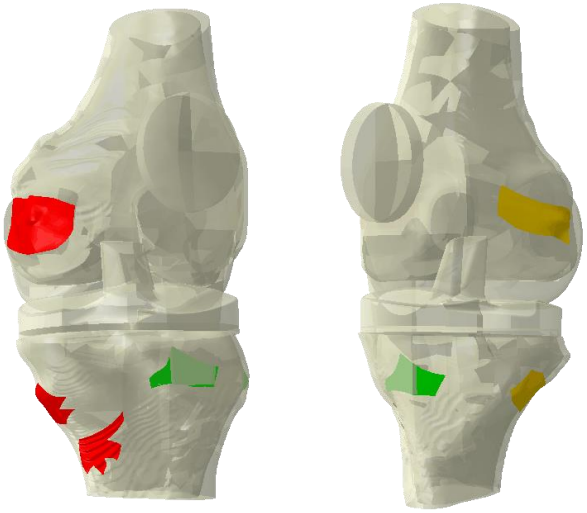

Fig. 4-17. *Ligaments and tendon attachments modelled as coupling.*

4.7 Loads

To replicate exactly the experimental squat, a dynamic simulation was performed with loads and boundary conditions derived from cadaver test. The tibia bone is considered embedded and only the femur can move with 6 degrees of freedom. The flexion-extension from 20° to 120° was performed in 10 s around the flexion axis derived on the femur based upon the previously obtained anatomical landmarks.

An external force was added as numerical correction, applied in the anatomical reference point placed on Femoral Knee Centre (FKC). Furthermore, quadriceps and hamstrings forces, extracted again

from experimental test, were simulated as sinusoidal and constant loads, which are placed, respectively, on the patella and on the proximal region of femur since tibia is considered fixed.

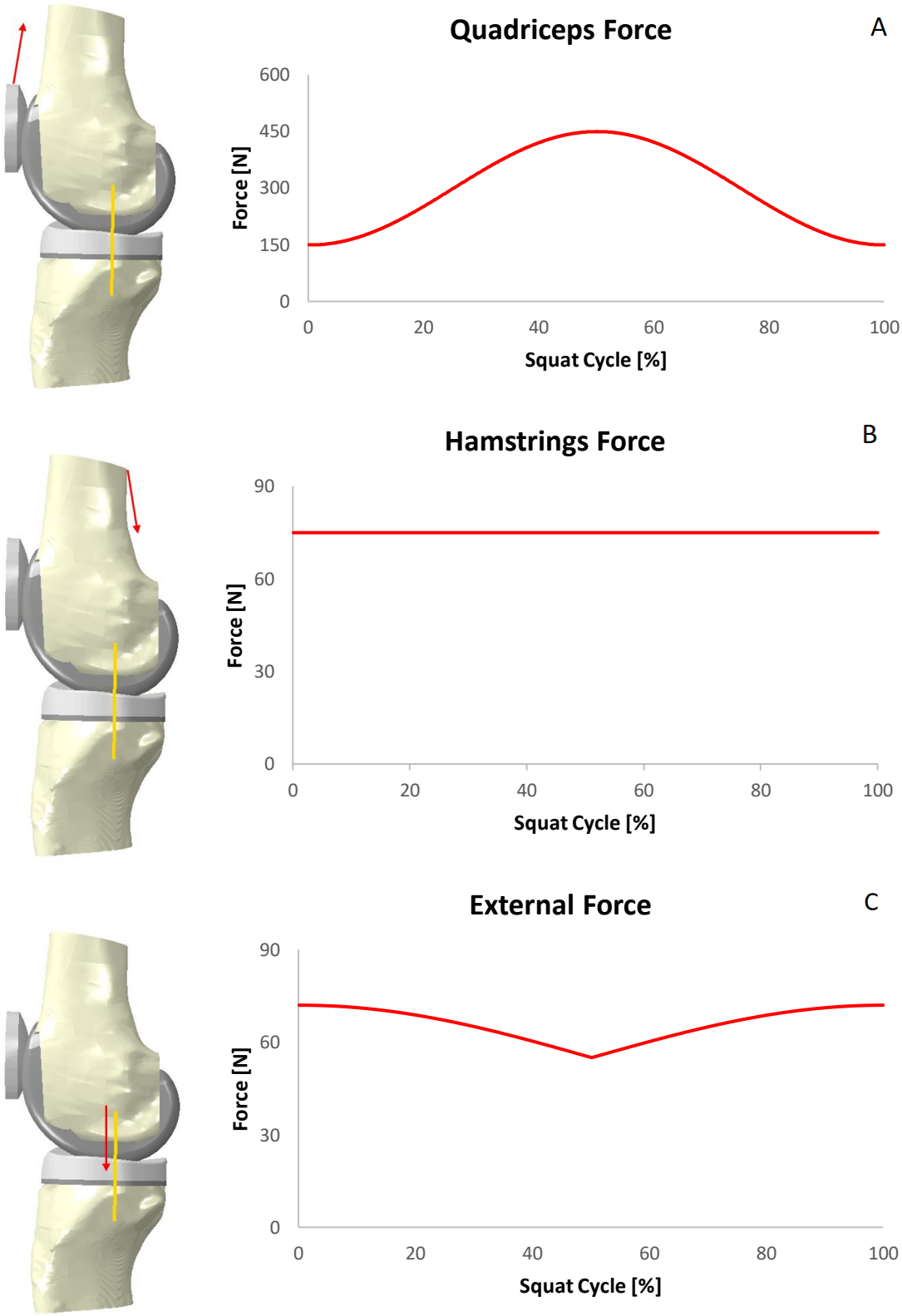

Fig.4-18. *Load applied to the model to replicate experimental set-ups: (A) quadriceps force, (B) hamstrings forces; (C) external force*

4.8 Mesh

Once interactions, loads and constrains were set, the finite element model is not yet ready to simulate squat motor task. A fundamental step in a numerical analysis is the meshing of the structures, which consist in the subdivision of each parts of model in 3D elements with variable dimension. These elements can have different types that allow different degree of distortion and sizes, selected according to the expected accuracy of the outputs and the available computational time.
The use of smaller elements allows to achieve a more accurate discretization, fitting better the original shape of the structure and improving the accuracy of the results. Unfortunately, the computational time increases, due to the raise of the number of nodes and consequently, the number of equation. On the contrary, using bigger elements, the computational time decrease introducing, simultaneously, approximations on outcomes. Therefore, a balance between computational time and accuracy can be achieved selecting different sizes of the element in function of the relevance of the region of interest.
For this study, due to the high complexity of the model, the geometries were all meshed with linear tetrahedral elements, after a preliminary convergence study about the femoral component, the patellar component and the tibial insert.

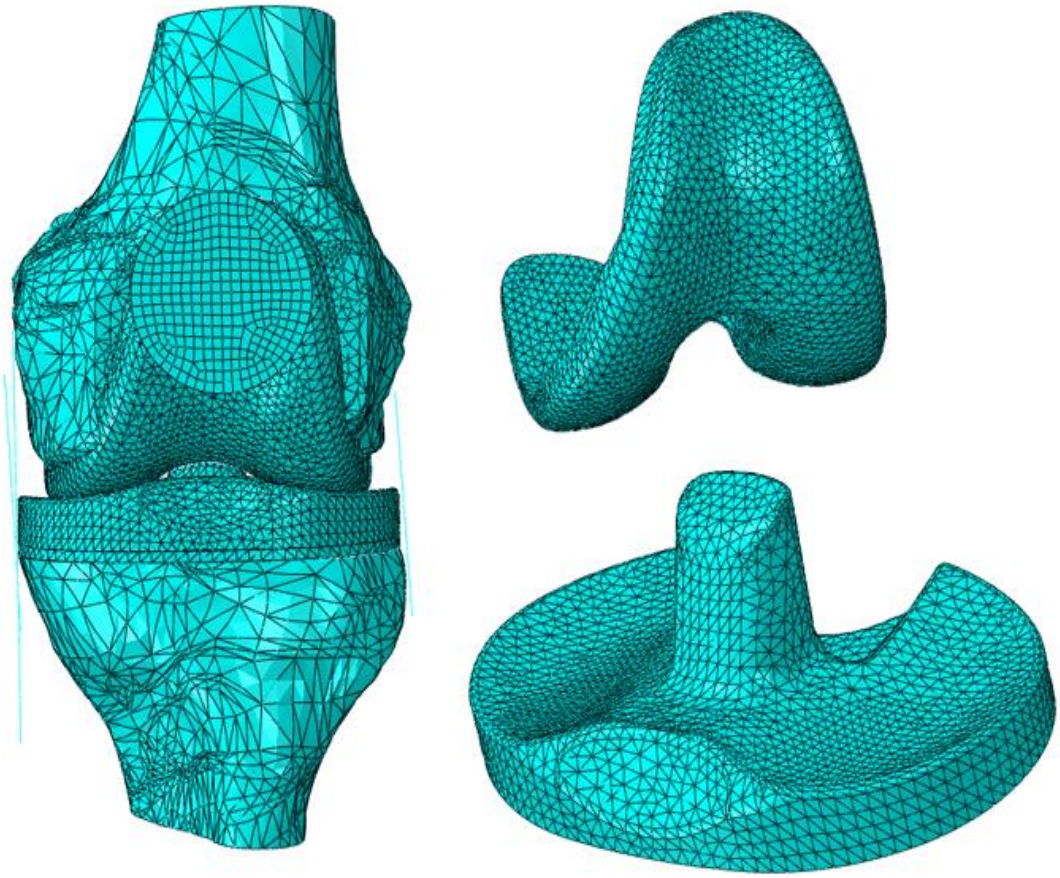

Fig.4-19. *Discretization of knee structures*

4.9 Model Outputs

To check the reliability of the model, kinetic on the region of interest and the kinematics have been compared to cadaver test results.
For the squat simulated, the contact pressure, the contact area and the magnitude of the contact force were investigated in the tibial insert and in patellar component. Tibial insert region was divided in medial and lateral compartment for a better analysis of the tibiofemoral joint. In addition, for the analysis of the kinematics, varus-valgus, internal-external rotations and medial-lateral, anterior-posterior and compress-distract translation were analysed.

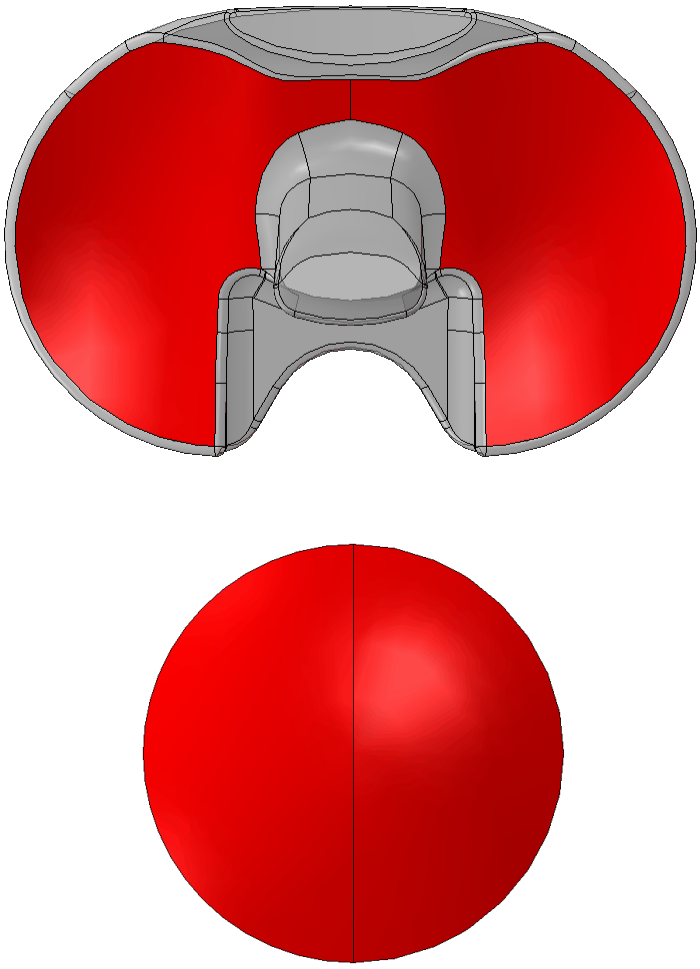

Fig.4-20. *Tibial insert and patellar component ROI*

4.10 Numerical Outputs

4.10.1 Kinetics

Figure 4.21 and figure 4.22 report results regarding the contact pressure on the tibial insert for the observed range of flexion and extension respectively. The contact zone moves from anterior to posterior part of tibial insert during the flexion, to go back in the initial position with the extension. Contact pressure increases with flexion achieving values in a range of 2-8 MPa. Maximum values of pressure are mainly located on the medial side in full extension. Observed contact pressures map are

comparable to literature data [33] for similar boundary conditions with the exception of the lower applied load that, as a consequence, results in lower pressure outcomes.

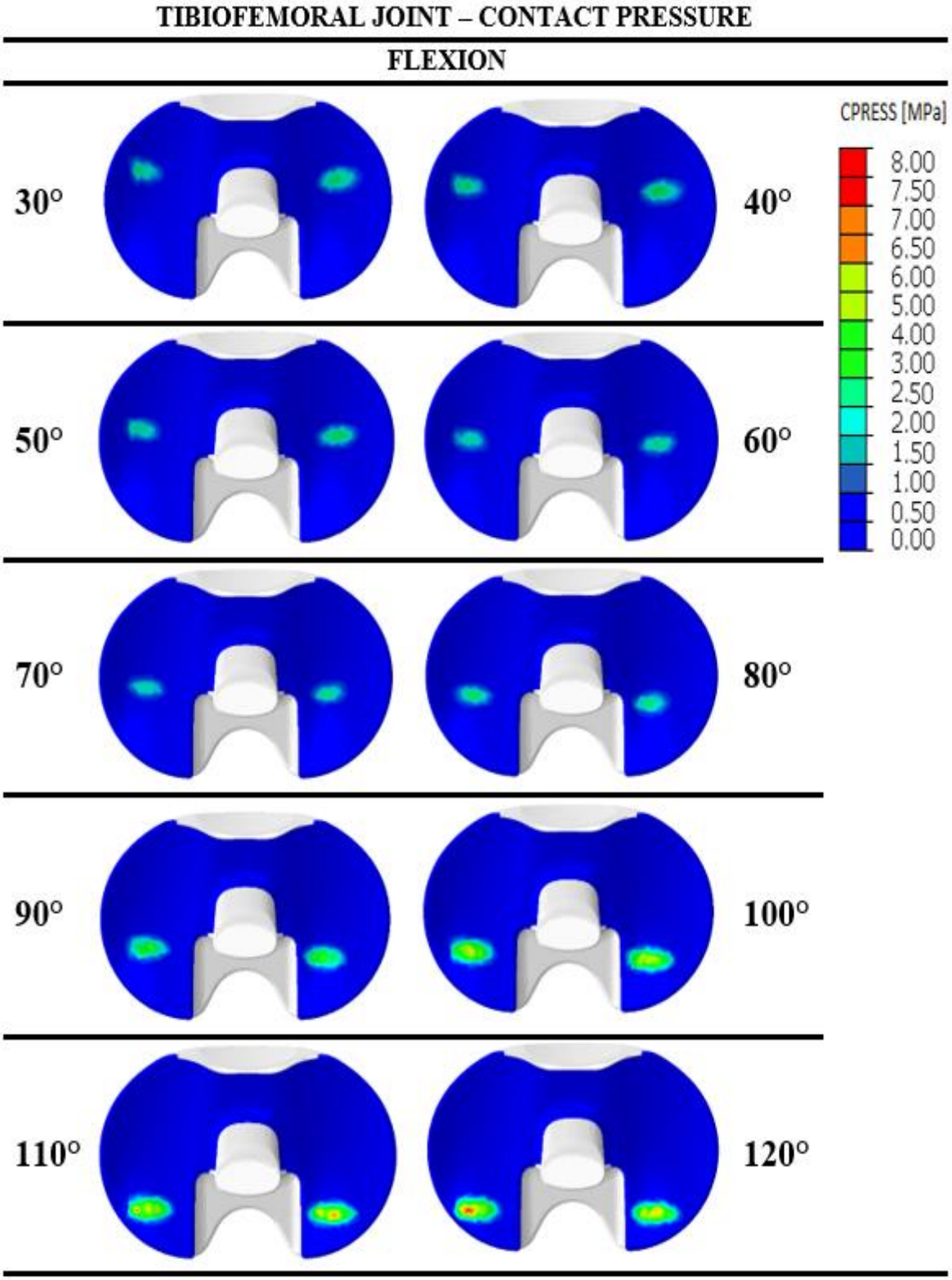

Fig. 4-21. *Contact pressure on tibial insert at each 10 of simulated flexion.*

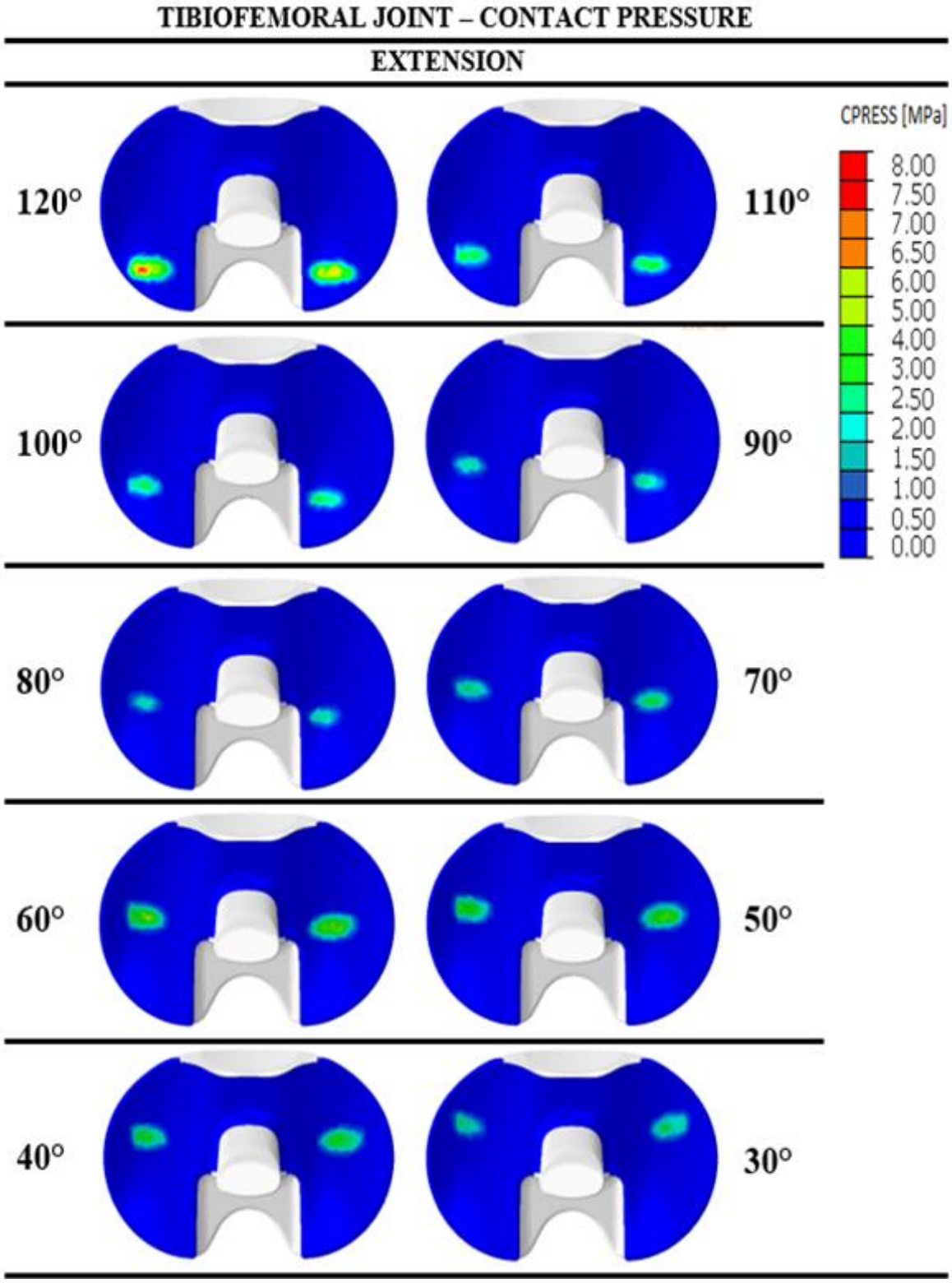

Fig. 4-22. *Contact pressure on tibial insert at each 10 of simulated extension.*

Focusing on the flexion movement, figure 4.23 shows quantitative results of contact pressures. Between 20 and 80 degrees the contact pressures fluctuate from 3 to 5 MPa. Afterwards, an increase is recorded until 8 MPa and 7.50 MPa, for medial and later side respectively.

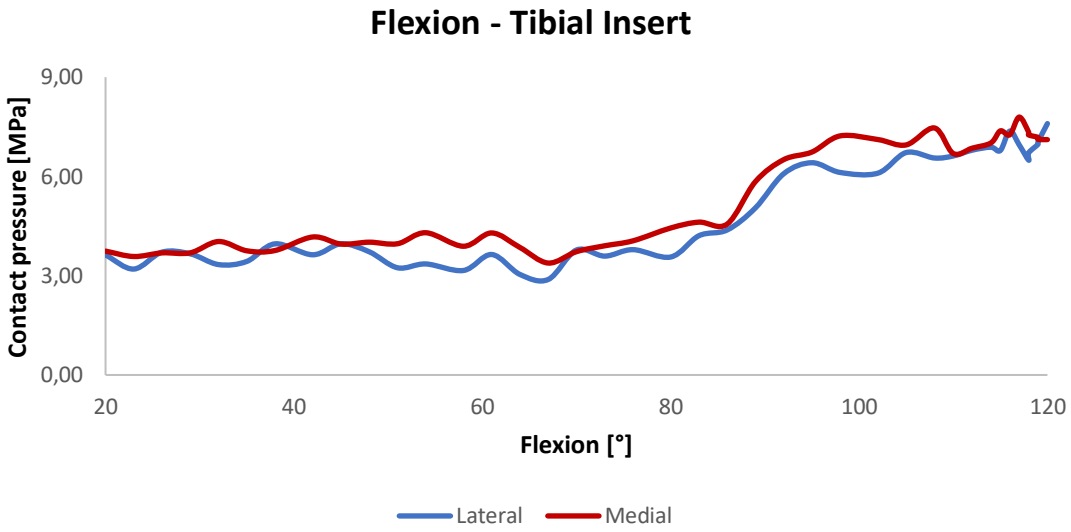

Fig. 4-23. *Contact pressure on the medial and lateral tibial insert during simulated flexion.*

Analysed contact areas on lateral tibial insert shows an average steady trend from 20 to 80 degrees and then an increase until 170 mm^2 at 120 degrees. Otherwise on the medial side, at beginning of flexion there are higher contact areas values, then can be observed a first reduction until 70-80 degree followed by an increase in full extension achieving 160 mm^2.

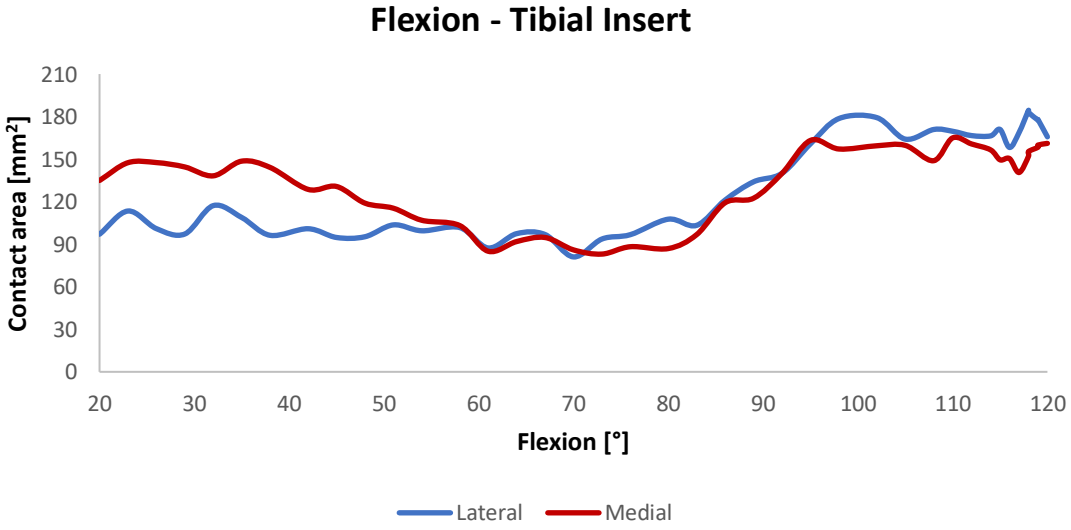

Fig. 4-24. *Contact area on the medial and lateral tibial insert during simulated flexion.*

Concerning to patellar component, figure 4-25 and figure 4-26 resume the contact pressure outputs during flexion and extension movements simulated. As showed, the contact zone moves from central to superior part in flexion and turns back during the extension.

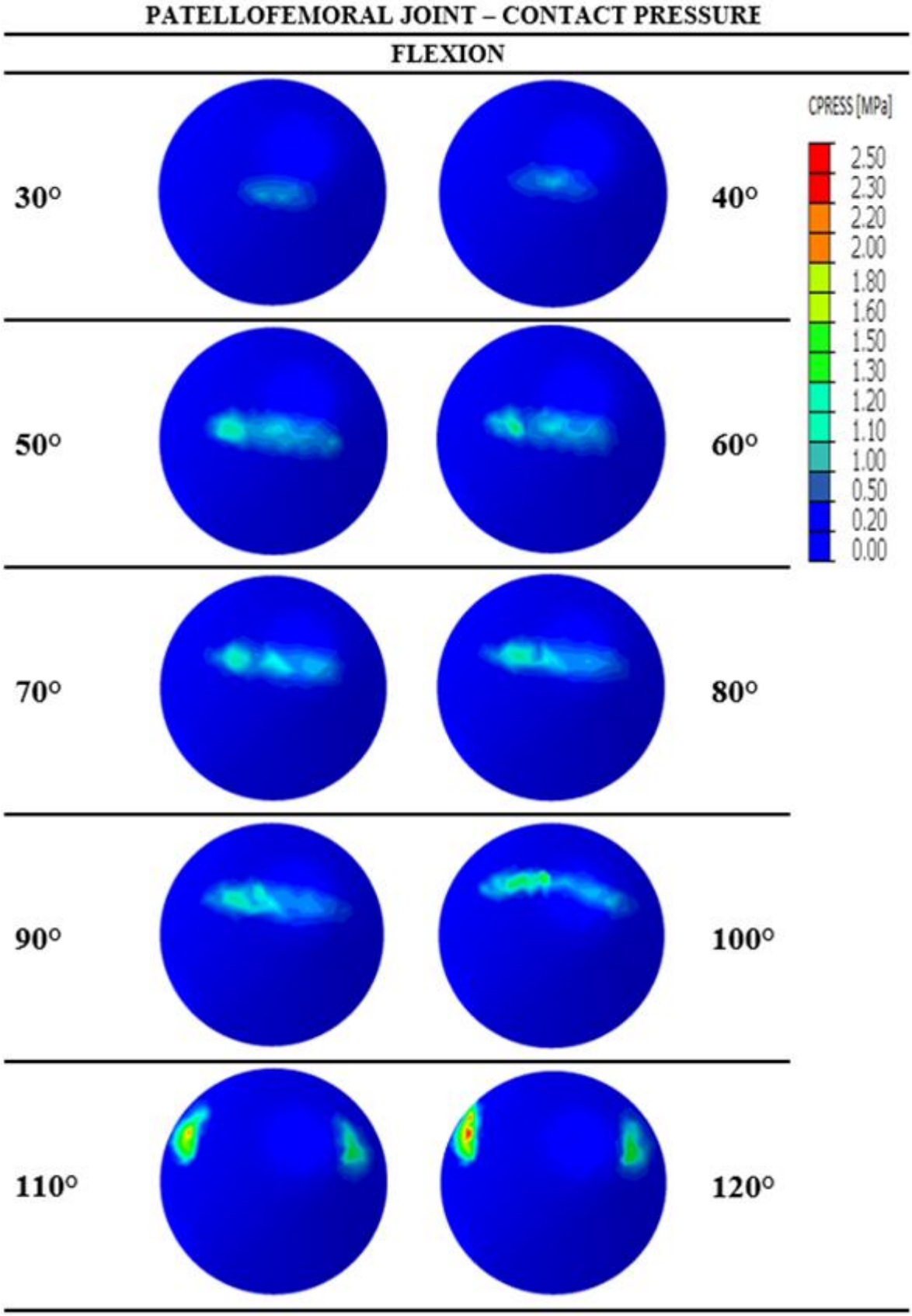

Fig. 4-25. *Contact pressure on tibial insert at each 10 of simulated flexion.*

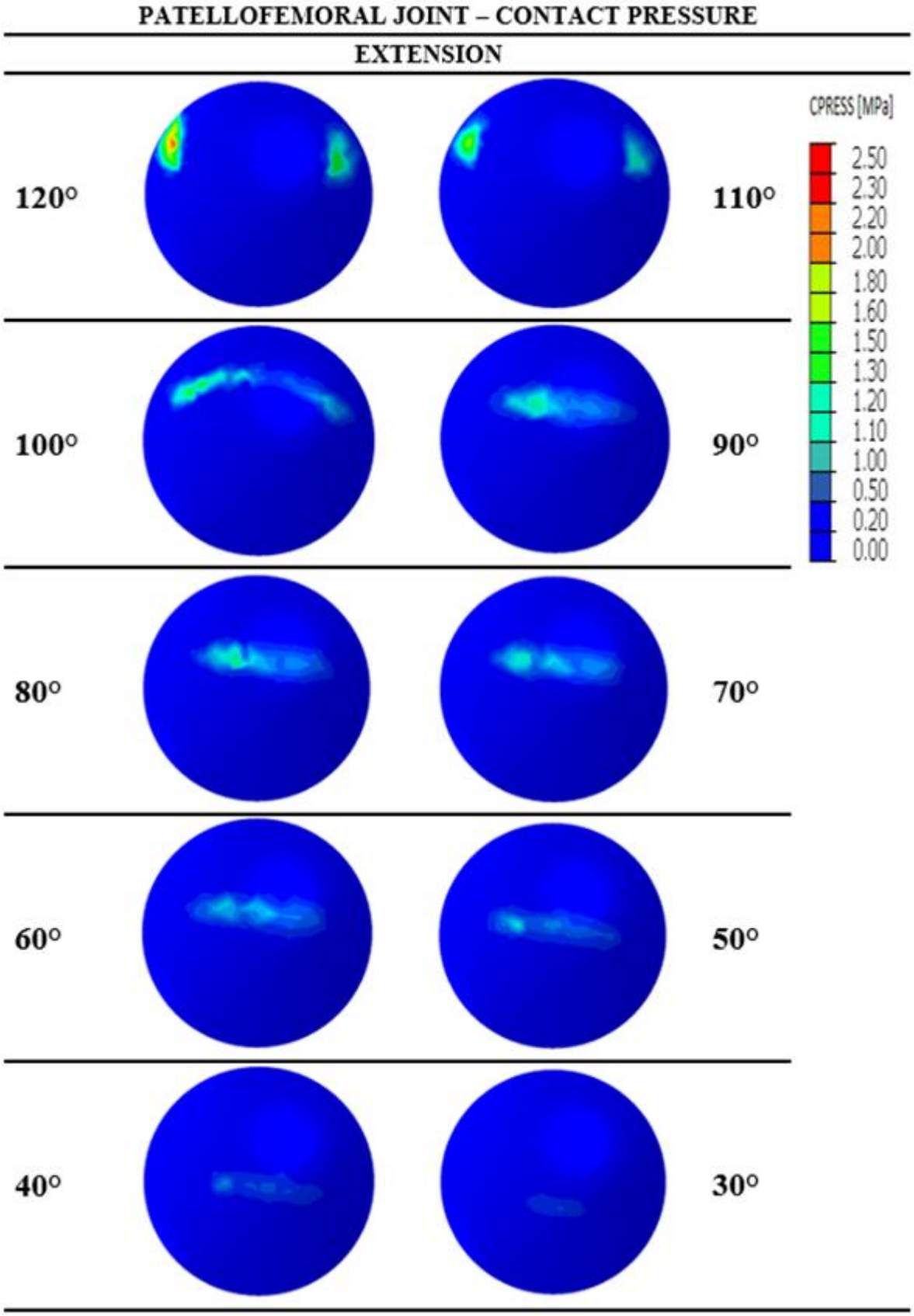

Fig. 4-26. *Contact pressure on tibial insert at each 10 of simulated extension.*

Figure 4-27 shows how the contact pressures trend in the patella component grows from the start of flexion to achieve a first peak of 1.90 MPa around 60 degrees. Afterwards, contact pressure decreases up to a value of 1.10 MPa to quickly increase in full extension, reaching to 2.5 MPa. Furthermore, in figure 4-28 are reported the contact areas on the patellofemoral joint. There is an initial increase of contact area during the flexion with a final steady trend from 110 degrees to full flexion, where the contact pressure holds approximal constant. Patellar outcomes are in agreement with the literature [34].

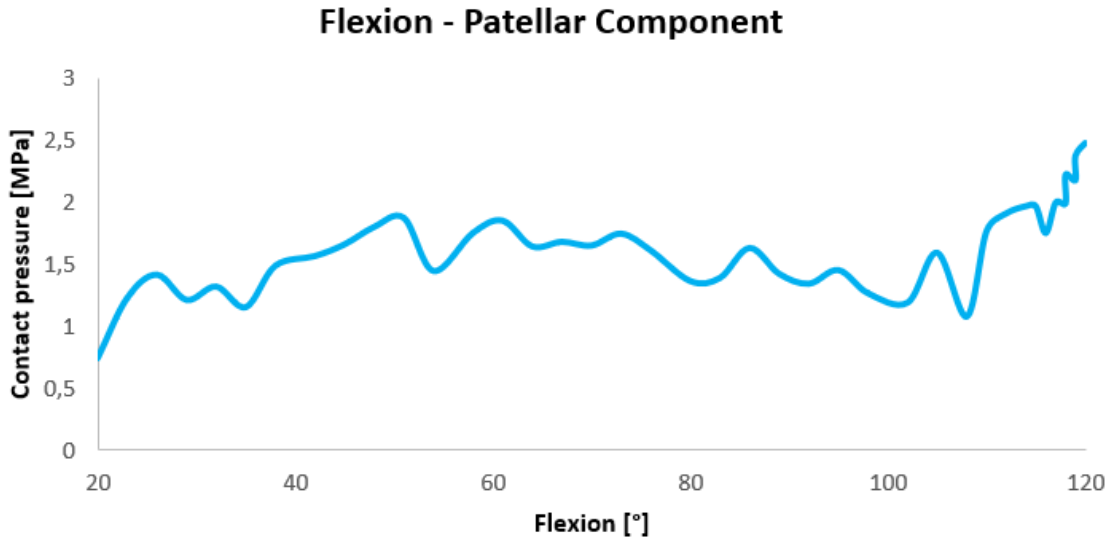

Fig. 4-27. *Contact pressure on the patella component during simulated flexion.*

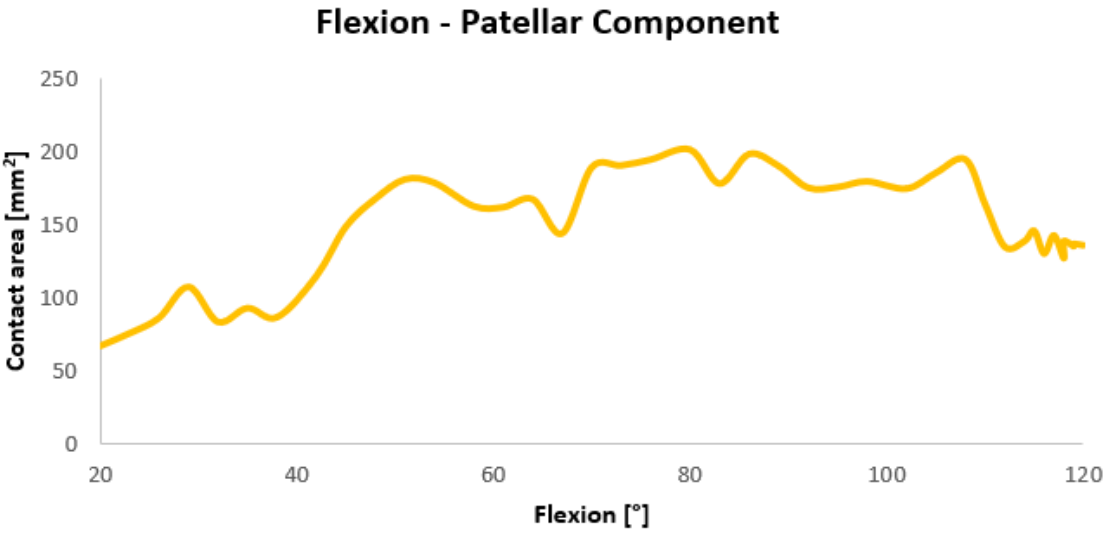

Fig. 4-28. *Contact area on the patella component during simulated flexion.*

4.10.1 Kinematics

Concerning to kinematics, Grood and Suntay methodology was adopted to evaluate rotations and translations of human knee during a squat. Figure 4-29 reports the anterior-posterior translation at each 10 degrees during the flexion. Results show a growing trend for both side with increased the flexion angle, with maximum values located in full extension. The anterior-posterior translation is in a range of 15 mm, posteriorly oriented, with higher values in the medial side. The medial-lateral translations, showed in figure 4-30, are characterize by a constant trend during the flexion with a range of 1 mm in both side. Figure 4-31 represents the compression-distraction translations during the simulated motion task. The medial side shows a range of motion of 8 mm, wider than the lateral one, characterized by a range of 2 mm. In both cases, the maximum values are recorded at 80 degrees. Extracted translations are similar and comparable with the literature [35].

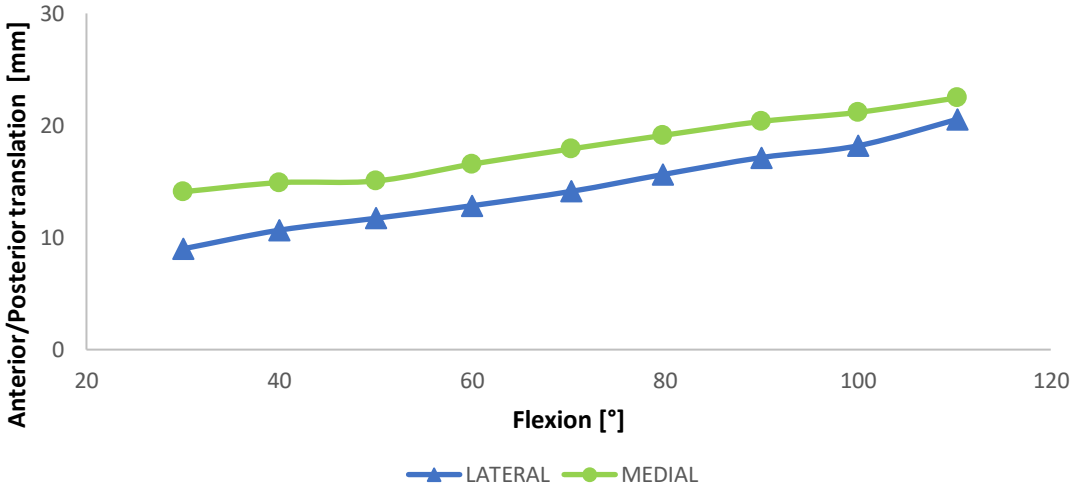

Fig. 4-29. *Anterior-posterior translation of medial and lateral condyle at each 10 degrees of simulated flexion.*

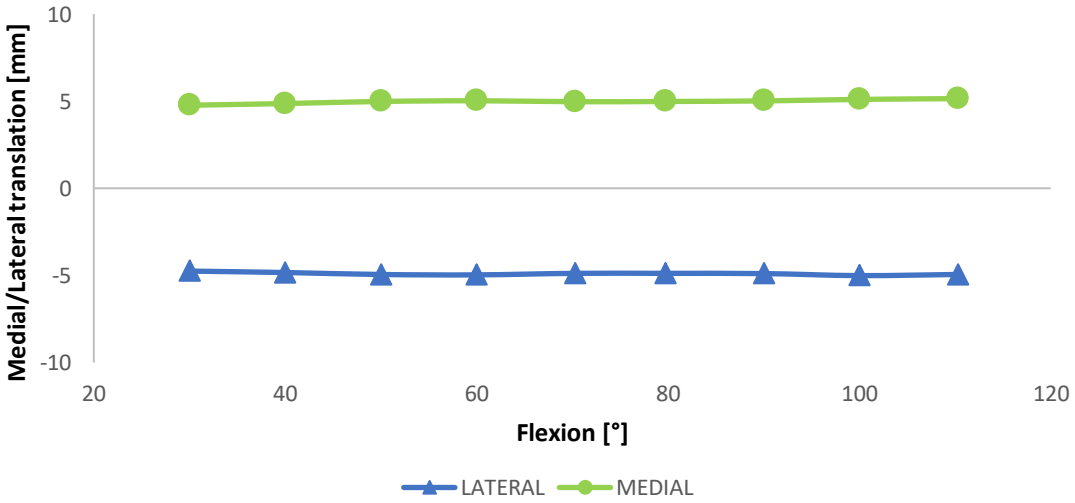

Fig. 4-30. *Medial-lateral translation of medial and lateral condyle at each 10 degrees of simulated flexion.*

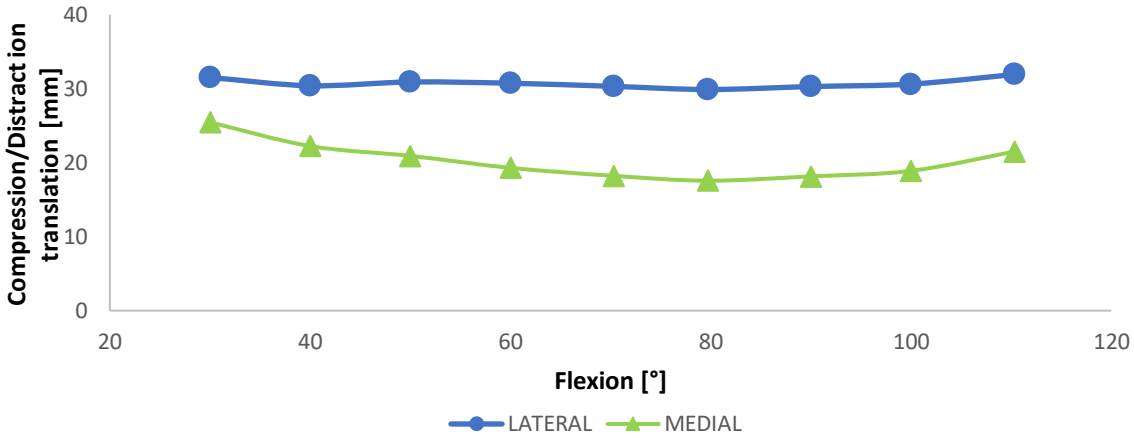

Fig. 4-31. *Compression-distraction translation of medial and lateral condyle at each 10 degrees of simulated flexion.*

As regard to rotations, varus-valgus and internal-external were calculated and are showed in the followed figures (4-32 and 4-33). The internal-external rotation presents a range of 4 degrees starting from around 7.5° and decreasing during the motion up to 2.5°. Considering the range of motion between 30 and 80 degrees this range is reduced to 1 degree. Instead, varus-valgus rotation shows a parabolic trend with increased values from 30 to 80 degrees and decreased values in full extension.

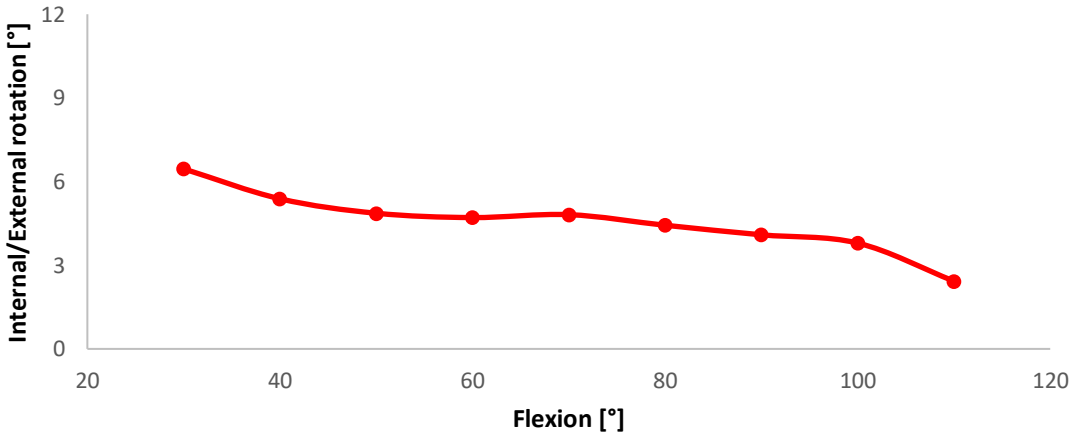

Fig. 4-32. *Internal-external rotation at 10 degrees of simulated flexion.*

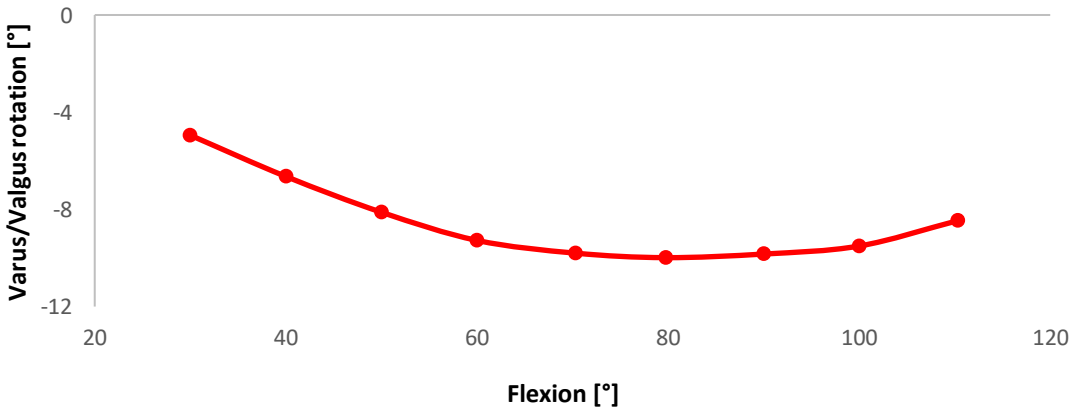

Fig. 4-33. *Internal-external rotation at 10 degrees of simulated flexion.*

CHAPTER V – VALIDATION

As mentioned before, nowadays the use of numerical models in orthopaedic research is becoming fundamental to better understand and predict the 3D behaviour of knee joint overcoming several limitations of the experimental procedures, namely ethical issues, high costs and shortage of repeatability. Before using extracted biomechanical outputs, in surgical practice or in improving knee prosthetic designs, an appropriate validation must be performed. Generally, regardless the type of Finite Element Analysis, the validation is always a critical step.
In this research project the validation of the patient specific knee model developed in Chapter 4 was based on cadaver test performed in UZ Ghent Hospital, under the same boundary conditions and knee prosthesis design illustrated in Chapter 3. For this purpose, numerical kinematics and kinetics outputs were compared with the experimental ones demonstrating a partial validation of Finite Element Model developed. In particular, experimental limitations due to the use of Tekscan pressure mapping systems were highlighted.

5.1 Comparison between numerical and experimental kinematics data

All kinematics patterns extracted in both approaches were compared in terms of translation and rotations. Graph 5-1 shows the anterior-posterior translations for the experimental and numerical model. Numerical outcomes show the same trend of those recorded with motion capture system, with slightly higher values. The only deviation trend is observed in full flexion for the lateral side, where experimental data are higher than the numerical. Output divergences are in a range of 2 mm, while it is reduced to 1mm considering the range of flexion between 50-90 degrees.
The medial-lateral translations are compared in figure 5-2. In this case, kinematics translations are completely identical between 20 and 30 degrees with a divergence on 0.1 mm. Increasing the flexion angle, range divergence grow up to achieve maximum in full flexion with range divergence value of 2.4 mm. Moreover, from 50 degrees to the end of flexion experimental values are lower than numerical ones.

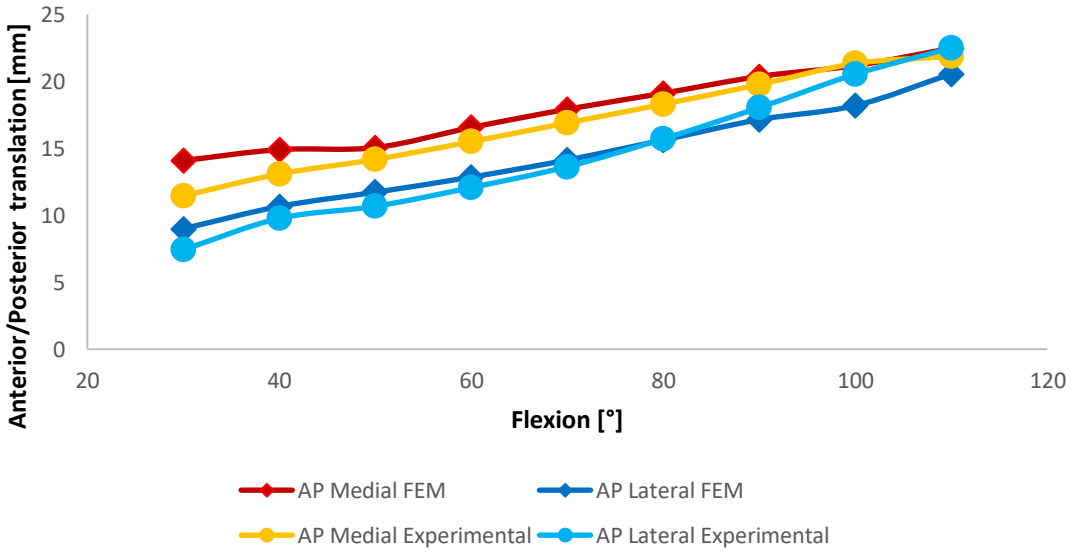

Fig. 5-1. *Comparison between numerical and experimental anterior-posterior translation of medial and lateral condyles.*

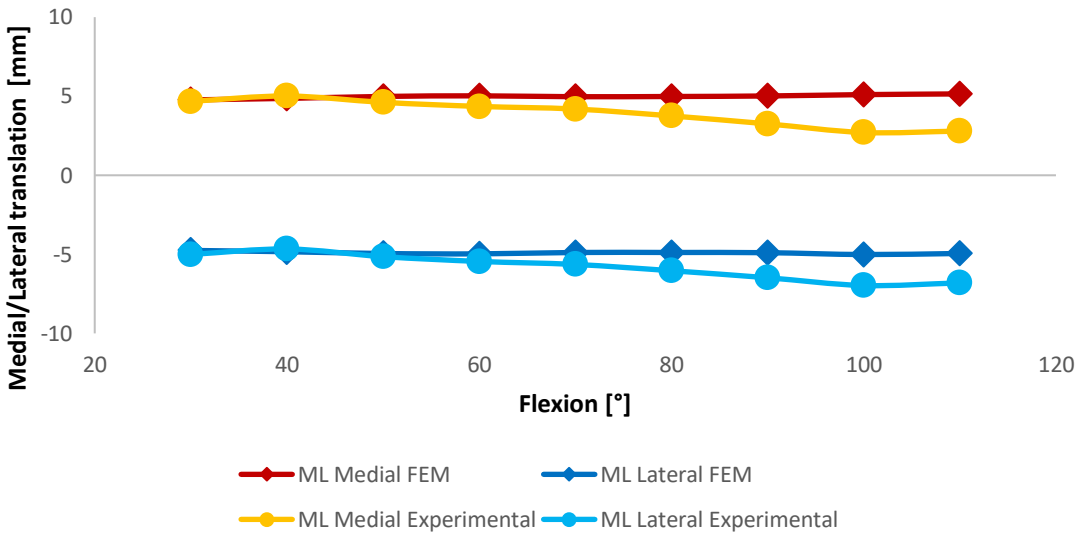

Fig. 5-2. *Comparison between numerical and experimental medial-lateral translation of medial and lateral condyles.*

Concerning to compression-distraction translations, the contrast of results shows a pronounced deviation on the medial side compare to the other translations found in anterior-posterior and medial-lateral directions. In detail, a range of divergences of 6.5 mm and of 2.7 mm characterize the medial and lateral side respectively. Regarding the medial side, this deviation remains steady with an average of 4.2 mm until 90 degrees to increase rapidly in full flexion. Instead, on the lateral side, excluding the 30 degrees where it was found the maximum value of divergence, the numerical outputs portray correctly kinematic evaluated during the cadaver test.

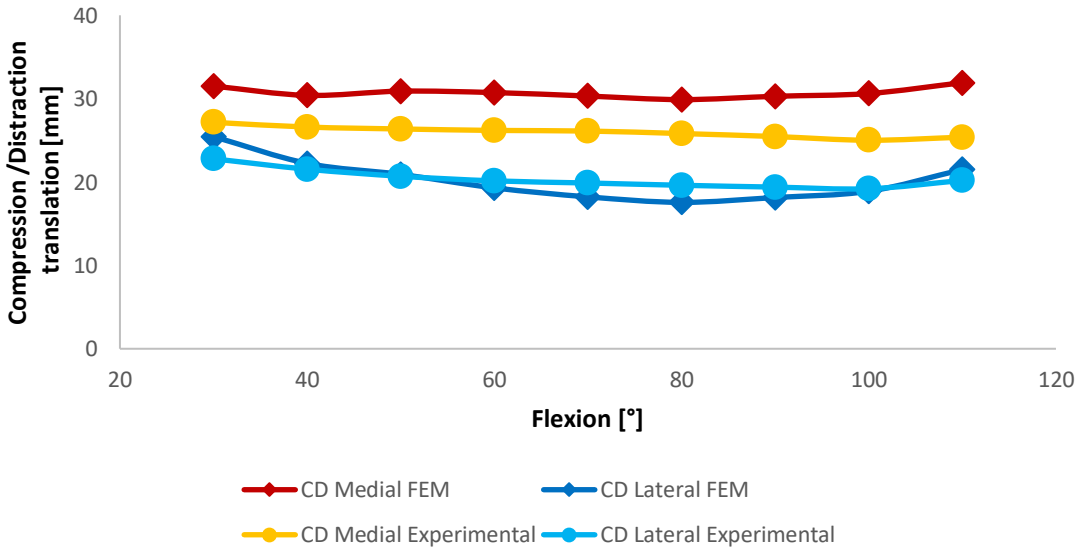

Fig. 5-3. *Comparison between numerical and experimental compression-distraction translation of medial and lateral condyles.*

The numerical translations exhibit higher value in comparison with experimental data. This can be attributed to the more constrained environment that characterize the human knee during the cadaver

test in contrast with the numerical setting, where few ligaments were considered neglecting all the joint capsule.
Figure 5-4 shows the contrast in terms of internal-external rotation. Numerical outputs follow the experimental trend until to 90 degrees with few divergences in a range of 1 degree. Instead, in full flexion the deviation rises to 1.6 degree. Figure 5-5 reports the valgus-varus rotation in the two models. Outcomes divergences inferior to 0.7 degree are recorded during all the motor task following the experimental trend.

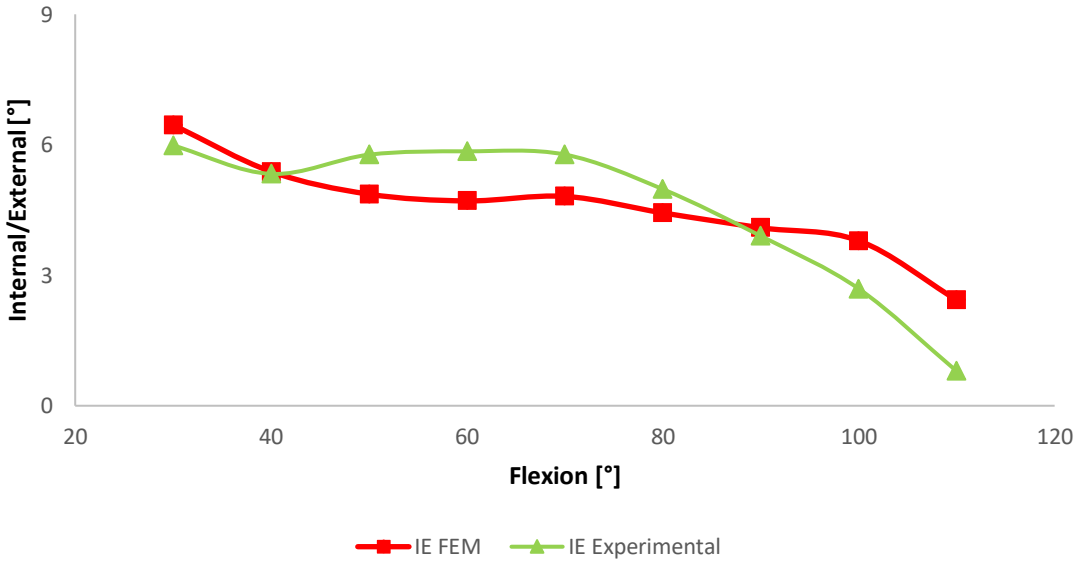

Fig. 5-4. *Comparison between numerical and experimental internal-external rotation.*

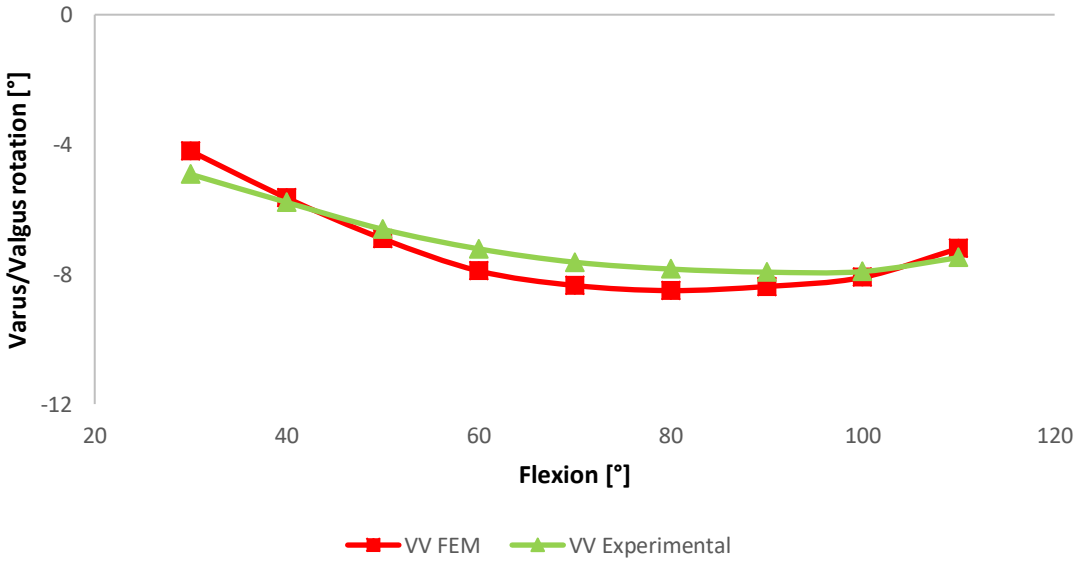

Fig. 5-5. *Comparison between numerical and experimental varus-valgus rotation.*

5.2 Comparison between numerical and experimental kinetics data

Once compared patient-specific kinematical outcomes, contact pressure and contact area in tibial insert and patella component were compared. Analysing the most significant degrees, figure 5-6 and figure 5-7 show, for the lateral and medial side of the tibial insert, the contact areas evaluated in vitro using Tekscan sensors and the numerical ones. The two patterns exhibit similar behaviour at the beginning of motor task to increase the range of divergence from 90 degrees to full flexion.

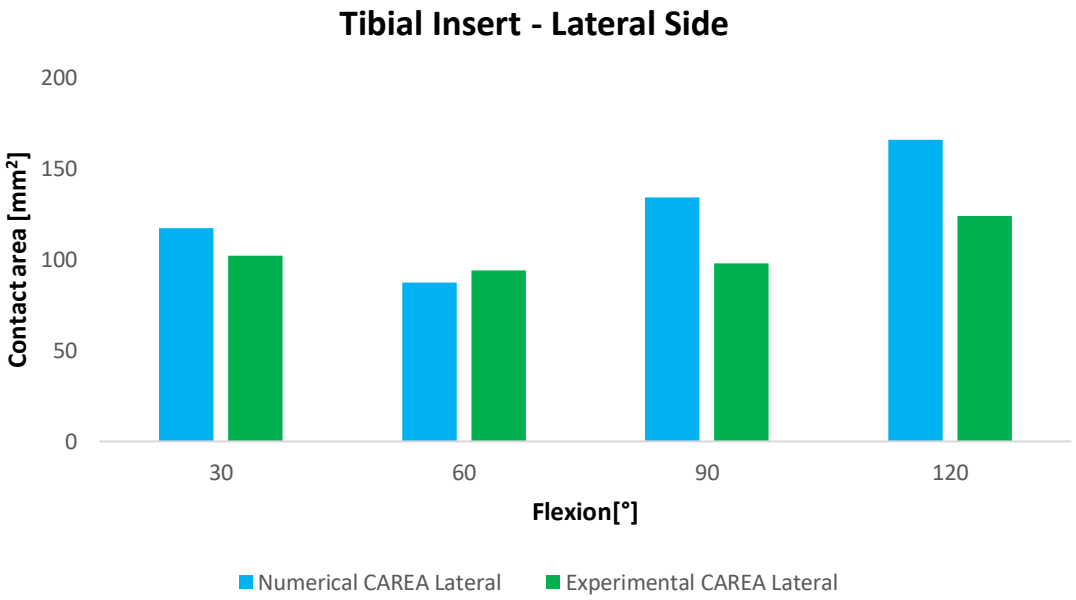

Fig. 5-6. *Comparison between numerical and experimental contact area on lateral side of tibial insert.*

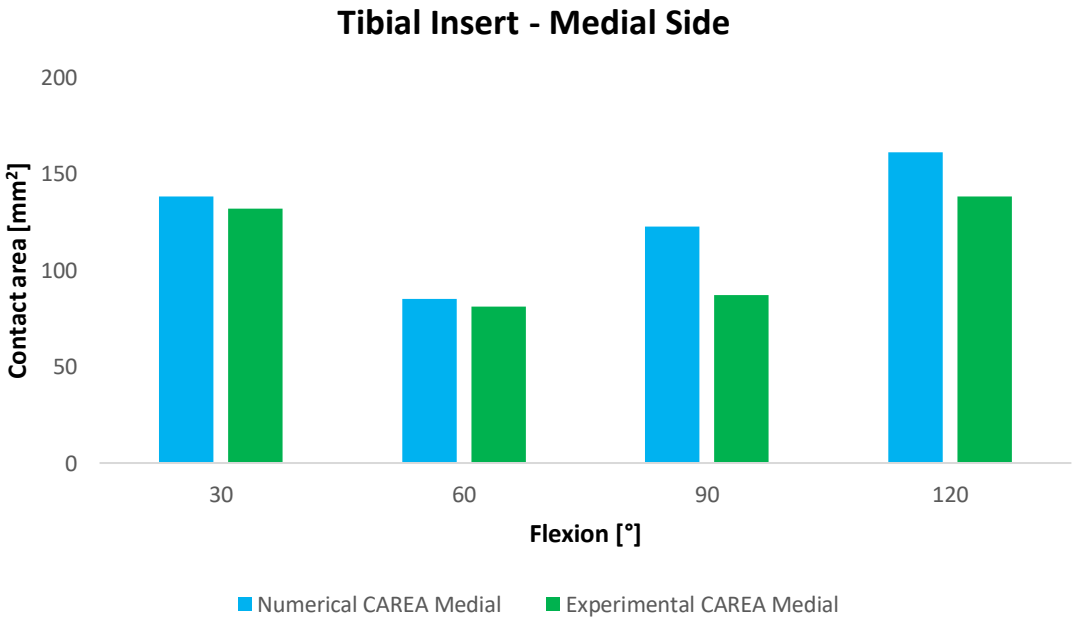

Fig. 5-7. *Comparison between numerical and experimental contact area on medial side of tibial insert.*

As concerning to the contact pressures, figure 5-8 and 5-9 represent relative trend for lateral and medial side of region of interest made a comparison between numerical outputs and experimental measurements. There is a pronounced range of divergences in both case. As mentioned in chapter 3, contact pressures measured during the cadaver test results around 6 times lower than numerical ones and literature. However, a similar trend is showed during all the motion, except in the range between 90 and 120 degrees on the lateral side where numerically there is a highly increase.

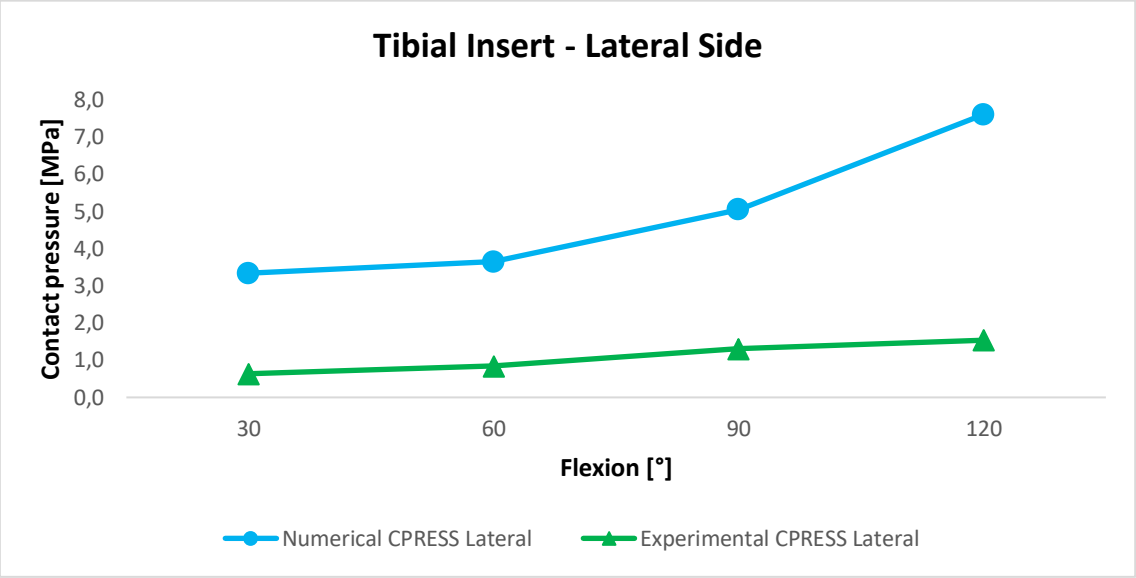

Fig. 5-8. *Comparison between numerical and experimental contact pressure on lateral side of tibial insert.*

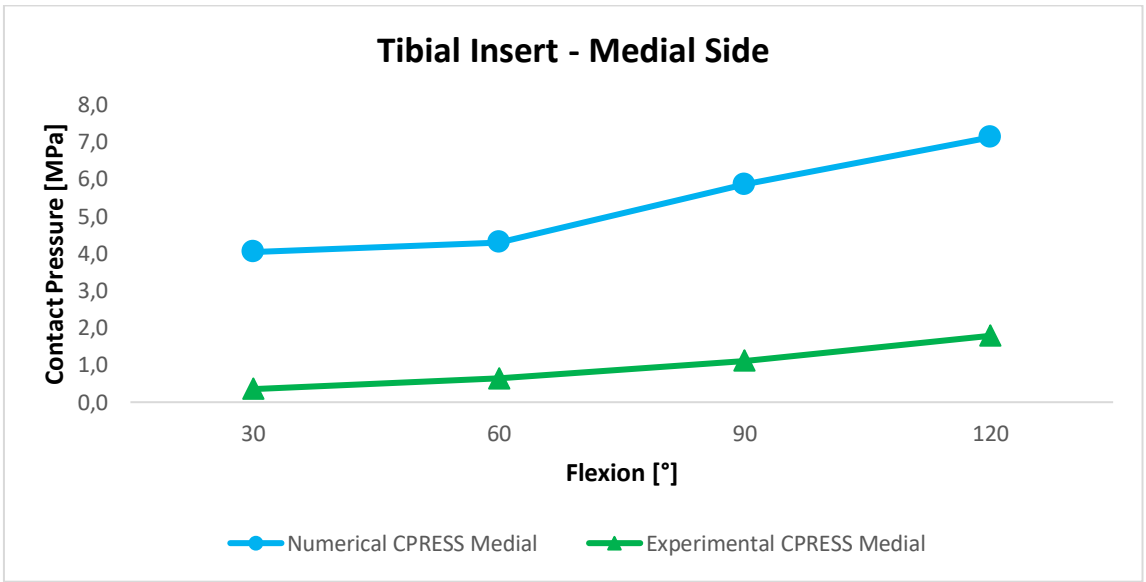

Fig. 5-9. *Comparison between numerical and experimental contact pressure on medial side of tibial insert.*

Relative to patellar component, figure 5-10 and figure 5-11 represent respectively the contact areas and the contact pressures during the flexion. The comparison shows comparable trend and range of values, also in terms of pressure, from 30 to 90 degrees. At the end of motion, due to a shift of sensor during the cadaver test, experimental measures show a remarkable decrease in full flexion in contrast to the values extracted from Finite Element Analysis and found in literature.

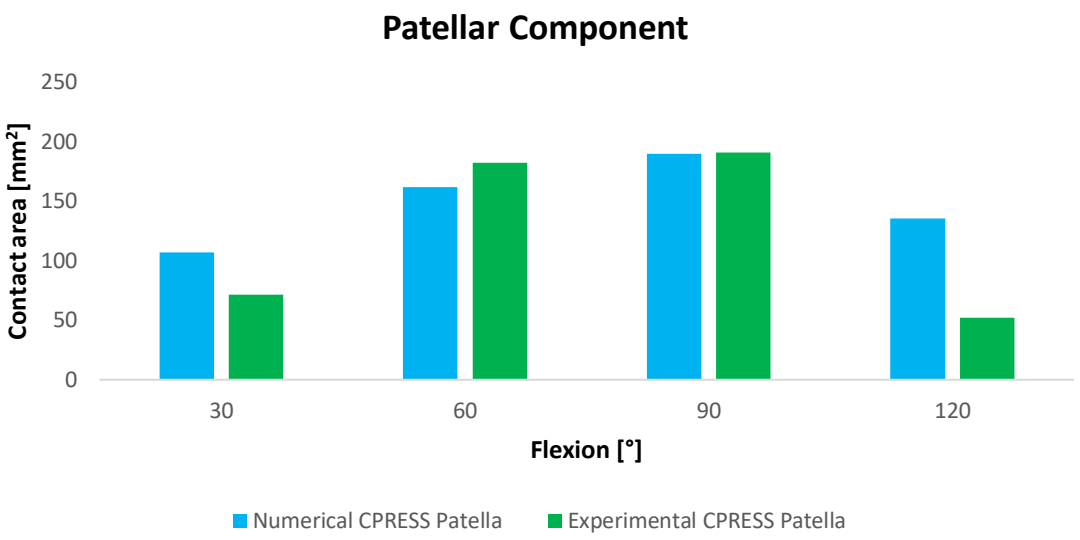

Fig. 5-10. *Comparison between numerical and experimental contact area on patellar component.*

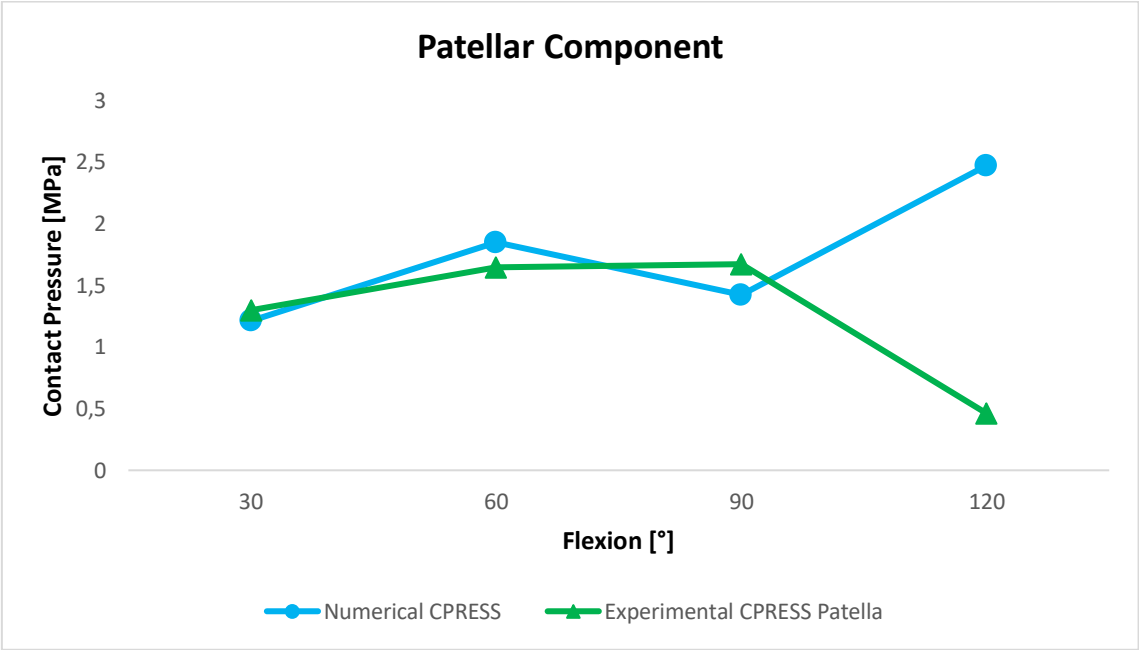

Fig. 5-11. *Comparison between numerical and experimental contact pressure on patellar component.*

Comparing outcomes with experimental data for the same specimen under the same boundary conditions, and considering also literature values, the patient-specific model developed could be considered reliable in terms of kinematics. Regarding the kinetic, the model could be validated from the perspective of contact areas both in the patellofemoral joint and in the tibiofemoral joint. Unfortunately, concerning the contact pressures, in vitro measurements of the tibiofemoral joint result incorrect and so can be validated only the patellofemoral joint.

CHAPTER VI – CONCLUSIONS

The research project shown in this thesis provides a complete protocol to develop and validate a subject-specific Finite Element Model of human knee after Total Knee Arthroplasty.
As mentioned before, the kinematic and kinetic knee joint activity results strongly patient-dependent. Therefore, a specific approach could represent the starting point to overcome failures and patient discontent after surgical treatment. For this reason, the main aims of this work have been to give, first, a cadaver test protocol which explains in detail all the steps to prepare and conduct experimental analysis on human specimen; second, to provide a protocol to develop a specific numerical model; third, to validate the latter comparing numerical outcomes and experimental measurements obtained these approaches.
The kinematic validation coupled with a partial kinetic validation demonstrate all the potentials of the finite element analysis in orthopaedic field and in particular in the knee studies. Starting from this cadaver test and finite element model protocols, researches and engineers could be able to conduct other studies in order to investigate and solve clinical issues. The kinematical validation allows to conduct deep analysis about translations and rotations before and after surgical treatment. In fact, different implants can be simulated in order to identify that one able to restore the best native kinematics. At the same time, a validate numerical approach can be used to compare different surgical strategy going to focus the kinematics deviations. Regarding to the kinetics, as marked for the kinematics, a patient specific FE model become a unique tool for surgeons to compare, for instance, how varying the pressure distributions during a motor task changing implants or surgical treatments.
However, this project certainly presents some limitations: regarding the experimental data recorded during cadaver test, it is known that the use of Tekscan sensors strongly depending of the user experiences and nevertheless the measurements can results affected by noise with the minimal environment changing. Moreover, uncertainties revealed during the experimental test could be correlated to the different work environments compared to the calibration one. Concerning to future projects, some improvements could regard a new Tekscan calibration protocol to overcome the previous mentioned problems and simulate different motor tasks, such as kneeling or stand up. Another improvement could also regard the study of the native knee with the purpose of developing a more complete model to permit deep specific clinical studies and a subsequent follow up.

BIBLIOGRAPHY

[1]. S H Palmer. Anatomy and Biomechanics of the Knee, 2009

[2]. Goldblatt, John P., and John C. Richmond. "Anatomy and biomechanics of the knee." *Operative Techniques in Sports Medicine* 11.3 (2003): 172-186.

[3].https://www.physio-pedia.com/Anterior_Cruciate_Ligament_(ACL)structure_and_ biomechanical _Properties

[4]. Hirschmann, Michael T., and Werner Müller. "Complex function of the knee joint: the current understanding of the knee." *Knee Surgery, Sports Traumatology, Arthroscopy* 23.10 (2015): 2780-2788.

[5]. Masouros, S. D., A. M. J. Bull, and A. A. Amis. "Biomechanics of the knee joint." *Orthopaedics and Trauma* 24.2 (2010): 84-91.

[6]. Komdeur, Prashant, Fabian E. Pollo, and Robert W. Jackson. "Dynamic knee motion in anterior cruciate impairment: a report and case study." *Baylor University Medical Center Proceedings*. Vol. 15. No. 3. Taylor & Francis, 2002.

[7]. Woo, Savio LY, et al. "Biomechanics of knee ligaments." *The American journal of sports medicine* 27.4 (1999): 533-543.

[8]. Draganich, L. F., T. P. Andriacchi, and G. B. J. Andersson. "Interaction between intrinsic knee mechanics and the knee extensor mechanism." *Journal of Orthopaedic Research* 5.4 (1987): 539-547.

[9]. Cooke, T. Derek V., Elizabeth A. Sled, and R. Allan Scudamore. "Frontal plane knee alignment: a call for standardized measurement." *Journal of Rheumatology* 34.9 (2007): 1796.

[10]. Yoshioka, Yuki, David Siu, and T. D. Cooke. "The anatomy and functional axes of the femur." *J Bone Joint Surg Am* 69.6 (1987): 873-880.

[11]. Pickering, Simon, and Dan Armstrong. "Focus on alignment in total knee replacement." *J Bone Joint Surg* (2012): 1-3.

[12]. Rand, James A. "Comparison of metal-backed and all-polyethylene tibial components in cruciate condylar total knee arthroplasty." *The Journal of arthroplasty* 8.3 (1993): 307-313.

[13]. Athwal, Kiron K., et al. "Clinical biomechanics of instability related to total knee arthroplasty." *Clinical Biomechanics* 29.2 (2014): 119-128.

[14]. Huang, Chun-Hsiung, Jiann-Jong Liau, and Cheng-Kung Cheng. "Fixed or mobile-bearing total knee arthroplasty." *Journal of orthopaedic surgery and research* 2.1 (2007): 1.

[15]. Callaghan, John J., et al. "Mobile-bearing knee replacement: concepts and results." *Instructional course lectures* 50 (2001): 431-449.

[16]. Innocenti, Bernardo, et al. "Can medio-lateral baseplate position and load sharing induce asymptomatic local bone resorption of the proximal tibia? A finite element study." *Journal of orthopaedic surgery and research* 4.1 (2009): 26.

[17]. https://www.stoneclinic.com/tkrillustration

[18]. Dorr, Lawrence D., and Richard A. Boiardo. "Technical considerations in total knee arthroplasty." *Clinical orthopaedics and related research* 205 (1986): 5-11.

[19]. Insall, JOHN N., and Michael Kelly. "The total condylar prosthesis." *Clinical orthopaedics and related research* 205 (1986): 43-48.

[20]. Leopold, Seth S. "Minimally invasive total knee arthroplasty for osteoarthritis." *New England Journal of Medicine* 360.17 (2009): 1749-1758.

[21]. Cheung, Alan, et al. "Complications of total knee arthroplasty." *Current Orthopaedics* 22.4 (2008): 274-283.

[22]. Verstraete, Matthias A., and Jan Victor. "Possibilities and limitations of novel in-vitro knee simulator." Journal of biomechanics 48.12 (2015): 3377-3382.

[23]. Victor, Jan, et al. "How precise can bony landmarks be determined on a CT scan of the knee?." The knee 16.5 (2009): 358-365.

[24]. Verstraete, Matthias A., et al. "3D printed guides for controlled alignment in biomechanics tests." Journal of biomechanics 49.3 (2016): 484-487.

[25]. Chen, Tony, Hongsheng Wang, and Bernardo Innocenti. "Tekscan measurements of interfacial contact area and stress in articulating joints." Experimental Methods in Orthopaedic Biomechanics. 2017. 267-283.

[26]. Grood, Edward S., and Wilfredo J. Suntay. "A joint coordinate system for the clinical description of three-dimensional motions: application to the knee." Journal of biomechanical engineering 105.2 (1983): 136-144.

[27]. Logan, Daryl L. A first course in the finite element method. Cengage Learning, 2011.

[28]. Oloyede, Kunle. ENB311– STRESS ANALYSIS. Australia: Pearson Higher Education, 2015.

[29]. Roylance, David. Finite Element Analysis. Cambridge, MIT OpenCourseWare (http://ocw.mit.edu), 2015. PDF.

[30]. Pianigiani, Silvia, and Bernardo Innocenti. "The use of finite element modelling to improve biomechanical research on knee prosthesis." New Developments in Knee Prosthesis Research. Nova Science Publishers, Inc., 2015.

[31]. Kluess, Daniel. "Finite element analysis in orthopaedic biomechanics." Finite Element Analysis. InTech, 2010.

[32]. Innocenti, Bernardo, et al. "Load sharing and ligament strains in balanced, overstuffed and understuffed UKA. A validated finite element analysis." The Journal of arthroplasty 29.7 (2014): 1491-1498.

[33]. Wang, Yuxing, Yubo Fan, and Ming Zhang. "Comparison of stress on knee cartilage during kneeling and standing using finite element models." Medical engineering & physics 36.4 (2014): 439-447.

[34]. Van Jonbergen, Hans-Peter W., et al. "Differences in the stress distribution in the distal femur between patellofemoral joint replacement and total knee replacement: a finite element study." Journal of orthopaedic surgery and research 7.1 (2012): 28.

[35]. Mootanah, Rajshree, et al. "Development and validation of a computational model of the knee joint for the evaluation of surgical treatments for osteoarthritis." Computer methods in biomechanics and biomedical engineering 17.13 (2014): 1502-1517.